**Title**
Temporal control of gene expression during neural circuit formation



**Author**
Lin, Ying

**Publication Date**
2021

Peer reviewed|Thesis/dissertation

UNIVERSITY OF CALIFORNIA

Los Angeles

# Temporal control of gene expression during neural circuit formation

A dissertation submitted in partial satisfaction of the requirements for the degree

Doctor of Philosophy in Molecular Biology

by

Ying Lin

2021

# ABSTRACT OF THE DISSERTATION

## Temporal control of gene expression during neural circuit formation

by

Ying Lin

Doctor of Philosophy in Molecular Biology

University of California, Los Angeles, 2021

Professor Stephen Lawrence Zipursky, Chair

Proper neural circuit formation is crucial for brain function and animal behavior. How neurons form connections with the right partners at the right subcellular locations is an essential question in neuroscience. Many mechanisms such as cell recognition, local signaling, and neural activity, have been shown to regulate neural circuit assembly, but the temporal regulation mechanisms of gene expression remain unclear. Recent improvement of single cell RNA-seq (scRNA-seq) method enables us to profile transcriptomes of many types of neurons at multiple developmental stages to study gene expression changes during neural development. By analyzing the transcriptomes of developing neurons in the Drosophila visual system, we identified that a cascade of transcription factors induced by steroid hormone ecdysone is expressed in a highly

synchronized fashion in all neurons during circuit assembly. We demonstrated that disrupting the ecdysone signaling leads to specific wiring defects in multiple types of neurons. Using scRNA-seq, we profiled 5 types of lamina neurons with different genetic perturbations that disrupt the ecdysone pathway. The results showed that a common set of genes required for neuronal maturation and a cell-type specific set of genes enriched for recognition molecules are controlled by the ecdysone pathway. Cell-type specific recognition molecules can be co-regulated by the globally controlled ecdysone pathway and constantly expressed cell-type specific transcription factors (i.e. Erm). These data showed that neurons integrate a global temporal program with cell-type specific transcription factors to express distinct sets of cell recognition molecules at different time points to regulate neural circuit assembly. By coordinating when and which recognition molecules are expressed in different neurons, the global temporal program could generate more molecular codes for neural interactions and choreograph circuit assembly.

The dissertation of Ying Lin is approved.

Alvaro Sagasti

Mark Arthur Frye

Kathrin Plath

William Edward Lowry

Stephen Lawrence Zipursky, Committee Chair

University of California, Los Angeles

2021

# TABLE OF CONTENTS

# LIST OF FIGURES

# ACKNOWLEDGEMENT

Pursuing my career in research has been an exciting journey and I have many people to thank for their kind help and encouragement along the way.

First, I would like to thank my thesis advisor, Dr. S. Lawrence Zipursky for his endless support and guidance. He is a true role model for me who has tremendous passion of scientific research. He has taught me how to be a rigorous scientist and has encouraged me to think creatively on important questions. With all his help and mentorship, I have grown as a scientist and as a person. He has also provided the perfect lab environment so that everyone is extremely collaborative, and I have learned so much from the other lab members. I could not have asked for a better mentor.

I would also like to thank my thesis committee, Dr. Alvaro Sagasti, Dr. Kathrin Plath, Dr. Mark Frye, and Dr. William Lowry for their precious research suggestions and valuable career advice.

I am very appreciated for everyone in the Zipursky lab. Thanks to Dr. Saumya Jain, Dr. Yerbol Kurmangaliev, Dr. Javier Valdes-Aleman and Dr. Sam LoCascio for their awesome collaboration on the project described in Chapter 2. I would also like to thank the great undergraduate students Parmis Mishahidi and Brianna Parrington for their contributions to this project. I am grateful that Dr. Qi Xiao and Dr. Shuwa Xu taught me fly genetics at the beginning so that I could contribute to the DIP/Dpr project. In addition, I would also like to thank Dr. Piero Sanfilippo, Dr. Liming Tan, Dr. Orkun Akin, Dr. Bryce Bajar, Dr. Sarah Cheng, Dr. Mark Dombrovskly, Juyoun Yoo and Alex Kim for inspiring discussion in various topics. Lastly, I extend special thanks to Dorian Gunning and Laura Schreiber for keeping the lab running.

The exciting journey started about eight years ago when I joined Dr. William Lowry's lab as an undergraduate student. Thanks to Dr. Yuan Xie for teaching me basic molecular techniques and intriguing my interests in biological research.

Finally, I would like to express my sincerest gratitude to my family and friends. My parents, Jianwan Lin and Jing Xu, are always extremely supportive for all my decisions. Without their love, I would not be able to pursue my passion in research. I would also like to thank my dear friends whom I have met throughout this exciting journey, and you all are precious treasure of my life.

My dissertation work was supported in part by Whitcome Fellowship. Chapter 2 is currently under revision at *Nature* and it is also available in bioRxiv. Jain, S., Lin, Y., Kurmangaliyev, Y.Z., Valdes-Aleman, J., LoCascio, S.A., Mirshahidi, P., Parrington, B., and Zipursky, S.L. (2021). A global timing mechanism regulates cell-type specific wiring programs. bioRxiv 2020.09.18.304410.

# VITA

| | |
|---|---|
| 2015 | Bachelor of Science in Molecular, Cell, & Developmental Biology |
| | with Computing Specialization and Biomedical Research Minor |
| | University of California, Los Angeles |
| | Los Angeles, CA |
| 2015 | Poster day Dean's Prize |
| | University of California, Los Angeles |
| | Los Angeles, California |
| 2015-present | Graduate student |
| | *Molecular Biology Interdepartmental Doctoral Program* |
| | University of California, Los Angeles |
| | Los Angeles, California |
| 2017 | Whitcome Pre-Doctoral Fellowship Award |
| | University of California, Los Angeles |
| | Los Angeles, California |
| 2018 | Whitcome Pre-Doctoral Fellowship Award |
| | University of California, Los Angeles |
| | Los Angeles, California |
| 2021 | Trainee Professional Development Award |
| | Society of Neuroscience |

# PUBLICATIONS AND PRESENTATIONS

1. Jain, S.*, Lin, Y.*, Kurmangaliyev, Y.Z., Valdes-Aleman, J., LoCascio, S.A., Mirshahidi, P., Parrington, B., and Zipursky, S.L. (2021). Temporal genetic program controls global wiring of post-mitotic neurons. Poster presentation at Society of Neuroscience Conference.
2. Jain, S.*, Lin, Y.*, Kurmangaliyev, Y.Z., Valdes-Aleman, J., LoCascio, S.A., Mirshahidi, P., Parrington, B., and Zipursky, S.L. (2020). A global timing mechanism regulates cell-type specific wiring programs. bioRxiv 2020.09.18.304410. (Under revision at *Nature*)
3. Jain, S.*, Lin, Y.*, Kurmangaliyev, Y.Z., Valdes-Aleman, J., LoCascio, S.A., Mirshahidi, P., Parrington, B., and Zipursky, S.L. (2020). A cascade of transcription factors provides temporal control of gene expression during neural circuit formation. Poster presentation at Cold Spring Harbor Laboratory Conference.
4. Xu, S., Xiao, Q., Cosmanescu, F., Sergeeva, A.P., Yoo, J., Lin, Y., Katsamba, P.S., Ahlsen, G., Kaufman, J., Linaval, N.T., et al. (2018). Interactions between the Ig-Superfamily Proteins DIP-α and Dpr6/10 Regulate Assembly of Neural Circuits. Neuron 100, 1369-1384.e6.

# Chapter 1 Introduction

## Overview

In our brain, there are billions of neurons that have distinct shapes and functions, and these neurons connect with each other through synapses and form complex neural networks. The precise neural connections are critical for proper brain functions. Defects in neural circuit assembly are associated with neuropsychiatric disorders (Penzes et al., 2011; Redies et al., 2012). Therefore, it is important to understand how specific connections between neurons are established during development.

Wiring specificity is largely determined by genetically encoded molecular mechanisms. From the electron microscopy (EM) reconstruction of C. elegans and Drosophila brains, each neuron encounters a large group of potential neurons, among which partners and subcellular regions are selected for synapse formation (Hulse et al., 2021; Takemura et al., 2015; Witvliet et al., 2021). Recognition molecules that are expressed in different neurons can act as adhesive or repulsive cues for neurons to form specific connections (Sanes and Zipursky, 2020). Precise spatial and temporal expression pattern of recognition molecules would be important for building functional neural networks.

During development, complex neural networks are generated from sequential steps of neuronal differentiation: cell fate determination, axon guidance, dendrite growth, and synapse formation. Temporal regulation of each step is crucial for neural circuit assembly. The timing of birth of neural progenitors determines their cell fate, projection pattern and connectivity (Deguchi et al., 2011; Imamura et al., 2011; Li et al., 2013; Meng et al., 2020). Post-mitotic neurons project to their target regions in a narrow time window and start spontaneous activity in a nearly

synchronized fashion (Akin and Zipursky, 2016; Akin et al., 2019). Experience-dependent neural plasticity is restricted in a critical period, which can be defined by glial cells (Ackerman et al., 2021; Ribot et al., 2021). The process of neural circuits assembly relies on accurate temporal control.

Accurate temporal control of neuronal differentiation can coordinate circuit assembly among different neurons. Waddington's landscape model in stem cell differentiation proposed that just like marbles rolling down a hill, the epigenetic landscape determines cell fate and reduces pluripotency over time. Similarly, during neural circuit formation, the landscape shaped by cell recognition molecules, local signaling, and neural activities directs neuronal interactions and synapse formation. Precise temporal control can specify when and where neurons interact with each other so that choices of synaptic partners or subcellular regions are restricted (Hassan and Hiesinger, 2015; Yogev and Shen, 2014). However, the timing mechanisms regulating neural circuit formation remain unclear. In this Chapter, we will focus on the temporal control of neural circuit assembly.

**Molecular strategies regulating wiring specificity**

From regeneration studies in vertebrate, John Langley and Roger W. Sperry proposed that the molecular differences between neurons determine their specific connections (Yogev and Shen, 2014). During development, neuronal processes encounter many neurons before choosing the right partners and subcellular regions to form synapses. In a brain, there are enormous number of synaptic connections ($10^{15}$ in human brain, $10^{9}$ in mouse brain, $10^{7}$ in Drosophila brain, 7600 in C. elegans) (DeWeerdt, 2019; Scheffer et al., 2020; Zhu et al., 2018). How do neurons form specific connections in such a complex environment? In this section, we will summarize different molecular strategies used to regulated wiring specificity.

*Cell recognition molecules*

Cell recognition molecules are proteins that have selective binding patterns with each other. The protein-protein recognition can lead to adhesive or repulsive interactions between neurons for proper wiring specificity. In addition to the canonical guidance-cue such as Netrin, Slits, Semaphorins, and Ephrins, adhesion molecules also play important roles in regulating neural wiring through homophilic or heterophilic binding (Honig and Shapiro, 2020). Based protein domains, adhesion proteins contain Cadherin family proteins and Immunoglobulin super family (IgSF) proteins (Figure 1-1a).

N-Cadherin, for example, which is broadly expressed in vertebrate and invertebrate systems, is a homophilic binding protein (Honig and Shapiro, 2020). In the Drosophila visual system, the organization of axon bundles and the axon targeting of photoreceptors are regulated by the expression level of N-Cadherin (Lee et al., 2001; Schwabe et al., 2014). High N-Cadherin L1 and L2 neurons are surrounded by low N-Cadherin R cells. Changing their relative levels of N-Cadherin alters their positions in the axon bundles, so differential adhesion can determine the

wiring structure (Schwabe et al., 2014). The dynamic expression of N-Cadherin correlates with growth cone movement and is required for the layer specificity of axon and dendrites (Nern et al., 2008; Özel et al., 2015). Therefore, changing when and where adhesion molecules are expressed, even a single molecule, significantly modifies neural circuit formation.

Immunoglobulin super family (IgSF) proteins form an important group of adhesion molecules. In this family, Sidekick, Dscam, DIP/Dpr, and Beat/Side proteins show specific homophilic or heterophilic binding properties providing molecular codes for neurons to distinguish between one another (Figure 1-1a) (Sanes and Zipursky, 2020). Interactome networks of IgSF proteins, both in vertebrate and invertebrate systems, have revealed extremely complex networks of protein-protein interactions (Li et al., 2017a; Özkan et al., 2013; Wojtowicz et al., 2020). In addition to qualitative methods, quantitative methods like Surface Plasmon Resonance (SPR) have also been used to determine binding affinities, and it showed that DIP/Dpr interactions have a broad range of affinities (Cosmanescu et al., 2018). In each cell type, only a subset of DIP/Dpr proteins are expressed and the protein binding patterns strongly correlate with synaptic connections (Tan et al., 2015). The specific bindings between cell recognition molecules provide diverse molecular codes for different neurons to distinguish from each other.

In addition to the proteins mentioned above, there are many other adhesion molecules that are required for synaptic specificity, including Leucine-rich repeat (LRR) proteins, Teneurin, Protocadherin proteins, etc. (Sanes and Zipursky, 2020; Schroeder and Wit, 2018). These adhesion molecules often work in combinations in different cell types and have dynamic expression over time.

*Combinatorial molecular code*

Multiple cell recognition molecules are expressed in a developing neuron. The combination of different recognition molecules increases the molecular complexity among neuronal interactions. In the antennal lobe of the Drosophila olfactory system, olfactory receptor neurons (ORNs) and projection neurons (PNs) form specific synaptic connections in different glomeruli. Different combination of Teneurins (Ten-a and Ten-m) and Leucine-rich repeats (LRR) proteins (Toll-6 and Toll-7) regulate their targeting to specific glomeruli (Figure 1-1b) (Sanes and Zipursky, 2020). Down Syndrome cell adhesion molecule 1 (Dscam1) generates thousands of isoforms through alternative splicing (Hattori et al., 2007). Each cell expresses different combinations of Dscam1 isoforms to generate a unique identifier, and their homophilic binding regulates neurite self-avoidance (Hattori et al., 2009). Similarly, 21 paralogs of Dpr proteins are expressed in different combinations in neurons with distinct synaptic connections, and matched DIP and Dpr proteins are often expressed in synaptic partners (Tan et al., 2015). All these examples underscore that the combination of recognition molecules can generate unique molecular codes that either promote or inhibit specific connections.

*Spatial-temporal specific gene expression pattern*

Another way to increase the complexity of molecular code with a limited set of cell recognition molecules is to restrict the spatial and temporal domain of their expression. With the rapid development of technology, especially high-throughput transcriptomic analysis, we learned that in different species, gene expression is highly dynamic and cell-type specific during brain development. For example, in the Drosophila visual system, there are more than a hundred types of neurons based on their morphology and they for neural circuits assembly mostly during metamorphosis (~ 100 hours at room temperature). Single cell RNA-seq (scRNA-seq) on developing neurons showed that many cell recognition molecules are expressed in a specific set of

neurons and their expression level changes dramatically over time (Figure 1-1c) (Kurmangaliyev et al., 2020; Özel et al., 2020). This complexity in gene expression is also seen in different brain regions of different species, including the Drosophila olfactory system, the mouse retina and neocortex, and the human prefrontal cortex (Alyagor et al., 2018; Clark et al., 2019; Li et al., 2017b; McLaughlin et al., 2021; Xie et al., 2021).

In addition to developmental transcriptomic data, there are studies showing a correlation between dynamic expression of adhesion molecules and the formation of specific synaptic connections. A recent paper in C. elegans provides an example showing that temporally regulated cell adhesion molecules SYG-1 controls synaptic specificity of AIB neurons (Figure 1-1c) (Sengupta et al., 2020). AIB neurons connect with both neurons in the anterior and posterior neighborhood in the layered nerve ring. Live imaging showed that the AIB neuron first attaches to the posterior neighborhood, and then exits the posterior neighborhood and then repositions itself onto the anterior neighborhood. Starting from the tip, the AIB neurite then zippers in a retrograde fashion as attaches to processes in the anterior neighborhood. This zippering process is mediated by the dynamic expression of SYG-1, which is first expressed in the posterior neighborhood and then in the anterior neighborhood. The timing of SYG-1 expression correlates with the timing of the zippering of AIB neurons and disruption of SYG-1 showed defects in layer specific connections of AIB neurons. However, there is little evidence showing that altering the temporal specificity of recognition molecules changes wiring specificity.

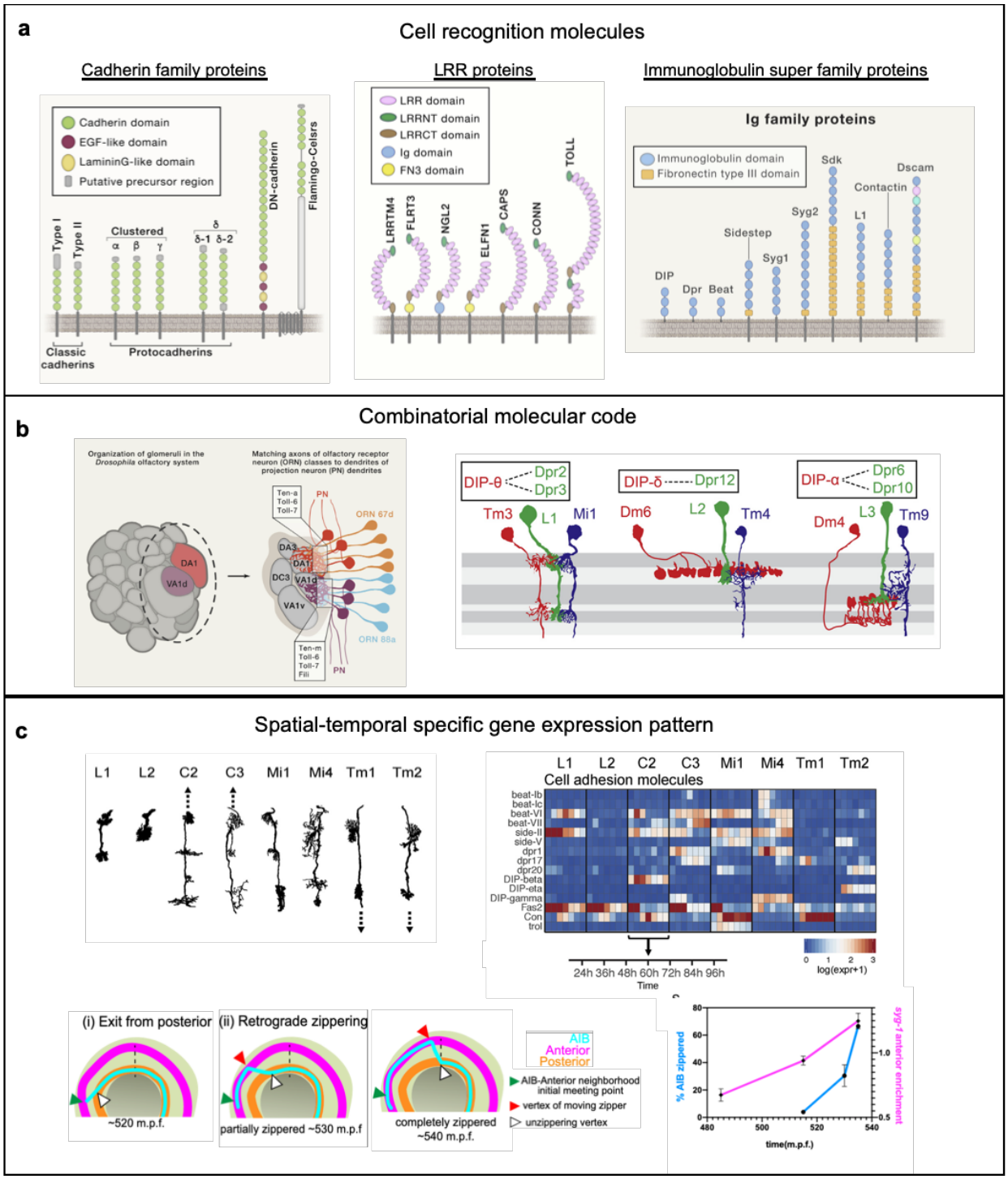


**Figure 1-1. Cell recognition molecules regulate wiring specificity.**

(a) Schematic of domain structures of Cadherin family proteins and IgSF proteins (Sanes and Zipursky, 2020) (b) Example of combinatorial molecular code in establishing specific connections.

Left: LRR protein and Teneurin proteins act together to determine the specific targeting of ORN and PN in glomeruli in the Drosophila olfactory system (Sanes and Zipursky, 2020). Right: different combinations of matching DIP/Dprs are expressed in synaptic partners (Tan et al., 2015).(c) Spatial-temporal specific gene expression patterns of wiring genes. Top, recent single cell RNA-seq data revealed that different cell adhesion molecules are expressed in a subpopulation of neurons dynamically during development (Kurmangaliyev et al., 2020). Bottom, example of dynamically expressed cell adhesion molecule directing wiring specificity in C. elegans (Sengupta et al., 2020). The AIB neuron is initially attached to the posterior neighborhood, and then it exits from posterior. The tip of the AIB neurite attaches to the anterior neighborhood and undergoes retrograde zippering to attach a segment of AIB to the anterior neighborhood. This correlates with the spatial-temporal expression pattern of SYG-1 shown on the right.

**Temporally regulated neuronal differentiation**

To form a functional brain, neural development is highly choreographed. Each step needs precise temporal control so that many neurons can establish proper networks during development. Many studies showed the dynamic process of neuronal development in different brain regions of different species (Cadwell et al., 2019; Miyares and Lee, 2019). In this section, we will highlight examples showing temporal regulation in neuronal differentiation.

*Temporal patterning of neural progenitors*

In both vertebrate and invertebrate, temporal cues help to specify neuronal diversity during neurogenesis. Neural progenitors sequentially express different temporal transcription factors (TFs), which marks their birth order. Different sets of temporal TFs are used in different developmental context, including Drosophila ventral nerve cord and optic lobe, and mouse retina.

The first series of temporal TFs (Hunchback (Hb), Kruppel (Kr), Pdm, Castor (Cas), and Grainyhead (Grh)) was discovered in Drosophila embryonic ventral nerve cord (Isshiki et al., 2001). The same series of temporal TFs can be used in distinct neural lineages to specify cell fate of their progenies. Altering the timing of these temporal TFs in neuroblast NB7-1 or NB3-1 disrupts normal neuromuscular synapse distribution and synaptic partner selection (Meng et al., 2019, 2020). A different cascade of temporal TFs is used in medulla neuroblast in the Drosophila optic lobe: Homothorax (Hth), Elyless (Ey), Sloppy paired (Slp), Dichaete(D) and Tailless (Tll) (Figure 1-2a) (Li et al., 2013). This temporal TF cascade, together with spatial input and Notch signaling, generates great neural diversity in medulla (Erclik et al., 2017).

Sequential temporal TFs like the ones discovered in Drosophila have not been found in mammalian system, but multiple studies have shown TFs that correlate with the timing of birth of neural progenitors. For instance, zinc-finger TF Ikaros and NFI TFs are expressed in early and late

retinal progenitors, respectively (Clark et al., 2019; Elliott et al., 2008). The birth order of neurons is often associated with their wiring specificity in many different systems, such as mouse olfactory sensory neurons (Figure 1-2a) (Deguchi et al., 2011). The regulatory mechanism that controls these temporal patterns in mammals remains unknown. These examples suggest that temporal patterning of neural progenitors is a common mechanism to generate neuronal diversity in both vertebrates and invertebrate systems.

*Axon and dendrite growth*

The developmental process of axon and dendrite growth is also highly dynamic. Although neurons are born in waves, their axon and dendrite growth can still be temporally regulated independently of their birthdate. The precise timing of neuronal growth might play important roles in establishing specifying neural networks.

In Drosophila visual system, photoreceptor R7 and R8 target to different layers in medulla region (M6 and M3 respectively). Recently developed ex vivo and in vivo live imaging methods allow us to observe the dynamic process of their axon development. Özel et al. used *ex vivo* imaging on cultured brains to analyze filopodial dynamics of R7 growth cones (Özel et al., 2015). They observed the fast R7 filopodial dynamics during layer formation. Akin and Zipursky (2016) used in vivo imaging to analyze the development of R8 (Akin and Zipursky, 2016). Through analysis of hundreds of wild type R8 neurons, they observed that growth cones of R8 neurons born at different times paused on the top of medulla (M0) for up to two days, and then all R8 neurons extended a thin process together around 38 hours after pupal formation (hAPF) (Figure 1-2b). After that, hundreds of R8s become stabilized and elongate from M0 to M3 to reach their final morphology within one day. The dynamic process of axon development suggests that there is a temporal control to direct hundreds of R7 and R8 to grow together. Although studies showed that

the transcription factor TF Sequoia, the cell adhesion molecule N-Cadherin, and the Netrin-Frazzled ligand receptor pair are important for R7 and R8 layer targeting, how these processes are temporally regulated remains unknown (Akin and Zipursky, 2016; Nern et al., 2008; Özel et al., 2015; Petrovic and Hummel, 2008).

Neural dendrites also undergo temporally regulated growth and remodeling during development. Drosophila class IV dendrite arborization sensory neurons (C4da) undertake extensive dendrite remodeling during metamorphosis. Their dendrites are almost completely pruned around 24 hours after pupa formation (Furusawa and Emoto, 2021). Then C4da neurons start to regrow the dendrite to form new arbors for adult-specific function. Right after eclosion, their radially shaped dendrites acquire a lattice shape. Similar dynamic dendritic growth or remodeling is also shown in Purkinje cells in cerebellum, mushroom body γ neurons, and Layer 4 pyramidal neurons (Nakazawa et al., 2018; Takeo et al., 2015; Yaniv and Schuldiner, 2016).

*Spontaneous neural activity*

In mammalian retina, neurons fire in almost synchronous bursts followed by silence, which form retinal waves even before receiving visual input (Meister et al., 1991). This experience-independent and correlated neural activity has also been observed in several brain regions during neural development, including hippocampus, cerebellum, and neocortex and it helps to shape neural circuits (Kirkby et al., 2013). It is remarkable how synchronized the patterned neural activity is without external input, raising the intriguing question of how this process is regulated by internal developmental processes.

In the Drosophila brain, spontaneous neural activity is also observed via calcium imaging on GCaMP expressing neurons by 2-photon microscopy (Akin et al., 2019). Akin et al. showed

that the central nervous system of Drosophila exhibits highly synchronized sensory-independent activity during metamorphosis (Akin et al., 2019). During the second half of pupal development (from ~50-100 hrs after pupal formation (hAPF)), the entire brain is active. This is characterized by regular active and inactive phases followed by a more turbulent phase (Figure 1-2c). Recent studies revealed that this actively regulates circuit development (Bajar et al., 2021, submitted). It is interesting that the onset, oscillation, and transition of the spontaneous activity is highly temporally controlled.

In this section, we highlighted examples of dynamic processes during neuronal differentiation, including temporal patterning of progenitors, axon/dendrite growth, and correlated neural activity. There might be more temporal regulated neural developmental events that have not been well characterized. It is important that all neurons coordinate with each other to form functional circuits. Therefore, molecular mechanisms controlling timing are highly desired to regulate every step of neuronal differentiation and circuit assembly.

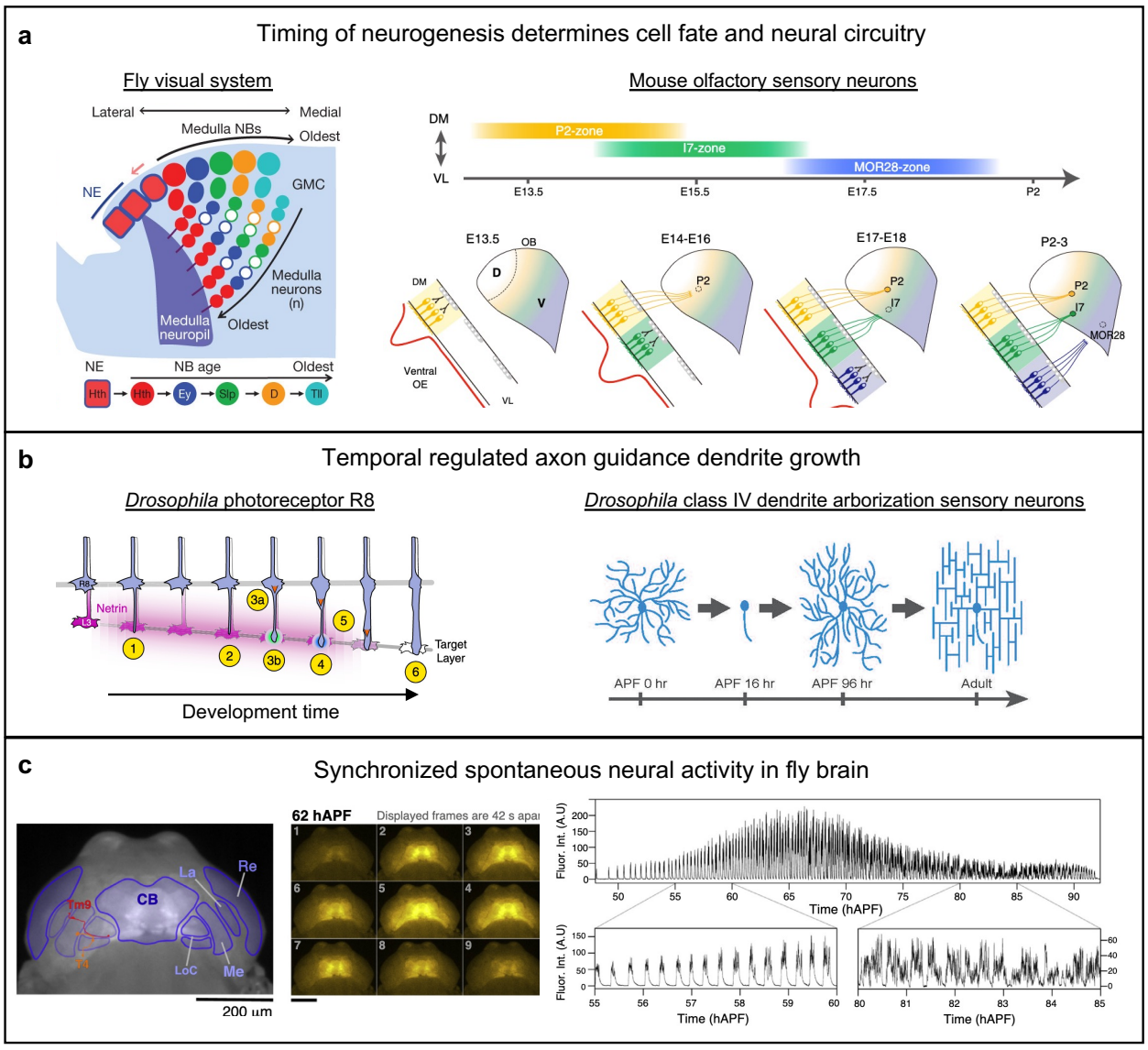


**Figure 1-2. Temporally regulated stepwise neuronal differentiation.**

(a) The timing of neurogenesis determines cell fate and neural circuity. Left, temporal TFs are used to determine the diverse neural types in Drosophila visual system (Li et al., 2013). Right, the timing of neural progenitor birth affects specific axon targeting in mouse olfactory sensory neurons (Deguchi et al., 2011). (b) Temporal regulated axon and dendrite growth. Left, temporally regulated photoreceptor R8 targeting in Drosophila (Akin and Zipursky, 2016). Right, dendrite pruning and regrowth of Drosophila class IV dendrite arborization sensory neurons (Furusawa and

Emoto, 2021). (c) Patterned stimulus-independent neural activity in the Drosophila brain. Calcium imaging of developing brains showed highly correlated experience-independent activity. The onset and pattern are highly synchronized across the entire brain (Akin et al., 2019).

**Timing mechanisms controlling neural development**

In the previous section, we discussed that series of temporal TFs can establish temporal patterns for progenitors and affect circuit formation. The dynamics of temporal TFs can be tuned by microRNAs (i.e., let-7 miRNA and lin4 miRNA) and post-translational modification (Kucherenko et al., 2012; Quan et al., 2016; Sun and Hobert, 2021). There are other mechanisms that provide temporal controls for neural development, including hormonal controls, local intercellular interactions, and neural activities (Akin and Zipursky, 2020; Pan and Monje, 2020; Salinas and Zou, 2008; Ting et al., 2014). In this section, we will focus on hormonal controls regulating timing in neuronal differentiation and circuit assembly.

*Steroid hormone ecdysone signaling in Drosophila*

In Drosophila, pulses of steroid hormone ecdysone act as temporal signals to regulate development from embryo to adult (Pak and Gilbert, 1987; Thummel, 2001). This timing mechanism is highly conserved across different insects (Truman, 2019). During larval stage, ecdysone is produced by prothoracic gland (PG), which expresses Halloween genes that encode enzymes to produce ecdysone (Yamanaka et al., 2013). Then ecdysone is actively released into the hemolymph via vesicular trafficking and enters receiving cells through a membrane transporter (Okamoto et al., 2018; Yamanaka et al., 2015). The timing of ecdysone synthesis/release in the PG is controlled by prothoracicotropic hormone (PTTH), insulin, MAPK, Activin, NO, and TOR signaling (Yamanaka et al., 2013). The circadian clock in the PG is also required for ecdysone production (Di Cara et al., 2016). However, since PG undergoes apoptosis during metamorphosis,

how ecdysone release is regulated during metamorphosis (the time when most circuits assembly occurs) is unclear (Dai and Gilbert, 1991).

After converting to the active form of ecdysone (20-hydroxyecdysone), the hormone binds to its receptor (ecdysone receptor (EcR), which often needs to form a heterodimer with ultraspiracle (USP) to bind to DNA. It then induces a series of gene expression cascade (Yamanaka et al., 2013). This cascade includes several key TFs, such as Hr3 and Ftz-f1, so that they can further activate/repress gene expression to regulate development (Gospocic et al., 2021; King-Jones et al., 2005). The genetic interactions among these TFs established their temporal relationships. For instance, Eip75 inhibits the activity of Hr3 so that only as Eip75 levels fall as Ecdysone decreases, is Hr3 induced leading to upregulation of Ftz-f1 transcription (Carney et al., 1997). Ftz-f1 can also be repressed by Blimp-1 when the ecdysone level is high (Agawa et al., 2007). The sequential order of these TF determines when their target genes are expressed. The targets of ecdysone signaling can differ between cell types (Shlyueva et al., 2014; Stoiber et al., 2016).

Ecdysone signaling regulates proliferation and gene expression in neuroblasts. Ecdysone signaling and the Mediator change the energy metabolism in neuroblasts and terminate proliferation and start differentiation (Homem et al., 2014). As discussed in the previous section, sequential expression of temporal TF in neuroblast can specify cell fate. During larval development, neuroblasts undergo an early to late gene expression transition. This transition is regulated by ecdysone signaling and larval brains can generate diverse types of neurons (Syed et al., 2017). These data show that ecdysone signaling plays an important role in controlling the number and type of neurons in Drosophila brain.

In addition to neuroblast, ecdysone signaling can also affect development of post-mitotic neurons. Mushroom body γ neurons prune their larval specific branches during early metamorphosis and grow adult-specific branches (Yaniv and Schuldiner, 2016). Disruption of ecdysone signaling leads to defect in their pruning and regrowth (Lee et al., 2000). Alyagor et al. performed RNA sequencing on developing g neurons with genetic perturbations that disrupt key TFs in ecdysone signaling (Alyagor et al., 2018). They revealed that the complex regulatory networks triggered by ecdysone signaling regulate the dynamics of neural remodeling. A recent study in Harpegnathos saltator (ants) showed that the transition between ecdysone and juvenile hormone can shift caste-specific behavior in adult through regulating the repressor function of TF Kr-h1 (Gospocic et al., 2021).

*Thyroid hormone signaling in mammals*

Thyroid hormones ($T_3$ and $T_4$) are important for development of mammalian brains. Similar with ecdysone signaling in Drosophila, thyroid hormones also affect a wide range of developmental processes, including neural migration, differentiation, synapse formation, and myelination (Bernal, 2007). Thyroid hormones act on their receptors, thyroid hormone receptors (TRs) to regulate gene expression patterns (Giannocco et al., 2020). Gene regulation exhibits temporal and regional specificity, because of the restricted expression of TFs (Bradley et al., 1992). Disruption of TRs induces morphological changes in hippocampus and behavior changes in rodents (Guadaño-Ferraz et al., 2003). Reduction of maternal thyroid hormone also causes brain development defects (Stenzel and Huttner, 2013).

In addition to the hormonal control discussed above, there are other examples of molecular or cellular mechanisms regulating timing during neuronal differentiation. For instance, glial cells can define the critical period, in which neural circuits can be modified by activity. The Drosophila motor circuits can be changed by activity before 8h after larval hatching (ALH) and this length of critical period is defined by astrocytes through Nrx-1 and Nlg interaction (Ackerman et al., 2021). In mouse visual cortex, astrocytes also control critical-period closure (Ribot et al., 2021). The temporal mechanisms discussed above suggest that the timing of neuronal development can be regulated on a global scale or through local interactions. It is important to understand how timing is regulated during neural development and how it integrates with spatial cues to achieve specific connections.

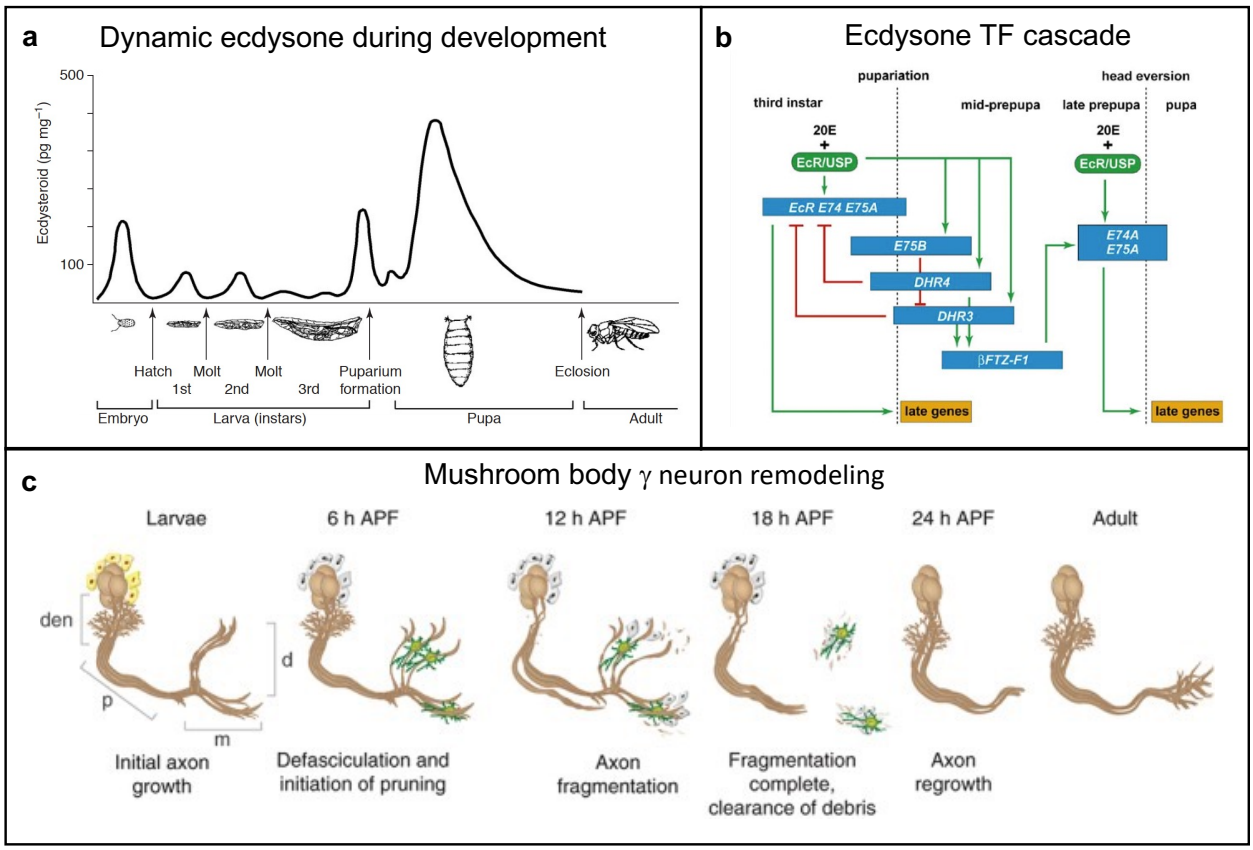

**Figure 1-3. Ecdysone signaling controls timing of neural development.**

(a) Dynamic ecdysone development. Ecdysone pulses are important temporal signals in Drosophila. The biggest pulse of ecdysone occurs during metamorphosis when the majority of CNS is developed (Thummel, 2001). (b) Ecdysone TF cascade. Ecdysone bind to its receptor EcR and then triggered the expression of a series TFs (King-Jones et al., 2005). (c) Mushroom body γ neuron remodeling. This drastic change of neurons require ecdysone signaling (Yaniv and Schuldiner, 2016).

**High-throughput transcriptomic analysis in developing neurons**

*Single cell RNA-seq (scRNA-seq)*

Bulk RNA-seq has been widely used to study gene expression patterns, but it only shows average expression of thousands of cells. Developing neurons have diverse transcriptional profile across cell types, so cell-type purification methods such as Fluorescence-Activated Cell Sorting (FACS) or microdissection are required prior to bulk RNA-seq. Many types of neurons in different species cannot be analyzed due to the lack of purification methods. Additionally, it is inevitable that other cells contaminate sample preparation.

Single cell RNA-seq (scRNA-seq) technology has revolutionized transcriptomic analysis because of its single cell resolution, which allows us to distinguish diverse cell types and to remove contaminated cells for downstream analysis (Macosko et al., 2015; Zheng et al., 2017). Currently, the commonly used scRNA-seq method is a droplet-based method that individual cells are captured in droplets using a microfluidic device and followed by reverse transcription reaction and library preparation. In each droplet, there is also a barcoded gel bead that gives a unique barcode for each cell and a unique molecular identifier (UMI) for each mRNA transcript (Macosko et al., 2015). After sequencing, we can use bioinformatic tools to identify individual cells and count the number of UMIs for each gene to assess the gene expression level in each cell. This method has been applied to various species in diverse types of tissues, including brain tissue (Chen et al., 2019; Simon and Konstantinides, 2021). Recently developed bioinformatic algorithms allow us to cluster cells into different groups based on their transcriptomic profile so distinct types of neurons can be processed in parallel (Butler et al., 2018; Cao et al., 2019). Compared to bulk RNA-seq, scRNA-seq significantly reduces the time and cost for sample preparation.

Although scRNA-seq has transformed transcriptional profiling, it still has its limitations. First, there are more variation across individual cells in scRNA-seq compared to samples in bulk RNA-seq. The noise of scRNA-seq data creates challenges in data analysis especially for developing tissues where heterogeneity is prevalent across cell types and time points (Kiselev et al., 2019). Second, doublet or multiplets could appear when two or more cells accidentally get in one droplet during library preparation. For a targeted 10,000 recovered cell in scRNA-seq, 7.6% of "cells" might be multiplets (https://kb.10xgenomics.com/hc/en-us/articles/360001378811-What-is-the-maximum-number-of-cells-that-can-be-profiled-).

*Multiplexing samples using natural genetic variations*

scRNA-seq enables massive profiling of single-cell transcriptome in parallel, but technical batch effects during sample preparations make it challenging to compare gene expression levels across samples. One solution is to perform more technical replicates, but the cost increases accordingly.

Kang et al. provides another solution, which is using natural genetic variation to determine sample identity if samples are from different individuals (Kang et al., 2018). The computational method Kang et al. developed allows us to pool samples from different individuals together during library preparation to minimize batch effects and then assign the source of each cell *in silico*. In adaptation of this approach, Kurmangaliyev et al. used natural genetic variation in wild-type strains from the Drosophila Genetic Reference Panel (DGRP) to label neurons at different developmental stages (Kurmangaliyev et al., 2020). Developing neurons in Drosophila visual system at 12-hour interval were transcriptionally profiled. This dataset provides a great atlas of developing neurons to analyze dynamic gene expression across cell types.

There are three advantages of multiplexing samples in scRNA-seq. First, batch effects will not affect differentially expressed gene analyses, since samples from different time points or conditions are prepared in a pooled fashion. Second, it helps to remove doublets or multiplets generated from scRNA-seq for downstream analysis. Multiplets could significantly affect average gene expression level, especially for cell types that have low number of cells. Third, it reduces cost by including many different conditions in one reaction so that we can perform RNAi or CRISPR screen using scRNA-seq. Multiplexing samples using natural genetic variation helps to make up for some of the shortcomings of scRNA-seq.

Overall, high-throughput transcriptomic analysis provides great opportunities to study the molecular mechanisms of neural circuit formation. Many datasets of wild type developing neurons were generated using either bulk RNA-seq or scRNA-seq (Alyagor et al., 2018; Cheng et al., 2021; Kurmangaliyev et al., 2020; Özel et al., 2020; Simon and Konstantinides, 2021; Yao et al., 2021). However, to understand the mechanisms underlying circuit formation, we need to improve our knowledge of the gene regulatory networks in distinct neurons during development. ScRNA-seq allows us to combine loss of function/gain of function analysis with transcriptional profiling and to process many samples in parallel. Additionally, single cell ATAC-seq (scATAC-seq) also provides useful information of accessible chromatin regions in different neurons (Janssens et al., 2021).

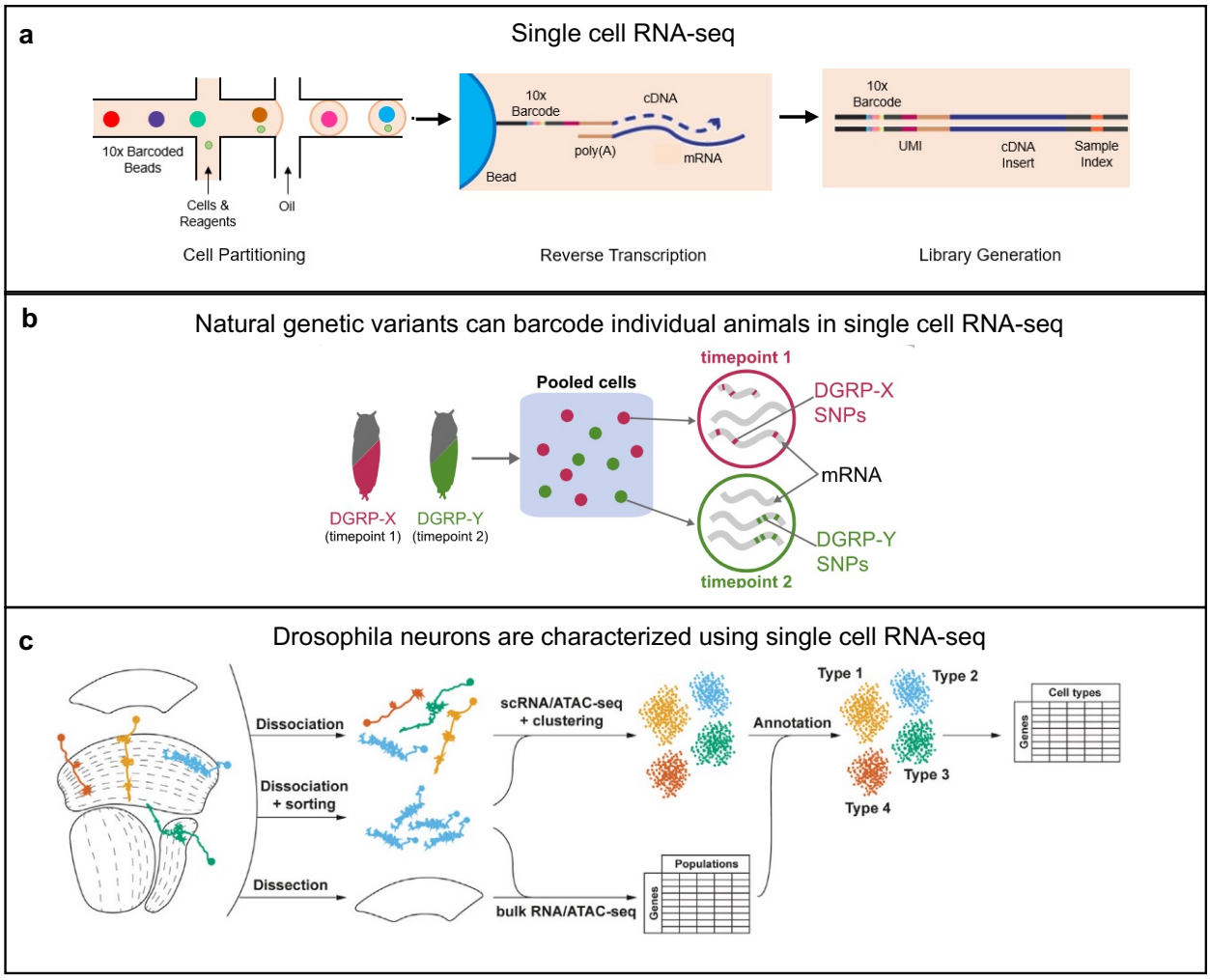


**Figure 1-4. scRNA-seq enables high-throughput transcriptomic profiling in developing neurons.**

(a) Schematic of droplet-based scRNA-seq. (https://web.genewiz.com/single-cell-faq) (b) Natural genetic variants like SNPs are used as barcodes to distinguish individual animals in scRNA-seq (Kurmangaliyev et al., 2020). (c) Developing Drosophila visual system neurons has been carefully characterized using bulk RNA-seq, scRNA-seq and scATAC-seq (Simon and Konstantinides, 2021). These data provide great references to study the molecular mechanism of wiring specificity.

**References**

Ackerman, S.D., Perez-Catalan, N.A., Freeman, M.R., and Doe, C.Q. (2021). Astrocytes close a motor circuit critical period. Nature 592, 414–420.

Agawa, Y., Sarhan, M., Kageyama, Y., Akagi, K., Takai, M., Hashiyama, K., Wada, T., Handa, H., Iwamatsu, A., Hirose, S., et al. (2007). Drosophila Blimp-1 Is a Transient Transcriptional Repressor That Controls Timing of the Ecdysone-Induced Developmental Pathway ▿ . Mol Cell Biol 27, 8739–8747.

Akin, O., and Zipursky, S.L. (2016). Frazzled promotes growth cone attachment at the source of a Netrin gradient in the Drosophila visual system. ELife Sciences 5, e20762.

Akin, O., and Zipursky, S.L. (2020). Activity regulates brain development in the fly. Curr Opin Genet Dev 65, 8–13.

Akin, O., Bajar, B.T., Keles, M.F., Frye, M.A., and Zipursky, S.L. (2019). Cell-type-Specific Patterned Stimulus-Independent Neuronal Activity in the Drosophila Visual System during Synapse Formation. Neuron 101, 894-904.e5.

Alyagor, I., Berkun, V., Keren-Shaul, H., Marmor-Kollet, N., David, E., Mayseless, O., Issman-Zecharya, N., Amit, I., and Schuldiner, O. (2018). Combining Developmental and Perturbation-Seq Uncovers Transcriptional Modules Orchestrating Neuronal Remodeling. Developmental Cell 47, 38-52.e6.

Bernal, J. (2007). Thyroid hormone receptors in brain development and function. Nat Clin Pract Endoc 3, 249–259.

Bradley, D., Towle, H., and Young, W. (1992). Spatial and temporal expression of alpha- and beta-thyroid hormone receptor mRNAs, including the beta 2-subtype, in the developing mammalian nervous system. J Neurosci 12, 2288–2302.

Butler, A., Hoffman, P., Smibert, P., Papalexi, E., and Satija, R. (2018). Integrating single-cell transcriptomic data across different conditions, technologies, and species. Nat Biotechnol 36, 411–420.

Cadwell, C.R., Bhaduri, A., Mostajo-Radji, M.A., Keefe, M.G., and Nowakowski, T.J. (2019). Development and Arealization of the Cerebral Cortex. Neuron 103, 980–1004.

Cao, J., Spielmann, M., Qiu, X., Huang, X., Ibrahim, D.M., Hill, A.J., Zhang, F., Mundlos, S., Christiansen, L., Steemers, F.J., et al. (2019). The single-cell transcriptional landscape of mammalian organogenesis. Nature 566, 1.

Carney, G.E., Wade, A.A., Sapra, R., Goldstein, E.S., and Bender, M. (1997). DHR3, an ecdysone-inducible early-late gene encoding a Drosophila nuclear receptor, is required for embryogenesis. Proc National Acad Sci 94, 12024–12029.

Chen, G., Ning, B., and Shi, T. (2019). Single-Cell RNA-Seq Technologies and Related Computational Data Analysis. Frontiers Genetics 10, 317.

Cheng, S., Butrus, S., Xu, V., Sagireddy, S., Tan, L., Shekhar, K., and Zipursky, S.L. (2021). Vision is Required for Cell Type Specification in the Visual Cortex. Biorxiv 2021.08.10.455824.

Clark, B.S., Stein-O'Brien, G.L., Shiau, F., Cannon, G.H., Davis-Marcisak, E., Sherman, T., Santiago, C.P., Hoang, T.V., Rajaii, F., James-Esposito, R.E., et al. (2019). Single-Cell RNA-Seq

Analysis of Retinal Development Identifies NFI Factors as Regulating Mitotic Exit and Late-Born Cell Specification. Neuron 102, 1111-1126.e5.

Cosmanescu, F., Katsamba, P.S., Sergeeva, A.P., Ahlsen, G., Patel, S.D., Brewer, J.J., Tan, L., Xu, S., Xiao, Q., Nagarkar-Jaiswal, S., et al. (2018). Neuron-Subtype-Specific Expression, Interaction Affinities, and Specificity Determinants of DIP/Dpr Cell Recognition Proteins. Neuron 100, 1385-1400.e6.

Dai, J., and Gilbert, L.I. (1991). Metamorphosis of the corpus allatum and degeneration of the prothoracic glands during the larval-pupal-adult transformation of Drosophila melanogaster: A cytophysiological analysis of the ring gland. Dev Biol 144, 309–326.

Deguchi, Y., Donato, F., Galimberti, I., Cabuy, E., and Caroni, P. (2011). Temporally matched subpopulations of selectively interconnected principal neurons in the hippocampus. Nat Neurosci 14, 495–504.

DeWeerdt, S. (2019). How to map the brain. Nature 571, S6–S8.

Di Cara, King-Jones, Francesca;, and Kirst (2016). The Circadian Clock Is a Key Driver of Steroid Hormone Production in Drosophila. Current Biology 26, 2469–2477.

Elliott, J., Jolicoeur, C., Ramamurthy, V., and Cayouette, M. (2008). Ikaros Confers Early Temporal Competence to Mouse Retinal Progenitor Cells. Neuron 60, 26–39.

Erclik, T., Li, X., Courgeon, M., Bertet, C., Chen, Z., Baumert, R., Ng, J., Koo, C., Arain, U., Behnia, R., et al. (2017). Integration of temporal and spatial patterning generates neural diversity. Nature 541, 365.

Furusawa, K., and Emoto, K. (2021). Scrap and Build for Functional Neural Circuits: Spatiotemporal Regulation of Dendrite Degeneration and Regeneration in Neural Development and Disease. Front Cell Neurosci 14, 613320.

Giannocco, G., Kizys, M.M.L., Maciel, R.M., and Souza, J.S. de (2020). Thyroid hormone, gene expression, and Central Nervous System: Where we are. Semin Cell Dev Biol 114, 47–56.

Gospocic, J., Glastad, K.M., Sheng, L., Shields, E.J., Berger, S.L., and Bonasio, R. (2021). Kr-h1 maintains distinct caste-specific neurotranscriptomes in response to socially regulated hormones. Cell.

Guadaño-Ferraz, A., Benavides-Piccione, R., Venero, C., Lancha, C., Vennström, B., Sandi, C., DeFelipe, J., and Bernal, J. (2003). Lack of thyroid hormone receptor α1 is associated with selective alterations in behavior and hippocampal circuits. Mol Psychiatr 8, 30–38.

Hassan, B.A., and Hiesinger, P.R. (2015). Beyond Molecular Codes: Simple Rules to Wire Complex Brains. Cell 163, 285–291.

Hattori, D., Demir, E., Kim, H.W., Viragh, E., Zipursky, S.L., and Dickson, B.J. (2007). Dscam diversity is essential for neuronal wiring and self-recognition. Nature 449, 223–227.

Hattori, D., Chen, Y., Matthews, B.J., Salwinski, L., Sabatti, C., Grueber, W.B., and Zipursky, S.L. (2009). Robust discrimination between self and non-self neurites requires thousands of Dscam1 isoforms. Nature 461, 644–648.

Homem, C.C.F., Steinmann, V., Burkard, T.R., Jais, A., Esterbauer, H., and Knoblich, J.A. (2014). Ecdysone and mediator change energy metabolism to terminate proliferation in Drosophila neural stem cells. Cell 158, 874–888.

Honig, B., and Shapiro, L. (2020). Adhesion Protein Structure, Molecular Affinities, and Principles of Cell-Cell Recognition. Cell 181, 520–535.

Hulse, B.K., Haberkern, H., Franconville, R., Turner-Evans, D.B., Takemura, S., Wolff, T., Noorman, M., Dreher, M., Dan, C., Parekh, R., et al. (2021). A connectome of the Drosophila central complex reveals network motifs suitable for flexible navigation and context-dependent action selection. Elife 10, e66039.

Imamura, F., Ayoub, A.E., Rakic, P., and Greer, C.A. (2011). Timing of neurogenesis is a determinant of olfactory circuitry. Nat Neurosci 14, 331–337.

Isshiki, T., Pearson, B., Holbrook, S., and Doe, C.Q. (2001). Drosophila Neuroblasts Sequentially Express Transcription Factors which Specify the Temporal Identity of Their Neuronal Progeny. Cell 106, 511–521.

Janssens, J., Aibar, S., Taskiran, I.I., Ismail, J.N., Spanier, K.I., Gonzalez-Blas, C.B., Quan, X.J., Papasokrati, D., Hulselmans, G., Makhzami, S., et al. (2021). Decoding gene regulation in the fly brain. BioRxiv.

Kang, H.M., Subramaniam, M., Targ, S., Nguyen, M., Maliskova, L., McCarthy, E., Wan, E., Wong, S., Byrnes, L., Lanata, C.M., et al. (2018). Multiplexed droplet single-cell RNA-sequencing using natural genetic variation. Nat Biotechnol 36, 89–94.

King-Jones, K., Charles, J.-P., Lam, G., and Thummel, C.S. (2005). The Ecdysone-Induced DHR4 Orphan Nuclear Receptor Coordinates Growth and Maturation in Drosophila. Cell 121, 773–784.

Kirkby, L.A., Sack, G.S., Firl, A., and Feller, M.B. (2013). A Role for Correlated Spontaneous Activity in the Assembly of Neural Circuits. Neuron 80, 1129–1144.

Kiselev, V.Y., Andrews, T.S., and Hemberg, M. (2019). Challenges in unsupervised clustering of single-cell RNA-seq data. Nat Rev Genet 20, 273–282.

Kucherenko, M.M., Barth, J., Fiala, A., and Shcherbata, H.R. (2012). Steroid-induced microRNA let-7 acts as a spatio-temporal code for neuronal cell fate in the developing Drosophila brain. The EMBO Journal 31, 4511–4523.

Kurmangaliyev, Y.Z., Yoo, J., Valdes-Aleman, J., Sanfilippo, P., and Zipursky, S.L. (2020). Transcriptional Programs of Circuit Assembly in the Drosophila Visual System. Neuron 108, 1045-1057.e6.

Lee, C.-H., Herman, T., Clandinin, T.R., Lee, R., and Zipursky, S.L. (2001). N-Cadherin Regulates Target Specificity in the Drosophila Visual System. Neuron 30, 437–450.

Lee, T., Marticke, S., Sung, C., Robinow, S., and Luo, L. (2000). Cell-Autonomous Requirement of the USP/EcR-B Ecdysone Receptor for Mushroom Body Neuronal Remodeling in Drosophila. Neuron 28, 807–818.

Li, H., Watson, A., Olechwier, A., Anaya, M., Sorooshyari, S.K., Harnett, D.P., Lee, H.-K. (Peter), Vielmetter, J., Fares, M.A., Garcia, K.C., et al. (2017a). Deconstruction of the beaten Path-

Sidestep interaction network provides insights into neuromuscular system development. Elife 6, e28111.

Li, H., Horns, F., Wu, B., Xie, Q., Li, J., Li, T., Luginbuhl, D.J., Quake, S.R., and Luo, L. (2017b). Classifying Drosophila Olfactory Projection Neuron Subtypes by Single-Cell RNA Sequencing. Cell 171, 1206-1220.e22.

Li, X., Erclik, T., Bertet, C., Chen, Z., Voutev, R., Venkatesh, S., Morante, J., Celik, A., and Desplan, C. (2013). Temporal patterning of Drosophila medulla neuroblasts controls neural fates. Nature 498, 456–462.

Macosko, E.Z., Basu, * Anindita, Satija, R., Nemesh, J., Shekhar, K., Goldman, M., Tirosh, I., Bialas, A.R., Kamitaki, 8 Nolan, Martersteck, 3 Emily M., et al. (2015). Highly Parallel Genome-wide Expression Profiling of Individual Cells Using Nanoliter Droplets. Cell 161, 1202–1214.

McLaughlin, C.N., Brbić, M., Xie, Q., Li, T., Horns, F., Kolluru, S.S., Kebschull, J.M., Vacek, D., Xie, A., Li, J., et al. (2021). Single-cell transcriptomes of developing and adult olfactory receptor neurons in Drosophila. Elife 10, e63856.

Meister, M., Wong, R.O., Baylor, D.A., and Shatz, C.J. (1991). Synchronous bursts of action potentials in ganglion cells of the developing mammalian retina. Science 252, 939–943.

Meng, J.L., Marshall, Z.D., Lobb-Rabe, M., and Heckscher, E.S. (2019). How prolonged expression of Hunchback, a temporal transcription factor, re-wires locomotor circuits. Elife 8, e46089.

Meng, J.L., Wang, Y., Carrillo, R.A., and Heckscher, E.S. (2020). Temporal transcription factors determine circuit membership by permanently altering motor neuron-to-muscle synaptic partnerships. Elife 9, e56898.

Miyares, R.L., and Lee, T. (2019). Temporal control of Drosophila central nervous system development. Current Opinion in Neurobiology 56, 24–32.

Nakazawa, S., Mizuno, H., and Iwasato, T. (2018). Differential dynamics of cortical neuron dendritic trees revealed by long-term in vivo imaging in neonates. Nat Commun 9, 3106.

Nern, Zhu, Aljoscha;, Zipursky, Yan;, and Lawrence, S. (2008). Local N-Cadherin Interactions Mediate Distinct Steps in the Targeting of Lamina Neurons. Neuron 58, 34–41.

Okamoto, N., Viswanatha, R., Bittar, R., Li, Z., Haga-Yamanaka, S., Perrimon, N., and Yamanaka, N. (2018). A Membrane Transporter Is Required for Steroid Hormone Uptake in Drosophila. Developmental Cell 47, 294-305.e7.

Özel, M.N., Langen, M., Hassan, B.A., and Hiesinger, R. (2015). Filopodial dynamics and growth cone stabilization in Drosophila visual circuit development. ELife Sciences 4, e10721.

Özel, M.N., Simon, F., Jafari, S., Holguera, I., Chen, Y.-C., Benhra, N., El-Danaf, R.N., Kapuralin, K., Malin, J.A., Konstantinides, N., et al. (2020). Neuronal diversity and convergence in a visual system developmental atlas. Nature 589, 1–8.

Özkan, E., Carrillo, R.A., Eastman, C.L., Weiszmann, R., Waghray, D., Johnson, K.G., Zinn, K., Celniker, S.E., and Garcia, K.C. (2013). An Extracellular Interactome of Immunoglobulin and LRR Proteins Reveals Receptor-Ligand Networks. Cell 154, 228–239.

Pak, M.D., and Gilbert, L.I. (1987). A Developmental Analysis of Ecdysteroids During the Metamorphosis of Drosophila Melanogaster. J Liq Chromatogr 10, 2591–2611.

Pan, Y., and Monje, M. (2020). Activity Shapes Neural Circuit Form and Function: A Historical Perspective. J Neurosci 40, 944–954.

Penzes, P., Cahill, M.E., Jones, K.A., VanLeeuwen, J.-E., and Woolfrey, K.M. (2011). Dendritic spine pathology in neuropsychiatric disorders. Nat Neurosci 14, 285–293.

Petrovic, M., and Hummel, T. (2008). Temporal identity in axonal target layer recognition. Nature 456, 800–803.

Quan, X.-J., Yuan, L., Tiberi, L., Claeys, A., De Geest, N., Yan, J., van der Kant, R., Xie, W.R., Klisch, T.J., Shymkowitz, J., et al. (2016). Post-translational Control of the Temporal Dynamics of Transcription Factor Activity Regulates Neurogenesis. Cell 164, 460–475.

Redies, C., Hertel, N., and Hübner, C.A. (2012). Cadherins and neuropsychiatric disorders. Brain Res 1470, 130–144.

Ribot, J., Breton, R., Calvo, C.-F., Moulard, J., Ezan, P., Zapata, J., Samama, K., Moreau, M., Bemelmans, A.-P., Sabatet, V., et al. (2021). Astrocytes close the mouse critical period for visual plasticity. Science 373, 77–81.

Salinas, P.C., and Zou, Y. (2008). Wnt Signaling in Neural Circuit Assembly. Annu Rev Neurosci 31, 339–358.

Sanes, J.R., and Zipursky, S.L. (2020). Synaptic Specificity, Recognition Molecules, and Assembly of Neural Circuits. Cell 181, 536–556.

Scheffer, L.K., Xu, C.S., Januszewski, M., Lu, Z., Takemura, S., Hayworth, K.J., Huang, G.B., Shinomiya, K., Maitlin-Shepard, J., Berg, S., et al. (2020). A connectome and analysis of the adult Drosophila central brain. Elife 9, e57443.

Schroeder, A., and Wit, J. de (2018). Leucine-rich repeat-containing synaptic adhesion molecules as organizers of synaptic specificity and diversity. Exp Mol Medicine 50, 10.

Schwabe, T., Borycz, J.A., Meinertzhagen, I.A., and Clandinin, T.R. (2014). Differential Adhesion Determines the Organization of Synaptic Fascicles in the Drosophila Visual System. Curr Biol 24, 1304–1313.

Sengupta, T., Koonce, N.L., Moyle, M.W., Duncan, L.H., Vázquez-Martínez, N., Han, X., Shao, L., Wu, Y., Santella, A., Fan, L., et al. (2020). A neurite-zippering mechanism, mediated by layer-specific expression of IgCAMs, regulates synaptic laminar specificity in the C. elegans nerve ring neuropil. Biorxiv 2020.08.28.271437.

Shlyueva, D., Stelzer, C., Gerlach, D., ˜ez-Cuna, J.O.Y. ´n, Rath, M., Bory, qukasz M., Arnold, C.D., and Stark, A. (2014). Hormone-Responsive Enhancer-Activity Maps Reveal Predictive Motifs, Indirect Repression, and Targeting of Closed Chromatin. Molecular Cell 54, 180–192.

Simon, F., and Konstantinides, N. (2021). Single-cell transcriptomics in the Drosophila visual system: Advances and perspectives on cell identity regulation, connectivity, and neuronal diversity evolution. Developmental Biology 479, 107–122.

Stenzel, D., and Huttner, W.B. (2013). Role of maternal thyroid hormones in the developing neocortex and during human evolution. Front Neuroanat 7, 19.

Stoiber, Celniker, Marcus;, Cherbas, Susan;, Brown, Lucy;, Cherbas, Ben;, and Peter (2016). Diverse Hormone Response Networks in 41 Independent Drosophila Cell Lines. G3 Genes Genomes Genetics 6, 683–694.

Sun, H., and Hobert, O. (2021). Temporal transitions in the post-mitotic nervous system of Caenorhabditis elegans. Nature 1–7.

Syed, M.H., Mark, B., and Doe, C. (2017). Steroid hormone induction of temporal gene expression in Drosophila brain neuroblasts generates neuronal and glial diversity. Elife 6, e26287.

Takemura, S., Xu, C.S., Lu, Z., Rivlin, P.K., Parag, T., Olbris, D.J., Plaza, S., Zhao, T., Katz, W.T., Umayam, L., et al. (2015). Synaptic circuits and their variations within different columns in the visual system of Drosophila. PNAS 112, 13711–13716.

Takeo, Y.H., Kakegawa, W., Miura, E., and Yuzaki, M. (2015). RORβ Regulates Multiple Aspects of Dendrite Development in Cerebellar Purkinje Cells In Vivo. J Neurosci 35, 12518–12534.

Tan, L., Zhang, K.X., Pecot, M.Y., Nagarkar-Jaiswal, S., Lee, P.-T., Takemura, S., McEwen, J.M., Nern, A., Xu, S., Tadros, W., et al. (2015). Ig Superfamily Ligand and Receptor Pairs Expressed in Synaptic Partners in Drosophila. Cell 163, 1756–1769.

Thummel (2001). Molecular Mechanisms of Developmental Timing in C. elegans and Drosophila. Developmental Cell 1, 453–465.

Ting, McQueen, Chun-Yuan;, Pandya, Philip G.;, Lin, Nishith;, Yang, Tzu-Yang;, Reddy, Meiluen;, O'Connor, O. Venkateswara;, McAuliffe, Michael B.;, Lee, Matthew;, and Chi-Hon (2014). Photoreceptor-Derived Activin Promotes Dendritic Termination and Restricts the Receptive Fields of First-Order Interneurons in Drosophila. Neuron 81, 830–846.

Truman, J.W. (2019). The Evolution of Insect Metamorphosis. Curr Biol 29, R1252–R1268.

Witvliet, D., Mulcahy, B., Mitchell, J.K., Meirovitch, Y., Berger, D.R., Wu, Y., Liu, Y., Koh, W.X., Parvathala, R., Holmyard, D., et al. (2021). Connectomes across development reveal principles of brain maturation. Nature 596, 257–261.

Wojtowicz, W.M., Vielmetter, J., Fernandes, R.A., Siepe, D.H., Eastman, C.L., Chisholm, G.B., Cox, S., Klock, H., Anderson, P.W., Rue, S.M., et al. (2020). A Human IgSF Cell-Surface Interactome Reveals a Complex Network of Protein-Protein Interactions. Cell 182, 1027-1043.e17.

Xie, Q., Brbic, M., Horns, F., Kolluru, S.S., Jones, R.C., Li, J., Reddy, A.R., Xie, A., Kohani, S., Li, Z., et al. (2021). Temporal evolution of single-cell transcriptomes of Drosophila olfactory projection neurons. Elife 10, e63450.

Yamanaka, N., Rewitz, K.F., and O'Connor, M.B. (2013). Ecdysone Control of Developmental Transitions: Lessons from Drosophila Research. Annu Rev Entomol 58, 497–516.

Yamanaka, N., Marqués, G., and O'Connor, M.B. (2015). Vesicle-Mediated Steroid Hormone Secretion in Drosophila melanogaster. Cell 163, 907–919.

Yaniv, S.P., and Schuldiner, O. (2016). A fly's view of neuronal remodeling. Wiley Interdiscip Rev Dev Biol 5, 618–635.

Yao, Z., Velthoven, C.T.J. van, Nguyen, T.N., Goldy, J., Sedeno-Cortes, A.E., Baftizadeh, F., Bertagnolli, D., Casper, T., Chiang, M., Crichton, K., et al. (2021). A taxonomy of transcriptomic cell types across the isocortex and hippocampal formation. Cell 184, 3222-3241.e26.

Yogev, S., and Shen, K. (2014). Cellular and Molecular Mechanisms of Synaptic Specificity. Annu Rev Cell Dev Bi 30, 417–437.

Zheng, G.X.Y., Terry, J.M., Belgrader, P., Ryvkin, P., Bent, Z.W., Wilson, R., Ziraldo, S.B., Wheeler, T.D., McDermott, G.P., Zhu, J., et al. (2017). Massively parallel digital transcriptional profiling of single cells. Nat Commun 8, 14049.

Zhu, F., Cizeron, M., Qiu, Z., Benavides-Piccione, R., Kopanitsa, M.V., Skene, N.G., Koniaris, B., DeFelipe, J., Fransén, E., Komiyama, N.H., et al. (2018). Architecture of the Mouse Brain Synaptome. Neuron 99, 781-799.e10.

# Chapter 2 A global timing mechanism regulates cell-type specific wiring programs

This chapter is adapted from the following publication with minor changes.

Jain, S.*, Lin, Y.*, Kurmangaliyev, Y.Z., Valdes-Aleman, J., LoCascio, S.A., Mirshahidi, P., Parrington, B., and Zipursky, S.L. (2020). A global timing mechanism regulates cell-type specific wiring programs. bioRxiv 2020.09.18.304410. (Under revision at *Nature*)

**Abstract**

The assembly of neural circuits is dependent upon precise spatiotemporal expression of cell recognition molecules[1–6]. Factors controlling cell-type specificity have been identified[7–9], but how timing is determined remains unknown. Here we describe the induction of a cascade of transcription factors by a steroid hormone (Ecdysone) in all fly visual system neurons spanning target recognition and synaptogenesis. We demonstrate through single cell sequencing that the Ecdysone pathway regulates the expression of a common set of targets required for synaptic maturation and cell-type specific targets enriched for cell surface proteins regulating wiring specificity. Transcription factors in the cascade regulate the expression of the same wiring genes in complex ways, including activation in one cell-type and repression in another. We show that disruption of the Ecdysone-pathway generates specific defects in dendritic and axonal processes and synaptic connectivity, with the order of transcription factor expression correlating with sequential steps in wiring. We also identify shared targets of a cell-type specific transcription factor and the Ecdysone pathway which regulate specificity. We propose neurons integrate a global temporal transcriptional module with cell-type specific transcription factors to generate different cell-type specific patterns of cell recognition molecules regulating wiring.

## Introduction

Animal behavior is dependent upon the formation of neural circuits with high fidelity. Many cell-surface proteins, particularly of the Immunoglobulin (Ig), Leucine-Rich Repeat and Cadherin families, promote interactions between neurons during circuit assembly[1,2]. How does a limited set of cell-surface protein coding genes (~$10^3$ genes in fruit fly[10]) specify a much larger number of synapses (~$10^7$ synapses amongst ~$10^5$ neurons in fly brain[11])? This is made possible by the use of several developmental strategies including the reuse of the same molecules to determine multiple, spatially and temporally separated neuron-neuron interactions[3,4,6,12]. Wiring specificity, thus, relies on genetic programs which regulate the cell-type and temporal specificity of genes encoding recognition molecules. Many programs that define cell-type specificity have been described[7–9]. Here we set out to discover how temporal specificity is determined.

## Results

### Dynamic expression of wiring genes

We defined metrics for cell-type specificity and temporal dynamics for each gene using our previously reported transcriptomic dataset of 97 neuron-types in the fly visual system across seven developmental time points (24 – 96 hours after pupal formation (hAPF))[12] (Fig. 1a). This period encompasses dendritic and axon terminal morphogenesis within target regions, selection of appropriate synaptic partners and synaptogenesis. We assigned two scores to each gene: 1) Cell-type variability score, which provides a measure of cell-type specificity; and 2) Temporal dynamicity score, which provides a measure of changes in expression across developmental time (see methods, Fig. 1a, Extended data Table 2).

"Housekeeping" genes, such as ribosomal protein coding genes (e.g. RpL36), generally have low scores on both scales, suggesting low variation in expression across cell-types and time. Many transcription factors (TFs) display high cell-type variability but low dynamicity scores (e.g. erm), consistent with their role in establishing and maintaining neuron types[6,12,13]. A previously identified set of genes representing a pan-neuronal program demonstrate low variability scores and a range of dynamicity scores (e.g. RNA-binding protein, Rbp9)[12]. Finally, we compiled a list of cell surface molecules (CSMs) with previously described roles in wiring (and paralogs thereof), into a group we hereafter refer to as 'wiring genes' (see methods, Extended data Table 3), and found that they have high cell-type variability and temporal dynamicity scores (e.g. dpr11). Dynamic, cell-type specific expression is consistent with previous reports for expression patterns for these genes[5,6,12]. While cell-type specific TFs have been identified which control wiring genes, what controls their temporal specificity remains unknown.

**A cascade of nuclear receptors is expressed in visual system neurons**

To identify candidates for temporal regulators, we focused on TFs with high dynamicity scores (Fig. 1a, Extended data Table 2). These were enriched for nuclear receptors (GO term: "nuclear receptor activity", p-value 9.3 X $10^{-5}$; Reactome pathway analysis: "Nuclear Receptor transcription pathway" p-value 8.3 X $10^{-10}$; also see Extended data Table 4). Nuclear receptor TFs (such as Hr3, Hr4 and ftz-f1) which exhibit high temporal dynamicity (Fig. 1a), are components of a cascade of TFs activated by the steroid hormone Ecdysone (Fig. 1b). Indeed, the Ecdysone Receptor (EcR) itself, as well as other TFs in this cascade are expressed in a synchronous way in all neurons in the developing visual system (at the mRNA and protein level, Fig. 1b, c, Extended data Fig. 1). This includes a synchronous change in isoform from EcR-B1 to EcR-A[14]. The timing and order of expression of these TFs correlates with a mid-pupal pulse of Ecdysone[15–19] (Fig. 1b).

Consistent with control of dynamic gene expression, ATAC-Seq[20] at 40hAPF, 60hAPF and 72hAPF in L1 neurons (see Methods) identified an enrichment for predicted binding sites for EcR, Hr3 and Ftz-f1 in regions with dynamic patterns of chromatin accessibility[21] (Extended data Fig. 2, Supplementary Table 5). Although these TFs are expressed in all neurons (Fig. 1b , c), they are known in other contexts to regulate a cell-type specific set of genes[22]. These observations raised the possibility that the Ecdysone-pathway has been co-opted as a temporal regulator to control the dynamic and cell-type specific expression of wiring genes.

**EcR controls neurite terminal morphology and synapse distribution**

To test the role of the Ecdysone-pathway in wiring, we sought tools available for disrupting the pathway. Given the proximity of the EcR gene to the centromere and the lethality of whole animal mutants, phenotypic analysis using null-mutants is difficult to perform across cell-types (see mosaic analysis with EcR mutants in L5 below). We thus, began by expressing a widely used dominant-negative allele of EcR (mutant with ligand binding defect[23], EcR-B1$^{W650A}$, EcR$^{DN}$) in a range of neuron-types arborizing in different neuropils and layers using the GAL4-UAS system (Fig. 2a, Extended data Fig. 3). Targeted expression of EcR$^{DN}$ led to profound defects in axonal and/ or dendritic branching across all neuron-types tested, namely lamina neurons (L1-L5), T4/T5, Mi4 and Dm4 (Fig. 2, Extended data Fig. 3). EcR$^{DN}$-induced defects in L1-L5 arborization were also seen with EcR-RNAi and could be largely rescued by overexpression of EcR-B1 from a cDNA transgene (Extended data Fig. 3a).

We also observed that expression of EcR$^{DN}$ in lamina neurons led to a redistribution of their presynaptic sites in the lamina neuropil from strictly proximal to more distal regions of the lamina (Fig. 2e). DIP-β mutants have been shown to produce a similar phenotype[24], and via scRNA-Seq

experiments described below, we identified DIP-β as a target of EcR in L4 neurons (Extended data Fig. 4a, b). That DIP-β is directly regulated by EcR, is consistent with the presence of a strong EcR binding site within the first intron of DIP-β (see methods, Extended data Fig. 4c). Thus, EcR controls dendritic and axonal terminal morphology and presynaptic site distribution across cell-types in the lamina, medulla and lobula plate.

**Different EcR pathway genes regulate specific steps in L5 wiring**

We next sought to investigate roles for the EcR-pathway at different steps in wiring of a single neuron-type (Fig. 2f). L5 axon terminals target to M5 during early pupal development[25,26], then arborize in M1 (between 48hAPF and 60hAPF), followed by extension of these arbors from M1 to M2 (between 75hAPF and 90hAPF) (Fig. 2f).

Targeted expression of $EcR^{DN}$ in developing L5 neurons did not disrupt targeting to the M5 layer, which is completed prior to the mid-pupal Ecdysone pulse. However, it led to a complete lack of branches in M1/M2 (Fig. 2g, Extended data Fig. 5a). To verify the role of EcR in establishing M1/M2 arbors, we generated a conditional null-allele for EcR using the FlpStop technology[27] ($EcR^{FlpStop}$, see methods, Extended data Fig. 5b). Similar to $EcR^{DN}$, we saw loss of M1/M2 arbors in: 1) $EcR^{FlpStop}$ over a frameshift mutation in the ligand binding domain ($EcR^{FlpStop/M554fs}$); 2) Heterozygous L5 neurons ($EcR^{FlpStop/+}$ or $EcR^{M554fs/+}$); and 3) knock-down of EcR via RNAi. EcR mutants were phenocopied by a homozygous hypomorphic allele of usp ($usp^{R160H}$). This gene encodes a cofactor which functions with EcR in different developmental contexts[28,29] (Fig. 2g). By contrast its role in promoting branching in M1/M2 medulla layers, EcR suppresses L5 branching in the lamina (Fig. 2h). Wildtype L5 neurons (unlike L1-L4 neurons) do

not elaborate branches in the medulla[30]. However, in response to either EcR RNAi or $EcR^{DN}$, robust ectopic branching (similar to L1-L3) was observed in the lamina.

While disruption of EcR activity blocks step 1 and step 2, knock-down of TFs downstream of EcR - Hr3 or ftz-f1, selectively disrupt step 2 (Fig. 2g, Extended data Fig. 5a). These findings are consistent with EcR regulating the expression of genes that promote extension of arbors into M1 and that Hr3 and Ftz-f1 execute a distinct developmental step ~ 24 hours later (Fig. 2g), promoting extension of arbors from M1 into M2. As Hr3 directly regulates ftz-f1[16] (Fig. 1b, see Extended data Fig. 10), Ftz-f1 may act alone or in combination with Hr3, to regulate the expression of genes required for branching in M2. Loss of Hr4, another TF directly downstream of EcR, results in ectopic branches terminating in M5 (Fig. 2g, Extended data Fig. 5a). By contrast to the medulla, suppression of branching in the lamina relies on Hr3, but not Ftz-f1 (Fig. 2h, i).

To see if the Ecdysone-pathway also affects communication between L5 and its postsynaptic partners, we used an L5-specific Gal4 to express Chrimson with or without $EcR^{DN}$ and recorded $Ca^{2+}$ responses in different postsynaptic cells (using GCaMP6s) upon activation of Chrimson by light. Given the near complete loss of M1 arbors with $EcR^{DN}$ (also see Extended data Fig. 5a), we focused on L5 postsynaptic partners in the M5 layer, Dm13 and Tm3[31]. Optogenetic stimulation of $EcR^{DN}$-expressing L5 neurons led to a stronger response in Dm13 (Fig. 2j), while responses from Tm3 remained unchanged (Extended data Fig. 6a). A postsynaptic neuron-type specific change in GCaMP6s response is consistent with perturbation of L5 synaptic connectivity upon disruption of the Ecdysone-pathway.

In summary, the Ecdysone-pathway sculpts L5 connectivity in multiple ways during development, including affecting branches at different times, in different ways and within distinct subcellular domains (see Summary in Figure 2i).

**The EcR cascade regulates pan-neuronal and cell-type specific genes**

To identify genes regulated by the EcR cascade, we focused on lamina neurons (L1-L5). These were enriched by Fluorescence-activated cell sorting[32] using a pan-lamina marker and profiled using a single-cell RNA-Seq (scRNA-Seq) based approach similar to the one used in Kurmangaliyev et al[12]. Transcriptional profiles of wildtype lamina neurons determined this way were similar to the ones determined from dissociated whole optic lobes[12] (Extended data Fig. 7). We then profiled the transcriptomes of $EcR^{DN}$, EcR RNAi or Hr3 RNAi-expressing lamina neurons and controls by scRNA-Seq at four timepoints (24hAPF, 48hAPF, 72hAPF and Adult, see Extended data Fig. 7a)[12].

By comparing the transcriptomes of wildtype and $EcR^{DN}$-expressing lamina neurons, we identified 872 downregulated and 517 upregulated genes in $EcR^{DN}$-expressing cells (fold change > 2, p-value < 0.05) (Fig. 3a; Extended data Fig. 8). Genes affected by $EcR^{DN}$ are similar to the set of genes affected by EcR RNAi, though the latter is significantly less effective at blocking the Ecdysone pathway in this context (Extended data Fig. 9, 11a, c, e). Hr3 RNAi also has a similar effect on gene expression as $EcR^{DN}$, especially at later time points (Extended data Fig. 10, 11b, d, e) consistent with the genetic relationship between EcR and Hr3 (Fig. 1b). In contrast to L1 and L3-L5, $EcR^{DN}$ had modest effects on gene expression in L2, consistent with lower $EcR^{DN}$ expression in L2 neurons at 48hAPF using the pan-lamina GAL4 driver (Extended data Fig. 8b – d, f). Thus, the EcR pathway regulates hundreds of genes in developing lamina neurons.

Analyses of the targets of the Ecdysone-pathway revealed that this pathway: 1) can both activate and repress gene expression (Fig. 3a, c, d, Extended data Fig.12); 2) does not affect cell-fate (Extended data Fig. 8e, 9e, 10e); and, 3) controls a larger number of genes with cell-type specific, dynamic expression than expected by chance (Fisher's exact test, p-value = 0.005, Fig.

3b). Together, these observations establish that the Ecdysone-pathway controls different sets of genes expressed in specific cell-types in a dynamic fashion. Importantly, we found many dynamic genes to not be affected by EcR mutants, suggesting roles for other temporal regulators as well (Fig. 3a, Extended data Fig. 11c, d, 12d).

Gene ontology analysis revealed that targets of the EcR pathway were enriched for genes required for mitochondrial ATP biogenesis and neurotransmitter loading into synaptic vesicles (see 'proton transport', Fig. 3b, c, Extended data Fig. 13b, Extended data Table 2), processes required for synapse development, function or both[33–36]. Importantly, they have low cell-type variability scores, and are thus likely regulated by the Ecdysone-pathway across neuron-types (Fig. 3b, also see common targets, Fig. 3a).

**Control of cell-type specific wiring genes**

The targets of EcR are also enriched for genes encoding CSMs, including wiring genes (Fig. 3b, c). As opposed to genes required for ATP-synthesis and vacuolar ATPases, CSMs and wiring genes regulated by the Ecdysone-pathway are largely composed of targets with cell-type specific expression (Specific targets, Fig. 3a, b). These genes can be repressed in one cell-type and activated in another (see dpr17 in L1 and L3, Fig. 3d), and can be regulated at different times in different cell types (e.g. dpr10 in L1 and L5). In some cases, bidirectional changes in gene expression resulted from activation by EcR, followed by repression by Hr3, indicative of a form of feedback inhibition (e.g. see dpr10 and dpr15 in L1 and dpr17 in L3, Fig. 3d). Thus, activation and repression by different Ecdysone-pathway TFs control cell-type and temporally specific patterns of gene expression of wiring genes.

To assess if genes encoding CSMs affected by disruption of EcR activity are responsive to hormone, we looked at the expression of some of these genes by controlling availability of Ecdysone in ex vivo preparations. We modified a protocol developed by Özel et al, wherein brains are removed from pupae (at 22hAPF) prior to the mid-pupal Ecdysone pulse, and then incubated in media with or without the active form of Ecdysone, 20 Hydroxyecdysone[37] (20E, Extended data Fig. 14a, see methods). Consistent with scRNA-Seq data, the expression of several targets of EcR depends upon inclusion of ligand in the media (Fig. 3e, Extended data Fig. 14b).

Together, these findings indicate that the Ecdysone-pathway, expressed in a common temporal fashion in all neurons, regulates genes required for proper circuit formation in different cell types in temporally specific ways.

**Erm and EcR co-regulate wiring genes in L3**

We next sought evidence that cell-type specific wiring programs are co-regulated by cell-type specific and EcR pathway TFs. Here, we focused on a conserved TF, Erm (Fezf1/2 in mammals) which is expressed in postmitotic L3, but not other lamina neurons, throughout development, and controls several L3-specific wiring programs[32,38]. Though Erm is expressed in a largely stable fashion throughout development, many of its known targets[38,39] (including wiring genes) show dynamic expression (Fig. 4a). Interestingly, dynamic targets of Erm are significantly enriched for genes affected by $EcR^{DN}$ (one-sided Fisher's exact t-test, p-value = 0.0331) and EcR pathway TFs are expressed sequentially in developing L3 neurons. These observations are consistent with Erm and the Ecdysone-pathway acting together to determine the spatiotemporal expression patterns of wiring genes in L3.

L3 neurons non-cell autonomously control the targeting of R8 neurons to the M3 layer. Netrin, which requires both Erm and EcR for proper dynamic expression in L3[38] (Fig. 3e, Extended data Fig. 16), is required for adhesion to the M3 layer, but not for recognition of the layer as its target. Indeed, in netrin mutants R8s target to the appropriate later but then retract to distal layers of the medulla[40]. While some R8s retract to distal medulla in erm and EcR mutants, most terminate beyond M3[38] (Fig. 4b, d, Extended data Fig. 15b). This is consistent with Erm and EcR acting together to control M3 target layer recognition and subsequent netrin-dependent stabilization. R8 terminals extending into deeper layers also contain ectopic presynaptic sites and show a modest overall decrease in synapse number (Fig. 4c, Extended data Fig. 15a), consistent with defects in R8 synaptic connectivity. We thus speculated that in addition to netrin, other genes coregulated by EcR and Erm (see Extended data Fig. 16) control R8 targeting.

To identify regulators of R8 targeting, we performed an RNAi screen for 12 genes coregulated by EcR and Erm (Fig. 4a, Extended data Fig. 15b, c, Extended data table 7, 8). Of these, RNAi for beat-IIa, CG4822, CG6044 and Tpr2, led to R8 targeting past the M3 layer (Fig. 4d). Beat-IIa and CG6044 are members of the Ig superfamily, a class of genes known to mediate cell recognition[1,2]. Tpr2 regulates the activity of steroid hormone receptors in mammals, and may play an analogous role in regulating EcR-pathway TFs. Indeed, as in mammals where either overexpression or knock-down of Tpr2 results in reduced hormone receptor activity[41,42], Tpr2 overexpression in L3 neurons phenocopies Tpr2 RNAi (Fig. 4d). And finally, CG4822, which belongs to a subfamily of ABC transporters involved in cholesterol and steroid efflux, is also implicated in steroid regulation[43,44].

Together these data indicate that the EcR-pathway and Erm coregulate the spatiotemporal specificity of several genes in L3 required for proper R8 wiring, including genes regulating steroid

abundance or steroid receptor function (CG4822 and Tpr2), genes encoding Ig superfamily proteins (Beat IIa and CG6044) and secreted proteins (NetA and B) required for targeting to and stabilization of R8 growth cones in M3.

**Discussion**

Wiring an animal brain requires precise cell-type and temporally specific expression of cell recognition proteins[3–5,32,45]. The Ecdysone-pathway functions as a temporal regulator of major developmental transitions, including larval molts and metamorphosis, as well as controlling sequential divisions of postembryonic neuroblasts and neuronal re-modelling[15,22,46–48]. Here we demonstrate that the EcR cascade has been co-opted for the temporal regulation of neuron-type specific wiring programs within the developing neuropil. Neuron-type specificity in this case is, at least in part, determined by the activity of cell-type specific TFs. The ability of the EcR cascade to function as a flexible temporal regulatory module may be similar to modules regulating spatial patterning (e.g. Hox genes and BMP/Wnt/Hh pathways[49–51]) which act in context-dependent ways to generate different morphological outcomes in many different developmental contexts.

Global pathways, including other steroid and peptide hormones, waves of stimulus independent neural activity, sensory experience as well as local intercellular interactions contribute to wiring more broadly in controlling temporal aspects of development in the vertebrate and invertebrate CNS (Fig. 4e)[52–57]. As in the EcR pathway in the fly visual system, these temporal signals may also alter the activity of broadly expressed TFs (e.g. via phosphorylation) which combine with cell-type specific TFs to control the expression of cell surface molecules regulating synaptic connectivity.

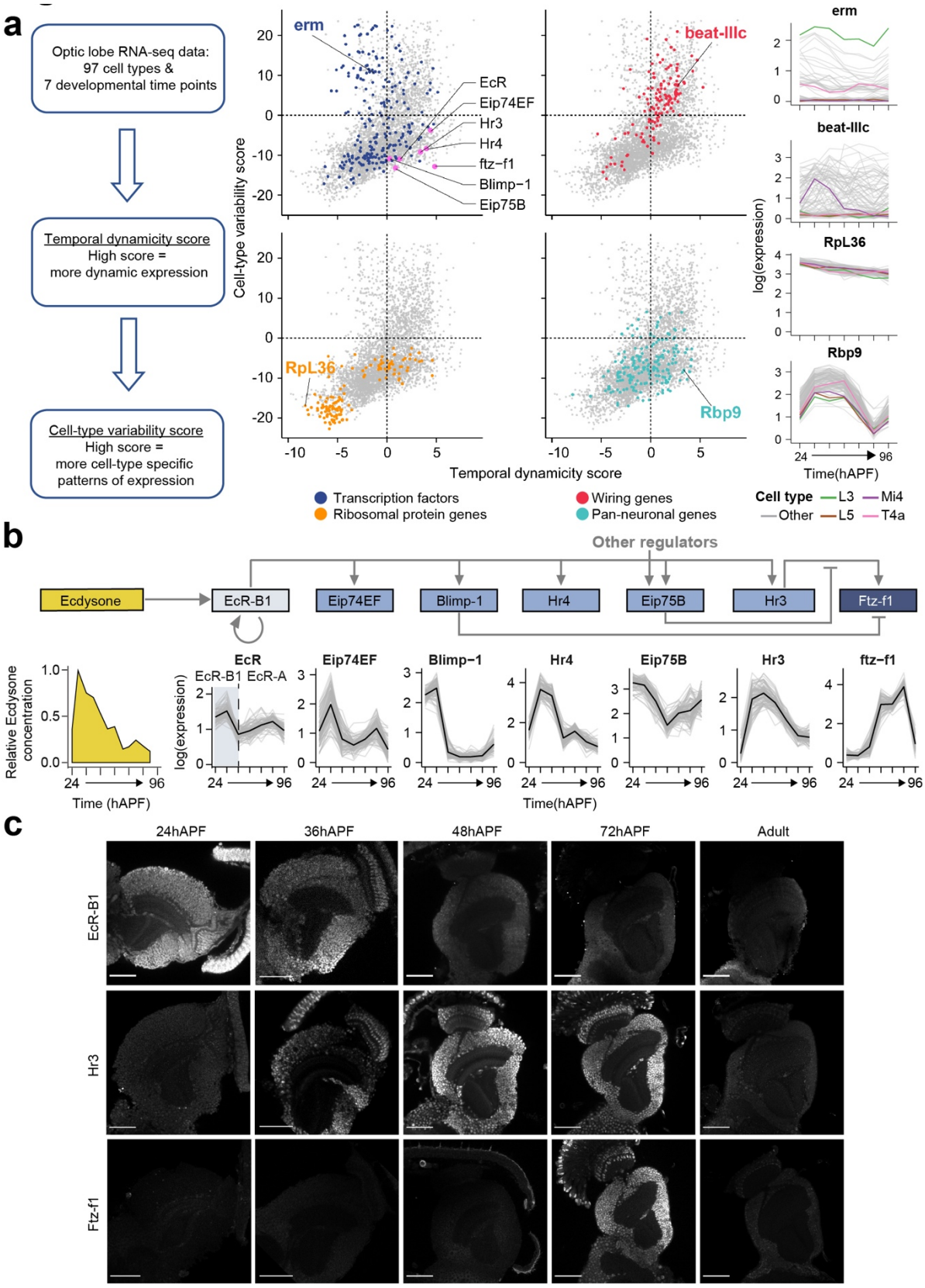
a
Optic lobe RNA-seq data:
97 cell types &
7 developmental time points
Temporal dynamicity score
High score =
more dynamic expression
Cell-type variability score
High score =
more cell-type specific
patterns of expression
erm
beat-IIIc
RpL36
Rbp9
EcR
Eip74EF
Hr3
Hr4
ftz−f1
Blimp−1
Eip75B
Cell-type variability score
Temporal dynamicity score
log(expression)
Time(hAPF)
Transcription factors
Ribosomal protein genes
Wiring genes
Pan-neuronal genes
Cell type
L3
Mi4
Other
L5
T4a
b
Other regulators
Ecdysone
EcR-B1
Eip74EF
Blimp-1
Hr4
Eip75B
Hr3
Ftz-f1
Relative Ecdysone concentration
Time (hAPF)
EcR-B1
EcR-A
c
24hAPF
36hAPF
48hAPF
72hAPF
Adult
EcR-B1
Hr3
Ftz-f1

**Figure 2-1 Dynamic expression of wiring genes and Ecdysone pathway TFs.**

a, Plots showing Cell-type variability and Temporal dynamicity scores calculated using data from Kurmangaliyev et al., 2020[12]. Each plot highlights genes belonging to the indicated gene group. Right, expression of one gene from each group, highlighting expression in L3, L5, Mi4, T4a neuron-types. Transcription factors of the Ecdysone-pathway are highlighted (pink) in top-left plot. b, Ecdysone-pathway showing a subset of known genetic interactions. Relative concentration of Ecdysone over development is shown (adapted from Pak and Gilbert, 1987[19]). Line plots: each grey line is expression in one neuron-type. Black line is mean across all neuron-types. Isoform change from EcR-B1 to EcR-A is highlighted (also see Extended data Fig. 1). All expression plots: time in hours after pupa formation (hAPF). All expression is log expression values from Kurmangaliyev et al. c, Images showing immunostaining for EcR-B1, Hr3 and Ftz-f1 at the indicated time points. Scale bar, 50 μm

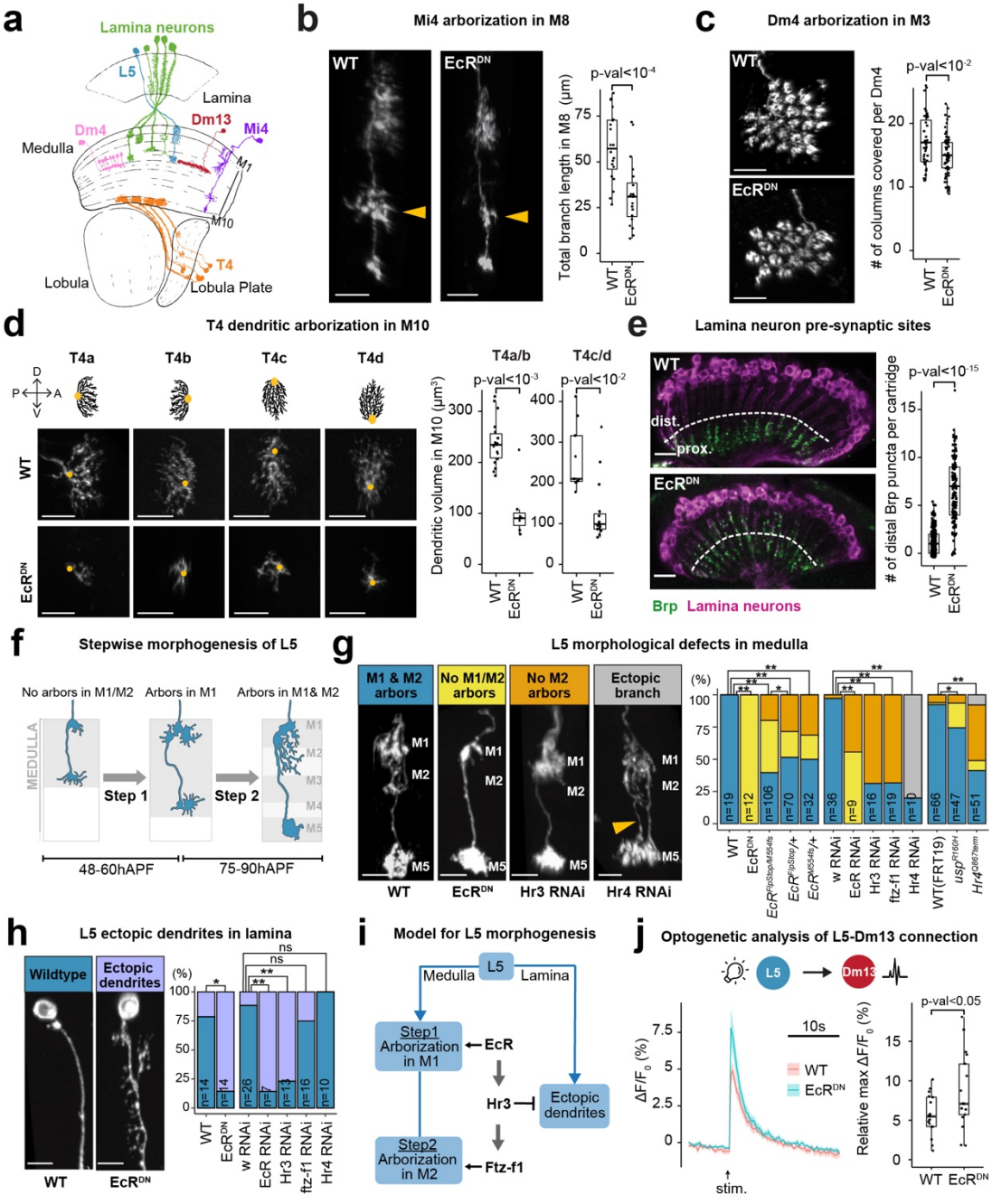


**Figure 2-2. Ecdysone-pathway TFs control multiple aspects of wiring.**

a, Schematic of Lamina (L1-L5), Mi4, Dm4, Dm13 and T4. b, Morphology of Mi4 ± EcR$^{DN}$. Yellow arrowhead: M8 layer. Scale bar, 10μm. Total branch length in M8 is quantified. (WT: 20

neurons, 3 animals. $EcR^{DN}$: 20 neurons, 4 animals). c, Morphology of Dm4 ± $EcR^{DN}$. Total number of columns covered/ neuron is quantified. (WT: 39 neurons, 5 animals. $EcR^{DN}$: 61 neurons, 5 animals). d, Schematic of dendrites of T4 a-d subtypes. Dorsoventral (D, V) and anterior-posterior (A, P) axes are shown. Below, dendrite morphology ± $EcR^{DN}$. Orange dot, dendritic stalk. Scale bar, 10μm. Dendritic volume for T4a, b and T4c, d subtypes is quantified. (WT: 18 T4a/b, 9 T4c/d neurons, 4 animals; $EcR^{DN}$: 7 T4a/b, 15 T4c/d neurons, 5 animals). e, Lamina neuron (magenta) presynaptic sites (Brp, green) in the lamina neuropil ± $EcR^{DN}$. Scale bar, 50μm. Distal Brp puncta/ cartridge is quantified. (WT: 409 cartridges, 7 animals. $EcR^{DN}$: 153 cartridges, 6 animals.) f, Schematic of stepwise morphogenesis of L5 arbors. g, L5 arborization defects and their distributions under the given genotypes (also see Extended data Fig. 5a). h, L5 ectopic dendrite phenotype with quantification under given genotypes. g, i, n = number of neurons (all conditions, animals ≥ 4). g, h, Scale bar, 5μm. i, Schematic showing roles for EcR, Hr3 and Ftz-f1 in L5 branching. j, GCaMP6s response in Dm13 upon optogenetic stimulation of WT and $EcR^{DN}$-expressing L5 neurons. Amplitude of peak response for each condition is given. b - e, j, p-values (Student's t-test) are given. g, h, *, p-value (Fisher's exact test) < 0.05, ** p-value < 0.001.

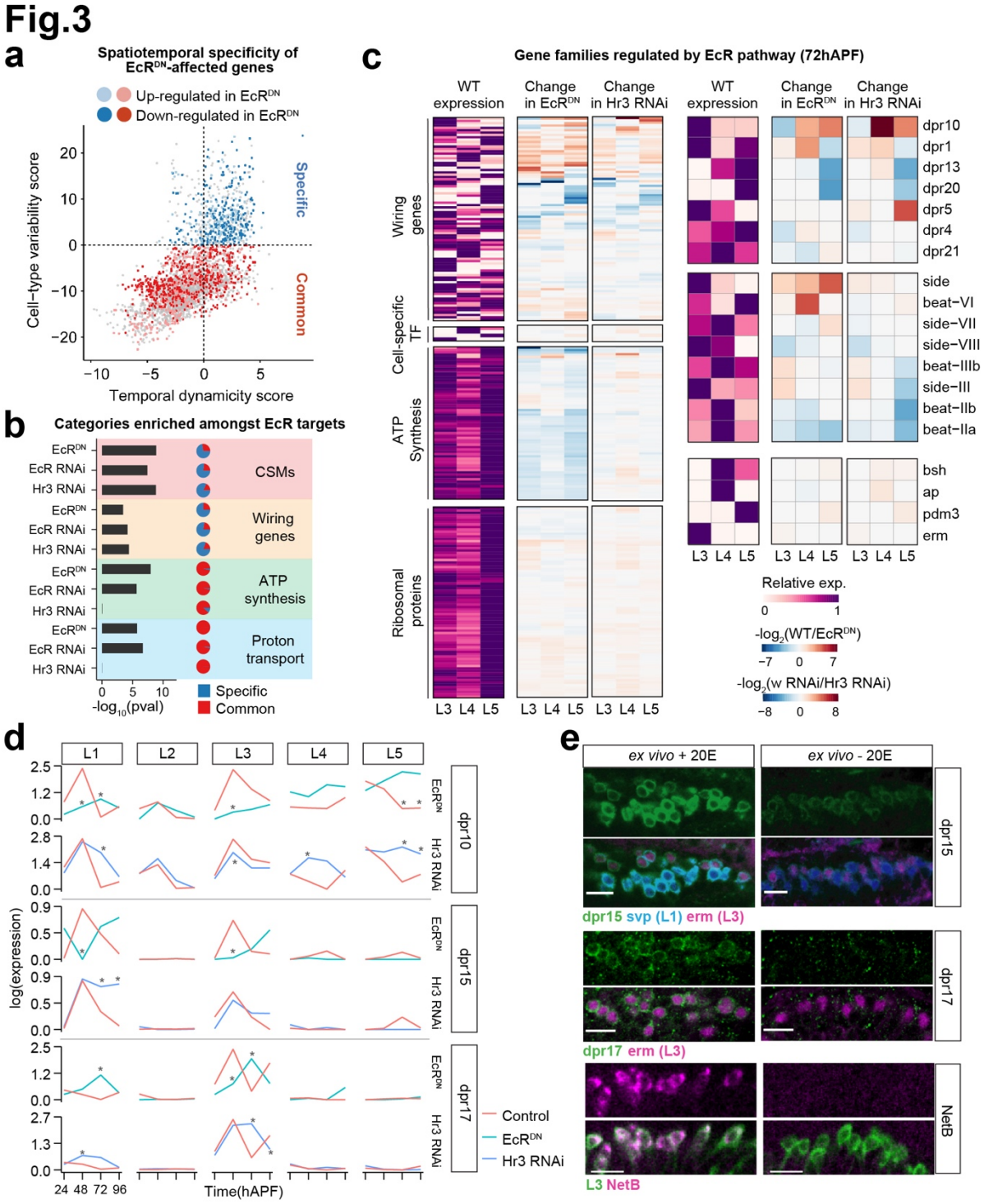


**Figure 2-3 Common and Cell-type targets of the Ecdysone-pathway.**

a, Cell-type variability vs Temporal dynamicity plot for EcR$^{DN}$-affected genes (fold change > 2, p-value < 0.05). Cell-type Specific (blue) and Common (red) targets are shown. Darker colors, genes

reduced in $EcR^{DN}$; lighter colors, genes increased in $EcR^{DN}$ (also see Extended data Fig. 11c, d). b, Gene groups enriched amongst genes reduced in $EcR^{DN}$. Fraction of targets common to all neurons (red) and neuron-specific (blue) targets in each category are shown as ratio of red to blue in small pie charts. c, Relative WT expression at 72 hAPF (left), change in expression with $EcR^{DN}$ (center), and change in expression with Hr3 RNAi (right) shown as heat maps for all genes expressed in L3-L5 neurons belonging to the specified gene categories at 72hAPF (also see Extended data Fig. 13a). Examples of genes belonging to the Dpr family, Side-Beat family and cell-type specific transcription factors are shown separately. d, dpr10, dpr15, dpr17 expression ± $EcR^{DN}$ (above) and ± Hr3 RNAi (below). * p-value < 0.05, fold change > 2. Expression is in log values. e, Staining for dpr15 and dpr17 reporters (MiMIC lines, see methods), and NetB (using anti-NetB antibody) in lamina neuron cell-bodies ± 20 Hydroxyecdysone (20E – active form of Ecdysone) in the medium (also see Extended data Fig. 14) in ex vivo preparations of pupal brains (see Methods).

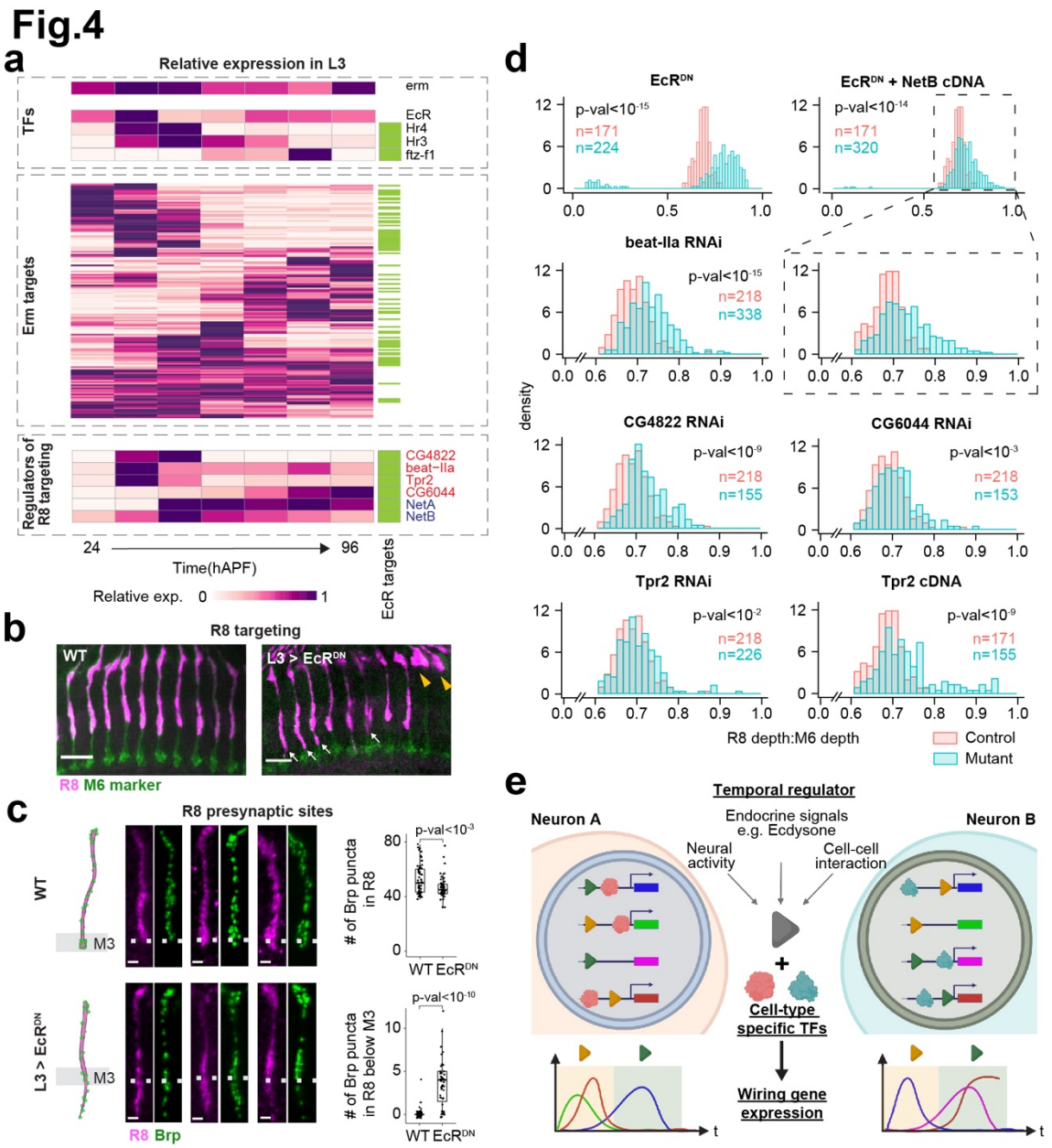


**Figure 2-4 Screening EcR and Erm co-regulated genes for wiring regulators.**

a, Heatmap showing relative expression of erm, EcR-pathway TFs and Erm targets in L3 neurons[38,39]. Green box indicates genes affected by EcR$^{DN}$ in L3 neurons. Genes that regulate R8 targeting are shown below. NetA and NetB (blue) are known regulators. Genes in red are identified in RNAi screen in this study. b, R8 axons ± EcR$^{DN}$ expression in L3. Magenta: R8 neurons. Green:

M6 marker (m24B10). Yellow arrowheads: Short R8's. White arrows: deep targeting R8's. Scale bar, 10μm. c, R8 presynaptic sites (Brp, green) ± $EcR^{DN}$ expression in L3. Right, quantification of Brp puncta number under the conditions shown. Scale bar, 5μm. (WT: 58 neurons, 3 animals; $EcR^{DN}$: 47 neurons, 3 animals). d, Distributions of R8 axon terminal depth (as in b) in control (red) or with expression of RNAi or cDNA (as shown, blue) in L3 neurons. Numbers of neurons/ condition are given. All conditions, number of animals ≥ 3. p-values (Student's t-test in c, Kolmogorov-Smirnov test in d) are given. e, Model for cell-type specific temporal control of wiring gene expression (see text).

## Methods

### Fly husbandry and stocks

Maintenance and rearing of fly lines, as well as staging of pupae was done as described in Tan et al.[32] Fly lines used in this work are listed in Supplementary Table 1.

### Data analyses of fly optic lobe RNA-seq

Measure of cell-type variability and temporal dynamicity for each gene

RNA-seq data of developing fly optic lobe were generated by Kurmangaliyev et al.[12], which contains 97 cell types covering 7 time points. For each gene, we assigned a cell-type variability score by their cell-type specific expression and a temporal dynamicity score by their expression changes over development. Cell-type variability score was calculated by the variance of gene expression at each time point when the gene is expressed, and then the maximum variance was normalized by the average expression across cell types that time point. Temporal dynamicity score was calculated by the sum of the absolute changes between consecutive time points for each cell type where the gene is expressed, and then the averaged value across cell types is normalized by the average of their peak expression. Both scores were centered their mean to 0 and transformed to natural log for visualization.

Wiring genes

Genes were designated to the category of 'wiring genes' if they satisfied the following criteria: 1) they were amongst the top 50% of the highest expressed cell-surface or secreted molecules in the developing optic lobe (from Kurmangaliyev et al.), 2) either themselves, or their paralogs (DIOPT v8.0 score ≥ 4) had published roles in establishing neuronal morphology or

connectivity in Drosophila. Extended data Table 3 contains a list of wiring genes along with references to published studies describing their roles in wiring.

Gene Ontology and REACTOME analysis of dynamic TFs

Dynamic TFs were defined as ones with temporal dynamicity score > 0 (see Fig. 1a, Extended data Table 2). Gene ontology analysis was performed using GOrilla (http://cbl-gorilla.cs.technion.ac.il) using dynamic TFs ranked on the basis of temporal dynamicity scores. All enriched categories are given in Extended data Table 4. For REACTOME pathway analysis, dynamic TFs were entered into the 'Analyze Data' tool on reactome.org (https://reactome.org/PathwayBrowser/#TOOL=AT). Reactome pathway analysis for Drosophila melanogaster was then run with default parameters.

**Bulk RNA-seq**

Bulk RNA-Seq analysis of L1 neurons at 40hAPF, 60hAPF and 72hAPF was performed as in Tan et al.[32] At least 2 replicates were generated for each timepoint. A minimum of 2000 cells were sorted for each experiment. cDNA libraries were created using the SMART-Seq2 protocol[58], which were then sequenced together using the HiSeq4000 platform (paired-end 50bp). Raw fastq reads files were mapped to FlyBase reference genome (release 6.29) using STaR (2.6.0) and only uniquely mapped reads were collected. Genes with counts per million (CPM) ≥ 4 in more than 2 samples were used for normalization with R package edgeR (3.26.8). Gene expression was quantified using RPKM units (Reads Per Kilobase of exon per Million reads mapped), calculated based on reads in the sum of exons using customized scripts. The correlation between biological replicates were calculated using Spearman correlation for top 500 genes with the highest variation across all samples. Coverage tracks were generated by bamCoverage(3.5.1).

**Bulk ATAC-seq**

At least 8000 L1 neurons were FACS purified at 40hAPF, 60hAPF and 72hAPF as described in Tan et al.[32] Biological duplicates were generated for each timepoint. ATAC-Seq libraries were generated as per the following protocol, which was modified from the one described in Buenrostro et al.[59]: 1) FACS purified cells were collected in 300ul 1X PBS and spun at 800xg for 8' at 4°C. 2) Cell pellet was then directly resuspended in 50µl of a tagmentation enzyme mix (25µl Nextera DNA library prep kit – Tagment DNA Buffer, 19µl Nuclease-free water, 5µl 1% IGEPAL CA630, 1µl Nextera DNA library prep kit - Tagment DNA Enzyme) and incubated at 37°C for 30' with constant agitation at 400rpm. 3) DNA was purified from the tagmentation mixes using the Qiagen minElute Reaction Cleanup Kit as per the manufacturer's protocol. 4) A 10µl qPCR reaction was setup to determine the optimum number of amplification 455 cycles (similar to Buenrostro et al.). 5) A larger PCR reaction (40µl) was then setup and PCR products in the 200-500bp range were gel purified. 6) Steps 4 and 5 were repeated, this time with barcoded primers (see Buenrostro et al.) to allow multiplexing of all libraries onto a single lane of HiSeq4000 (paired-end 50bp).

Raw fastq reads files were mapped to FlyBase reference genome (release 6.29) using Bowtie2 (2.2.9) and uniquely mapped genes were kept. All samples were pooled together prior to peak calling. Read start positions were shifted +4 or -5bp and used for peak calling using MACS2 (2.1.1) with parameters "-q 0.01 --nomodel --shift -100 --extsize 200". There were 26,122 peaks identified. Then bedtools multicov (2.27.1) was used to sum the total reads within each peak separately for each sample. Peaks with CPM ≥ 4 were used for counts normalization with edgeR. Correlations between biological replicates were calculated using Spearman correlation for the top 500 peak regions with the highest variation of peak levels across all samples. Distribution of the

top 5000 peaks across different genomic features at 40hAPF, 60hAPF and 72hAPF was determined using the R package ChIPseeker (1.20.0). Each ATAC peak was associated to the nearest gene based on proximity to the transcription start site using ChIPseeker. To compare change of ATAC-seq peak accessibility over time and change in expression of their nearest gene, $\log_2$(fold change ATAC-seq peak read coverage) was plotted against $\log_2$(fold change expression of nearest gene) for dynamic ATAC-Seq peak (Extended data Fig. 2b). Bulk RNA-Seq data was used for this, as this transcriptome dataset had been generated for the same time points as for ATAC-Seq. This was done separately for peaks differentially accessible between 40hAPF and 60hAPF (Extended data Fig. 2b (left)) and between 60hAPF and 72hAPF (Extended data Fig. 2b (right)). Differential peak analysis was performed using edgeR. Fold-change> 2 and adjusted p-value < 0.05 were chosen as the cutoffs to define peaks with differential accessibility between time points (dynamic peaks).

Binding sites for the EcR-usp complex (motif: Jaspar MA0534.1), Hr3 (motif: Fly Factor Survey, Hr46_SANGER_5) and Nr5a1, mammalian homolog of Ftz-f1 (motif: Jaspar 1540.1) across the genome were identified using the PWMscan (https://ccg.epfl.ch/pwmscan/). Cutoff of p-value < $10^{-5}$ were used to identify binding sites[60]. Enrichment of binding sites within different sets of ATAC-Seq peaks (Extended data Fig. 2d) was done using Homer (v4.7) mergePeaks utility. p-value ≤ 0.01 was considered as significantly more overlap than expected by chance.

**Calcium imaging**

Calcium imaging experiments were performed using a 3i VIVO Multiphoton upright microscope (Intelligent Imaging Innovations) with a water immersion objective (W Plan-Apochromat 20x/1.0 DIC, Zeiss). L5 neurons expressing CsChrimson (using 64B07 Gal4) were photo-stimulated with a 1040 nm laser (SpOne-8, Spectra-Physics) coupled to a 2-photon Phasor

(Intelligent Imaging Innovations) to generate a holographic pattern to restrict the stimulation area. GCaMP6s responses were recorded using an imaging laser tuned to 940 nm (Chameleon Discovery, Coherent).

Experimental crosses were set in vials with fly food supplemented with all-trans retinal (0.5 mM) and kept in the dark at 25 ºC. The brains of ≤ 5-day old adult flies were dissected in a saline solution (135 mM NaCl, 5 mM KCl, 2 mM $CaCl_2.2H_2O$, 4 mM $MgCl_2.6H_2O$, 5 mM TES, 36 mM Sucrose, pH 7.15) and mounted dorsal side on a poly-L-lysine-coated coverslip. Typically, the dissected brains were held for about 5 minutes before the start of the experiment to ensure a stable basal calcium signal. The photo-stimulation hologram was restricted to a rectangular area of 18 μm x 65 μm to roughly cover the middle third of the axon layer of L5 neurons in the medulla layers 1-2. The experimental protocol consisted of three consecutive iterations of a 30 s resting period and a 500 ms stimulation event. The stimulation laser power at the objective end was 335 mW, measured with a power meter (PM100D Thorlabs). GCaMP responses were recorded from a single Z plane at 3.05 frames/s. This protocol was executed on both optic lobes when possible.

Image processing

The GCaMP image data were processed using custom macros in Fiji and analyzed using custom code written in R. Briefly, a region of interest (ROI) was manually defined as the medulla layers that include the sub-arbors of the neurons expressing GCaMP. The average pixel value inside such ROI was measured across all time points for each sample. All fluorescence values were reported relative to a fluorescence baseline ($F_0$) defined as the median pixel value of the corresponding ROI during the entire imaging experiment. $\Delta F/F_0$ was calculated as $\Delta F/F_0 = (Ft - F_0)/F_0$, where Ft is the mean fluorescence value of the ROI at a given time point. The relative

maximum ΔF/F0 was defined in a 10 s time window immediately after stimulation offset from which the recent baseline (mean $\Delta F/F_0$ of the 6.5 s preceding stimulation onset) was subtracted. Those failed individual trials in which there were no detectable responses were discarded. The three individual stimulation events from left and right hemispheres trials were averaged to generate a single response trace per animal.

**Multiplexed single cell transcriptomic analysis**

For transcriptomic analysis of developing wildtype lamina neurons, w; UAS-H2A-GFP; 9B08-Gal4/Tm6B, tb females were crossed with males from different DGRP backgrounds (wildtype, see Supplementary Table 1 for list of DGRPs used). F1 prepupae were staged as in Kurmangaliyev et al.[12] Males were only included in the analysis if no significant differences in gene expression were found with female pupae of the same genotype and developmental time point. Pupae corresponding to different developmental stages (see Extended data Fig. 7a) were all dissected, dissociated and processed at the same time. Each developmental time point was represented by ≥ 2 DGRP heterozygotes, and only one animal/ DGRP heterozygote was dissected. Tissue dissociation, FACS and preparation of single-cell libraries using 10X Genomics Chromium (v3) were carried out similar to Kurmangaliyev et al., except that H2A-GFP expression was used to enrich for lamina neurons. All libraries were sequenced on a NextSeq500 platform (single-end 75bp).

For transcriptomic analysis involving UAS $EcR^{DN}$ (BDSC #6872), males carrying a single DGRP autonomous chromosome – w; (UAS $EcR^{DN}$ or UAS tdTom); DGRP/ Tm6b, tb were crossed with w; UAS-H2A-GFP; 9B08-Gal4/Tm6B females. For experiments involving UAS EcR RNAi (BDSC #9326) or UAS Hr3 RNAi (BDSC #27253), w; DGRP; (UAS wRNAi or UAS EcR

RNAi or UAS Hr3 RNAi)/ Tm6B, tb males were crossed with UAS Dcr2; UAS H2A-GFP; 9B08 Gal4/ Tm6B, tb females (see Extended data Fig. 7a and Supplementary Table 1). UAS tdTom and UAS wRNAi were used as controls.

scRNA-seq data pre-processing

Raw fastq read files were processed using Cell Ranger (3.1.0) with default parameters. Seurat V3 was used for all preliminary analyses. FlyBase reference genome (release 6.29) was used for alignment and annotation. Profiled single cells were identified as coming from a particular developmental time-point and genetic background based on the natural genomic variance within the different parent DGRP lines. This was done using the pipeline described in Kurmangalyev et al.[12], with the following modifications: the count of minor allele that equals to 2 among the analyzed DGRP strains were used as genomic variants to assign the profiled single cells to different DGRP parent lines. Only single cells with: 1) number of genes between 200 and 3000, 2) number of mitochondrial transcripts < 20% of all transcripts, and 3) assignment to a unique DGRP parent line; were used for all downstream analyses.

To identify different lamina neuron subtypes, all cells from a particular were integrated as described in Seurat v3 workflow and then subjected to unsupervised clustering, thus disregarding global temporal gene expression changes (similar to Kurmangaliyev et al.). Previously identified lamina neuron subtype specific genes[32] were used to assign each cluster to a cell-type. All cell cluster separations are visualized in tSNE plots. Cells not assigned to a lamina neuron-type cluster were removed from subsequent analyses. Average expression for each gene for each cell-type at a particular timepoint and genetic background was calculated using normalized expression values prior to integration.

**Comparison of scRNA-Seq with published dataset**

For comparison of lamina neuron transcriptomes generated here with lamina neuron transcriptomes generated in Kurmangaliyev et al., 500 genes with the highest variance across all cell types and all timepoints were used to calculate Spearman correlation.

**Differential gene expression analysis**

Wilcoxon rank-sum test (fold change > 2, adjusted p-value < 0.05) was used to identify genes differentially expressed between timepoints, cell-types or as a consequence of EcR/ Hr3 perturbations. All fold change calculation used pseudo number 0.01.

**Enrichment analysis amongst EcR and Hr3 targets**

For each of the four categories shown in Fig. 4b, enrichment was calculated using Fisher's exact test. Briefly, number of genes expressed in lamina neurons overlapping with genes in the stated category vs other genes expressed in lamina neurons, was used to define a null hypothesis. Then genes affected by $EcR^{DN}$, EcR RNAi or Hr3 RNAi were also divided into ones overlapping with genes in the stated category, and ones that don't overlap. Number of genes in these two categories, along with similar numbers from the null-hypothesis, were then used to create a 2X2 matrix, which was then subjected to Fisher's exact test.

Gene categories, Proton transport (proton transmembrane transport, GO:1902600) and ATP synthesis (ATP metabolic process, GO:0046034) were initially identified from GO analysis of targets of $EcR^{DN}$ and EcR RNAi.

**Gene group analysis for EcR and Hr3 perturbation effect**

Prior to clustering, all average gene expression from scRNA-seq transcriptomic analysis were normalized to maximum expression in each cell type across development. For each cell types, the relative expression of each gene was used to perform k-means clustering to assign expressed genes in different groups. The number of clusters for each cell type were determined by calculating Within-Clsuter of Squared Errors (WSS) and finding where the difference of WSS in consecutive cluster number first become less than 5. For Extended data Fig. 12, we presented the gene groups with the most up-regulated or the most down-regulated or the unchanged gene expression after expressing $EcR^{DN}$ in each lamina neuron.

***Ex vivo* culture of dissected brains**

We used a protocol similar to the one described in Özel et al.[37] Briefly, brains were dissected from 22hAPF pupae in pre-warmed Schneider's medium (ThermoFisher #2172004) with either 1:1000 dilution of 1mg/ml 20-HydroxyEcdysone (dissolved in 100% Ethanol, Sigma H5142) or equivalent volume of 100% ethanol. Brains were then incubated in ~ 200ul of medium ± 20-HydroxyEcdysone in 96 well plates for 26h at 25ºC in a humidified chamber. Thereafter, brains were fixed, stained and imaged using the aforementioned protocols for immunohistochemistry and microscopy (see Extended data Fig. 14a).

In the presence of 20-HydroxyEcdysone in the media, strong expression of EcR-B1 and Hr3 is observed throughout the optic lobe, while no expression of Ftz-f1 is seen (Extended data Fig. 14a). When 20-HydroxyEcdysone is omitted from the culture medium, no expression of Hr3 is seen (as expected), however weak induction of Ftz-f1 is observed. The transcriptional regulation of ftz-f1 is not completely understood, and previous work has shown that ftz-f1 can be induced even without Hr3 expression. Apart from Hr3, another target of EcR – Blimp-1 has also been shown to regulate ftz-f1 expression by functioning as a repressor. Indeed, loss of Blimp-1 leads to

ftz-f1 expression[17]. In brains incubated without Ecdysone, the weak induction of ftz-f1 may be (in part) due to lack of Blimp-1 expression.

**Immunohistochemistry and microscopy**

Immunohistochemistry and microscopy were performed as described in Xu et al.[61] with the following modifications: 1) For experiments involving staining of presynaptic sites and L5 morphology, brains were fixed using glyoxal (3.12% glyoxal, 0.75% acetic acid and 20% ethanol, pH adjusted to 5.0) for 30' at RT and then washed 3X with PBST. 2) All images were acquired using an LSM880 confocal microscope.

Primary antibodies used in this study were: mAb24B10 (1:20, DSHB), rabbit anti-NetB (1:500, gift from Akin Lab), rabbit anti-dsRed (1:400, Clontech 632496), chicken anti-GFP (1:1000, Abcam ab13970), rat anti-Flag (1:200, Novus Biologicals, NBP1-06712), mouse anti-EcR-B1 (1:20, DSHB AD4.4), mouse anti-EcR-A (1:10, DSHB 15G1a), rabbit anti-Hr3 (1:50, gift from Thummel Lab), mouse anti-Svp (1:20, DSHB 5B11), rabbit anti-Erm (1:100, gift from Wang Lab), rat anti-Bab2 (1:500, gift from Laski Lab), mouse anti-V5 (1:200, BioRad MCA1360), guinea pig anti-Bsh (1:400, see Tan et al. 2015), guinea-pig anti-DIP-β (1:300, gift from Pecot Lab). Secondary antibodies used in this study were: goat anti-mouse 488 (1:500, ThermoFisher A-32723), goat anti-mouse 568 (1:500, ThermoFisher A-11031), goat anti-mouse 647 (1:500, ThermoFisher A-21235), goat anti-chicken 488 (1:1000, ThermoFisher A-11039), goat anti-rabbit 568 (1:500, ThermoFisher A-11011), goat anti-guinea pig 647 (1:500, ThermoFisher A-21450), goat anti-rabbit 647 (1:200, ThermoFisher A-32733), goat anti-rat 568 (1:500, ThermoFisher A-11077), goat anti-guinea pig 568 (1:500, A-11075).

**Image analysis**

All images for figures were created using ImageJ (v2.1.0) or Imaris (v9.1.2). Details for quantification of phenotypes are given below.

**R8 targeting**

Imaris (v9.1.2) was used to measure the distance of R8 terminals from the top of the medulla (M0), as well as the distance of 6th medulla layer (M6) from the top of the medulla. The latter was estimated using mAb24B10 staining, which labels R7 neurons that terminate in M6. Values reported on the X-axis of Fig. 4d and Extended data Fig. 15b are (R8-M0)/ (M6-M0).

**L5 morphological defects**

Imaris was used to visualize individual neurons. Each neuron was then manually assigned to one of the stated categories.

**Quantification of BRP puncta**

For lamina neuron presynaptic sites in the lamina: the distance between the proximal end of the lamina and the distal end of the lamina was measured using Imaris individually for all lamina cartridges. A line was drawn at the measured distance divided by 2. All BRP puncta more distal of this line were counted manually. For R8 presynaptic sites: All Brp puncta were counted manually.

**Other statistics**

One-sided Fisher's exact test was used to determine the enrichment of dynamic genes (temporal dynamicity score > 0, calculated as in Fig. 1a, but specifically for L3) within common

targets of EcR and Erm as compared to targets of Erm alone. Targets of Erm were obtained from Peng et al. and Santiago et al.[38,39].

For all box-plots, solid line depicts median, while the upper and lower bounds of the box depict the third and first quantile of the data spread respectively.

Kolmogorov-Smirnov (KS) test (Fig. 4d, Extended data Fig. 15b, c), two-tailed Student's t-test (Fig. 2b-e, 2j, 4c, Extended data Fig. 6, 8c, 15a), two-tailed Fisher's exact test (Fig. 2g, h, Extended data Fig. 5a), one-tailed Fisher's exact test (Fig. 3b, Extended data Fig. 2d) were performed using the following basic R functions (R 3.6.1) respectively: ks.test, t.test, fisher.test. Raw data for all analyses is available upon request.

**Data and code availability**

All raw sequencing data and codes will be provided upon request. They will be made publicly available prior to publication.

**Supplemental Information**

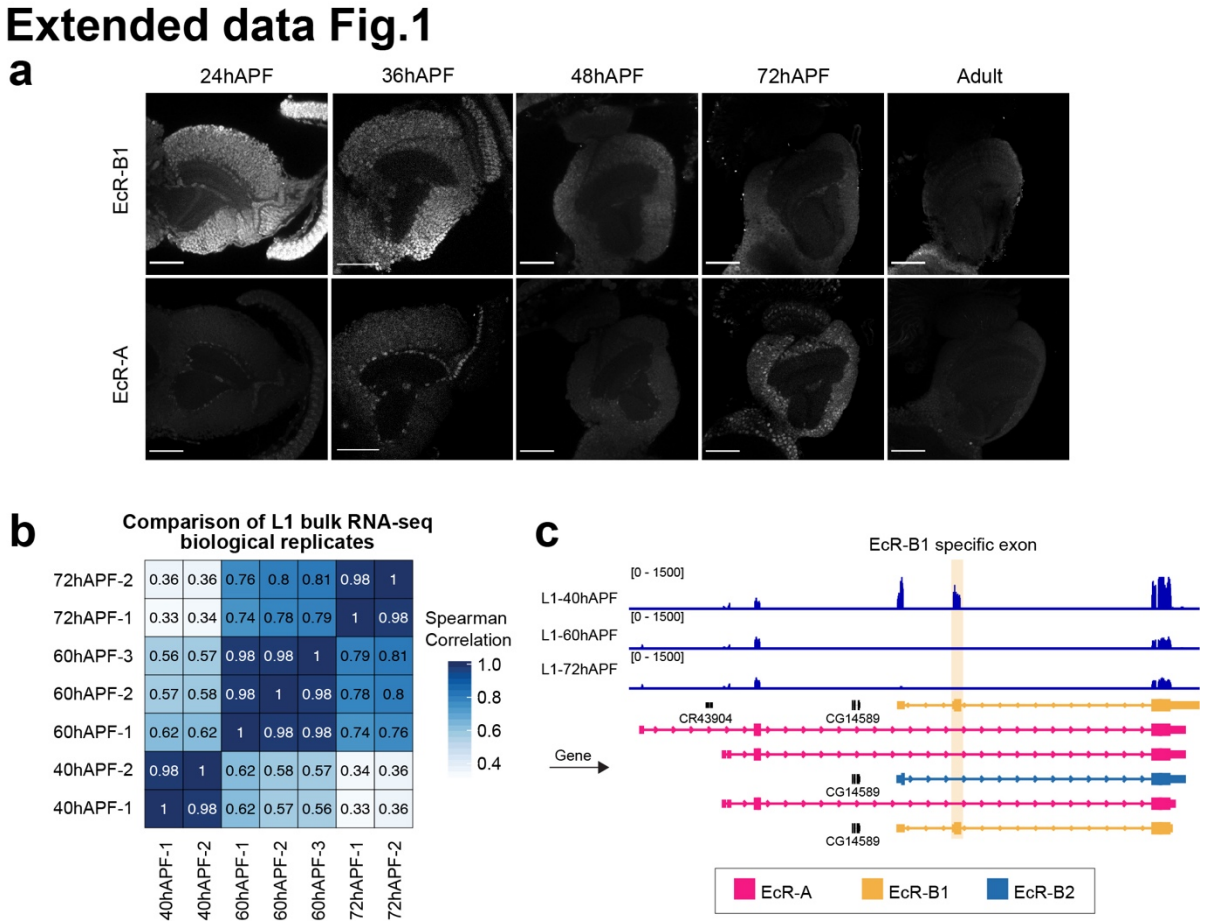


**Extended data Fig. 1. Development change from EcR-B1 to EcR-A isoform.**

a, Staining using anti-EcR-B1 or anti-EcR-A antibodies at the indicated times in development. Scale bar, 50 μm. Note: EcR-A positive cells at 36hAPF are glia. b, Comparison of replicates of bulk RNA-Seq of L1 neurons at 40hAPF, 60hAPF and 72hAPF. Values given are Spearman correlation values (see methods). c, Coverage tracks from L1 bulk RNA-Seq in the EcR locus at 40hAPF, 60hAPF and 72hAPF. EcR-A, EcR-B1 and EcR-B2 transcripts are shown, and EcR-B1 specific exon is highlighted.

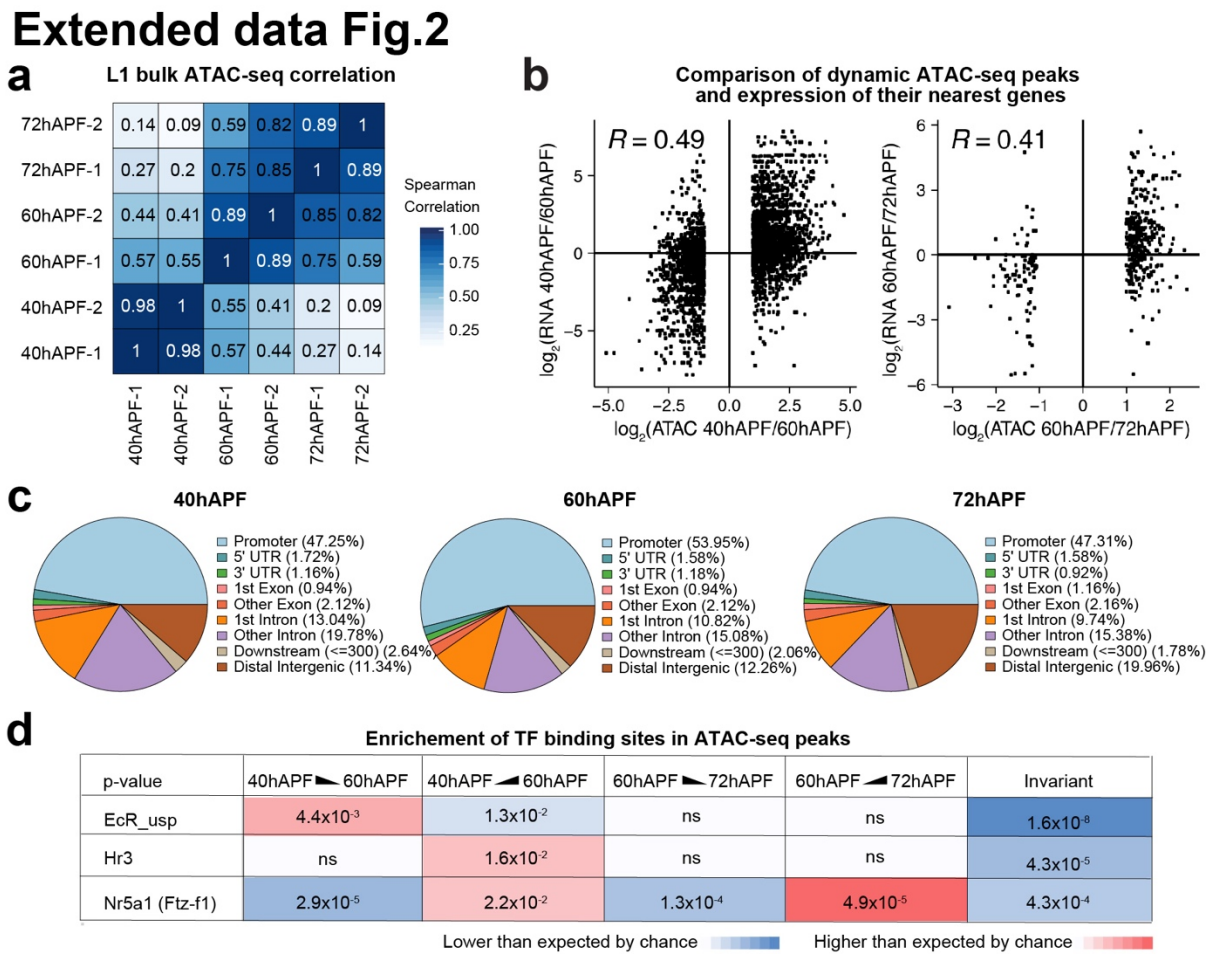


**Extended data Fig. 2. ATAC-Seq analysis of developing L1.**

a, Comparison of replicates of bulk ATAC-Seq data of L1 neurons at 40hAPF, 60hAPF and 72hAPF. Values shown are Spearman correlation values (see Methods). b, Comparison of change of ATAC-seq peak coverage (for regions with dynamic coverage over time) and change in expression of nearest gene. $\log_2$(fold change RPKM of nearest gene) vs $\log_2$(fold change ATAC-seq peak coverage) between 40hAPF and 60hAPF, and 60hAPF and 72hAPF. r, Pearson's correlation coefficient. c, Distribution of the top 5000 peaks at each time point between various genomic landmarks. d, p-values (Hypergeometric test) for enrichment of binding motifs of EcR-usp complex, Hr3 and Nr5a1 (mammalian homolog for Ftz-f1) amongst the following sets of

ATAC-Seq peaks: peaks going down from 40hAPF to 60hAPF, peaks going up from 40hAPF to 60hAPF, peaks going down from 60hAPF to 72hAPF, peaks going up from 60hAPF to 72hAPF, and peaks invariant over time. Red: occurrence of motif is higher than expected by chance, blue: occurrence of motif is lower than expected by chance (see methods).

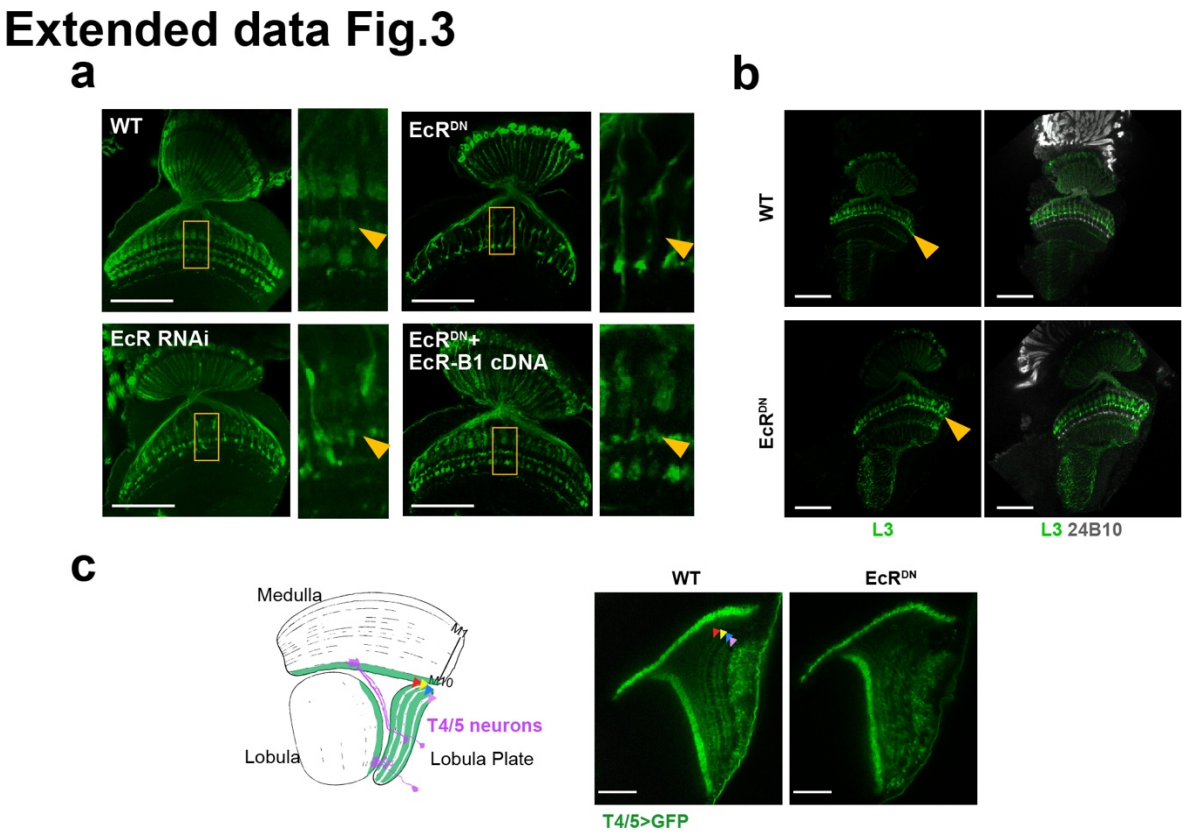


**Extended data Fig. 3. Analysis of morphology with or without EcR$^{DN}$ expression.**

a, Morphology of lamina neurons (L1-L5) in wildtype (WT) brains and upon pan-lamina expression (using 9B08 Gal4) of EcR$^{DN}$, EcR$^{DN}$ + EcR-B1 cDNA or EcR RNAi. Arrowhead in inset points to M3 medulla layer. Note: loss of arborization in M3 with EcR$^{DN}$ is likely due to loss of driver expression in L3 neurons (see Extended data Fig. 3b). b, Morphology of L3 neurons with or without EcR$^{DN}$ expression using an L3-specific driver (9D03 Gal4). Note, in adults 9D03 Gal4 also labels some L2 neurons. This is not the case during development (see Extended data Fig. 16b, c) a, b, Arrowhead points to M3 layer in the medulla. Scale bar, 50 μm. c, Effect of EcR$^{DN}$ expression on morphology of T4/T5 neurons. Four layers in the lobula plate, a, b, c and d, are marked with red, yellow, blue and pink arrowheads, respectively. Cartoons of one T4 (purple

neuron, top) and one T5 neuron (purple neuron, bottom) are shown to highlight wildtype morphology. Scale bar, 20μm.

# Extended data Fig.4

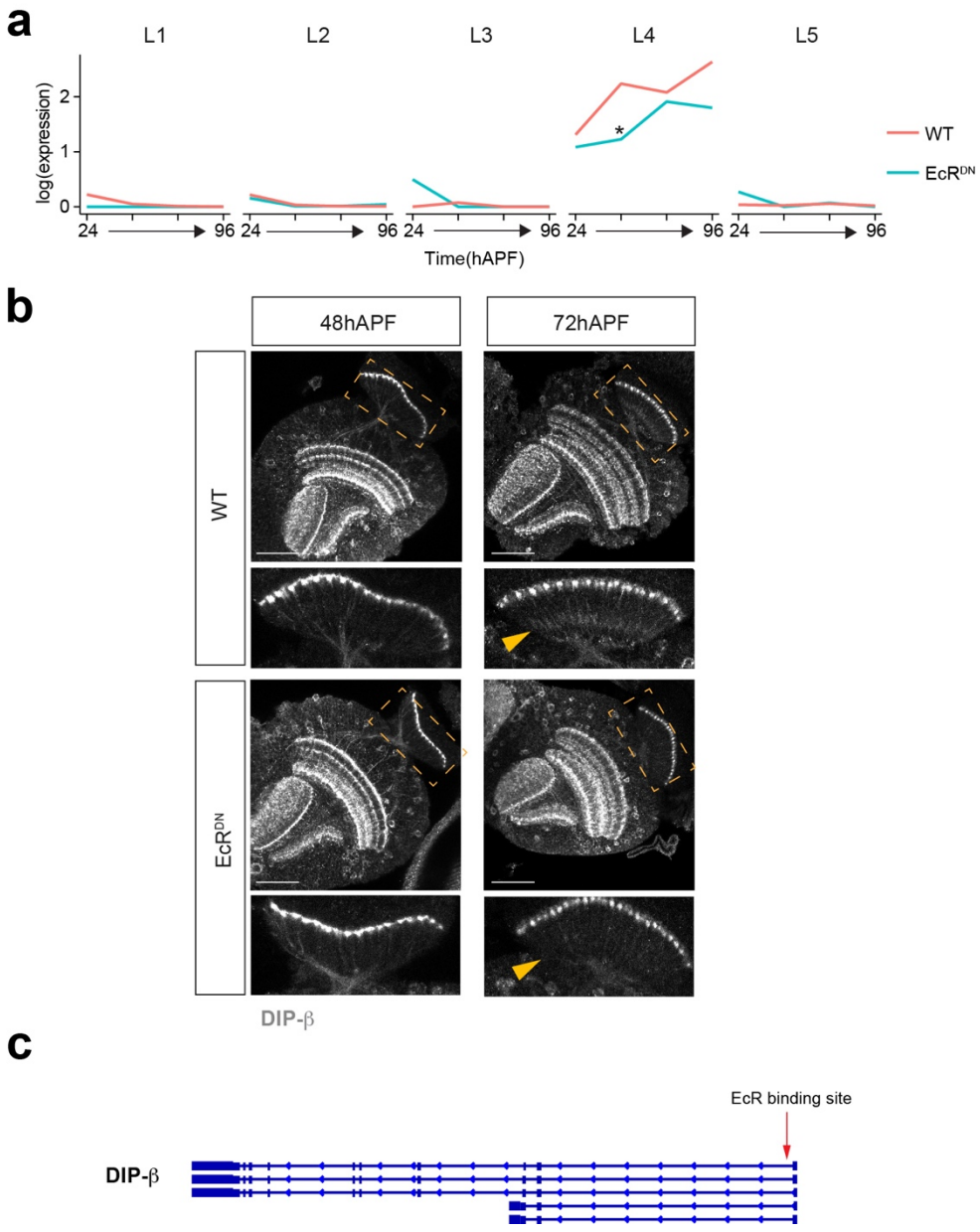


**Extended data Fig. 4. DIP- β expression with or without EcR$^{DN}$.**

a, DIP-β mRNA expression in L1-L5 neurons across development with or without pan-lamina expression of EcR$^{DN}$ (from scRNA-Seq based transcriptomic analyses, see Fig. 3, Extended data Fig. 7, 8). * significant difference between control and EcR$^{DN}$ (change in expression > 2fold, p-value < 0.05). b, Staining using anti-DIP-β antibody at the indicated time points in development

with or without pan lamina expression of $EcR^{DN}$. Inset shows the lamina neuropil. Arrowhead points to proximal lamina neuropil, positive for DIP- β staining at 72hAPF. Note that staining is largely absent from the lamina neuropil (yellow arrowheads). The level of DIP- β RNA is reduced in $EcR^{DN}$ at 48 but rises to near normal levels again at 72 hrs. We assume that the decrease in RNA leads to a lag in the accumulation of DIP- β protein. c, EcR-usp complex binding motif within the first intron of DIP- β (FDR < $10^{-7}$, see methods).

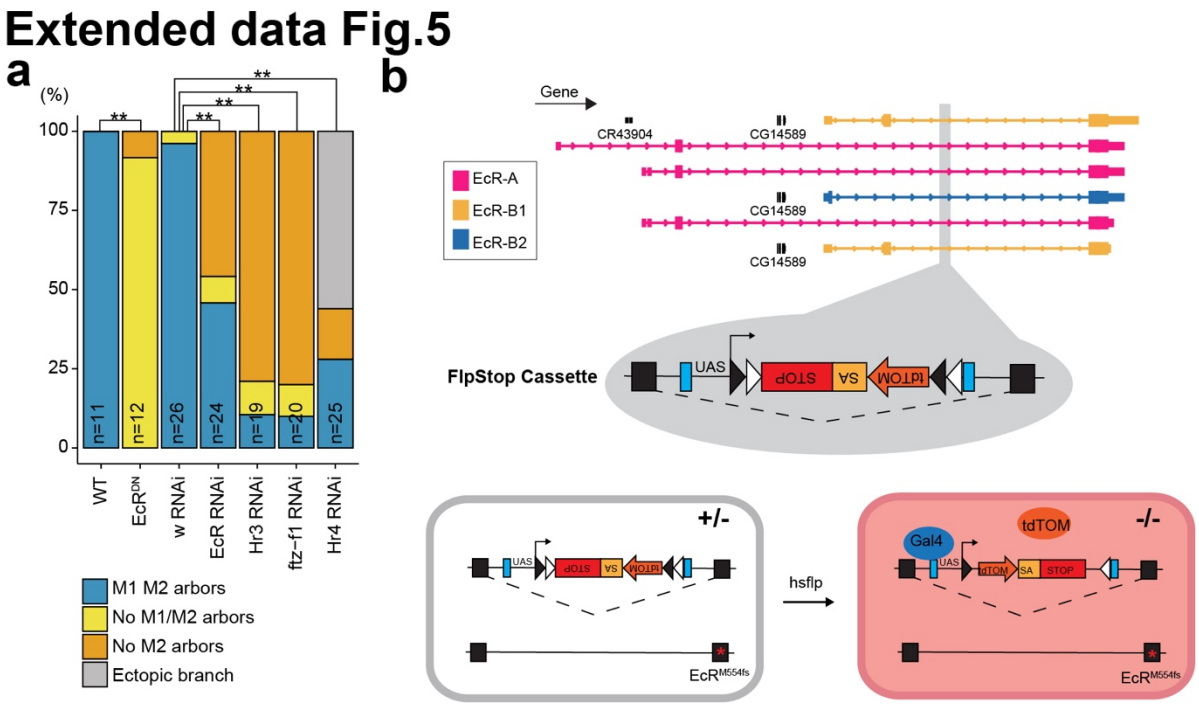


**Extended data Fig. 5. Cell and cell-type autonomous analysis of EcR function.**

a, Different L5 arborization defects and their distributions under the given genotypes (see Fig. 2g). All transgenes are expressed using an L5-specific driver (pan-lamina driver is used for data in Fig. 2g). n = number of neurons (all conditions, animals ≥ 4). **, p-value < 0.001. b, schematic showing the $EcR^{FlpStop}$ allele. FlpStop cassette is inserted in the first common intron of EcR (grey bar shows insertion site, Mi{MIC}EcRMI05320). Cells expressing Gal4, within which a stochastic, heat-shock FLP recombinase-mediated flipping of the cassette occurs, express tdTom.

# Extended data Fig.6

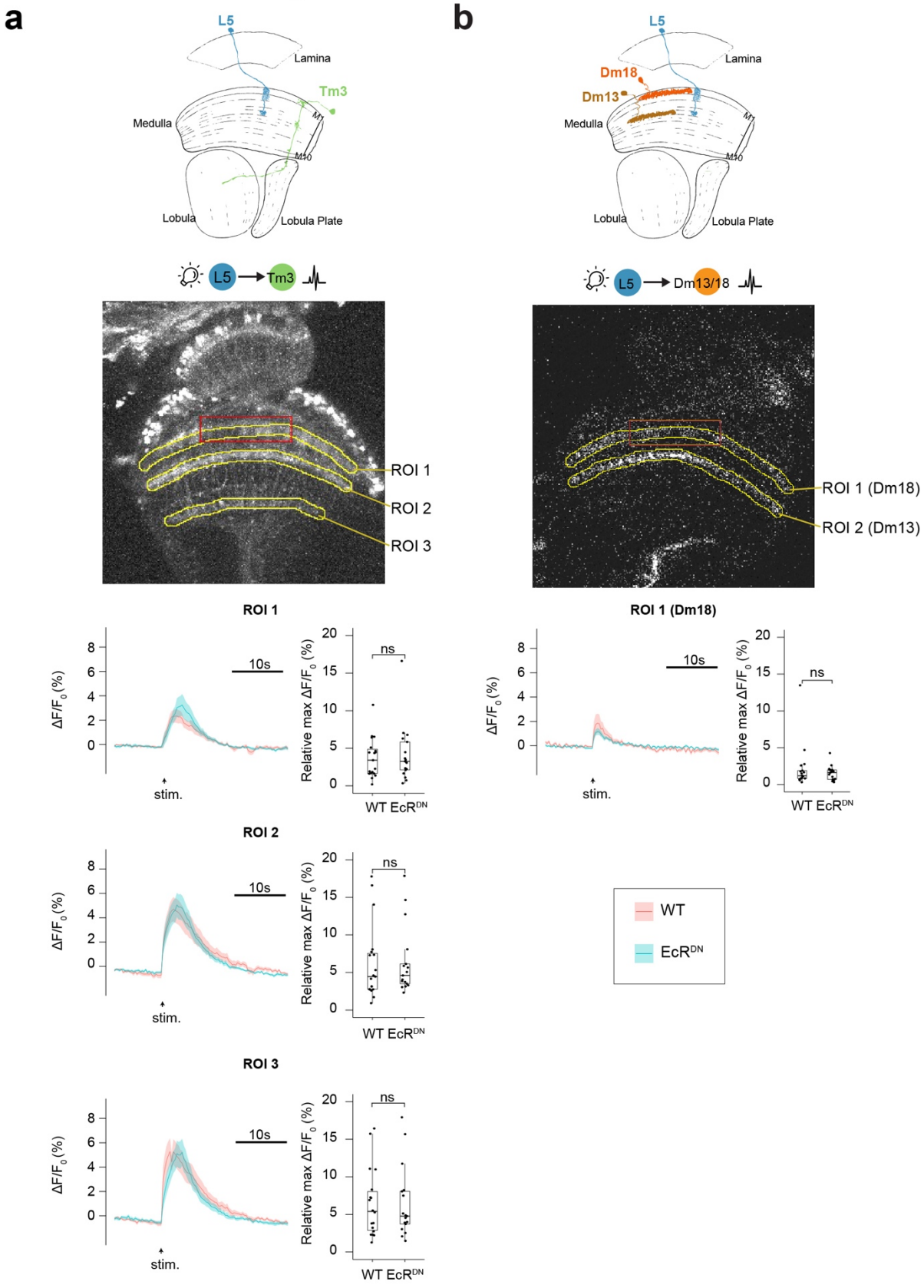

**Extended data Fig. 6. Optogenetics-based assay for communication between L5 and its postsynaptic partners.**

a, $Ca^{2+}$ response from Tm3 (measured using GCaMP6s) upon optogenetic stimulation of L5 with (blue line) or without (red line) $EcR^{DN}$ expression in L5. GCaMP6s responses were measured in 3 regions of interest (ROI). ROI 1, ROI 2 and ROI 3 span medulla layers M1, M5 and M10 respectively. b, $Ca^{2+}$ response from Dm13 and Dm18 (common LexA driver used yields expression in both Dm13 and Dm18, see Extended data Table 1) upon optogenetic stimulation of L5 with (blue line) or without (red line) $EcR^{DN}$ expression in L5. ROI 1 spans M1 and measures response from Dm18. ROI 2 spans M5 and measures response from Dm13. Note: weak response from Dm18 upon stimulation of L5 irrespective of condition. a, b, Amplitude of relative peak response for each condition is quantified. There is no significant difference between WT and $EcR^{DN}$ for any comparison shown here. For Dm13 response, see Fig. 2j.

# Extended data Fig.7

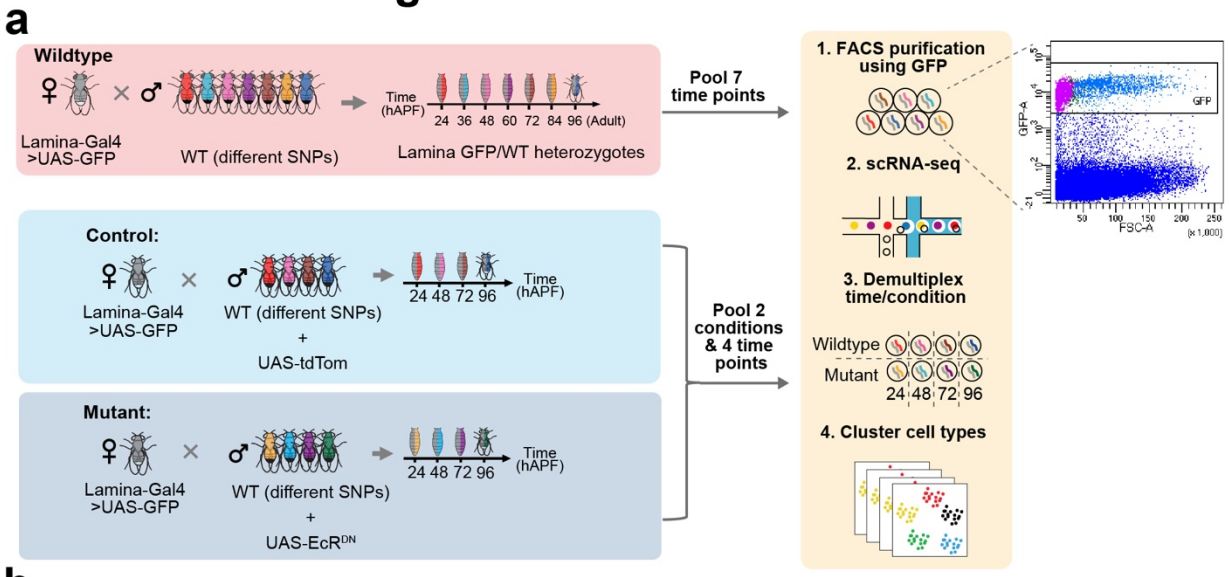


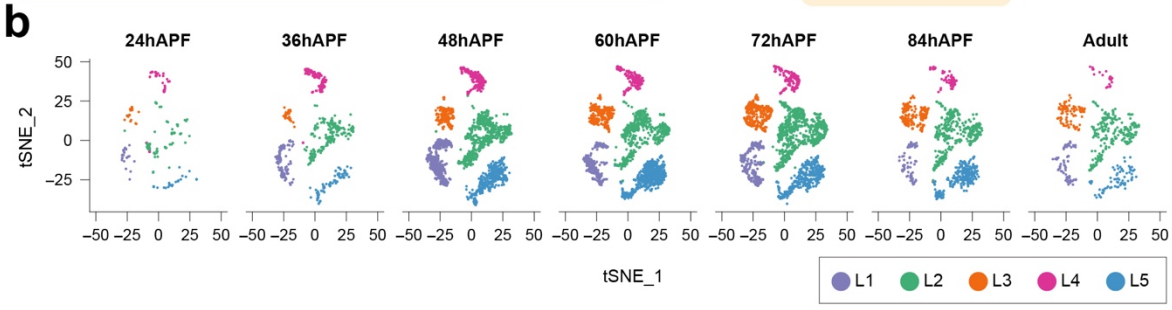


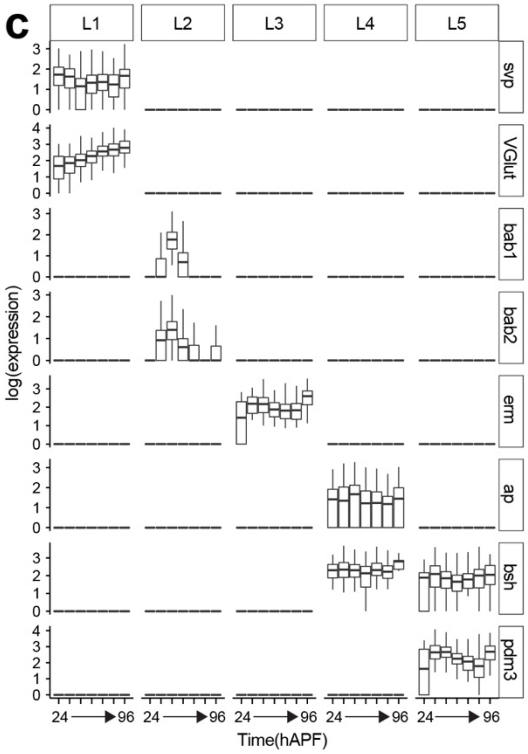


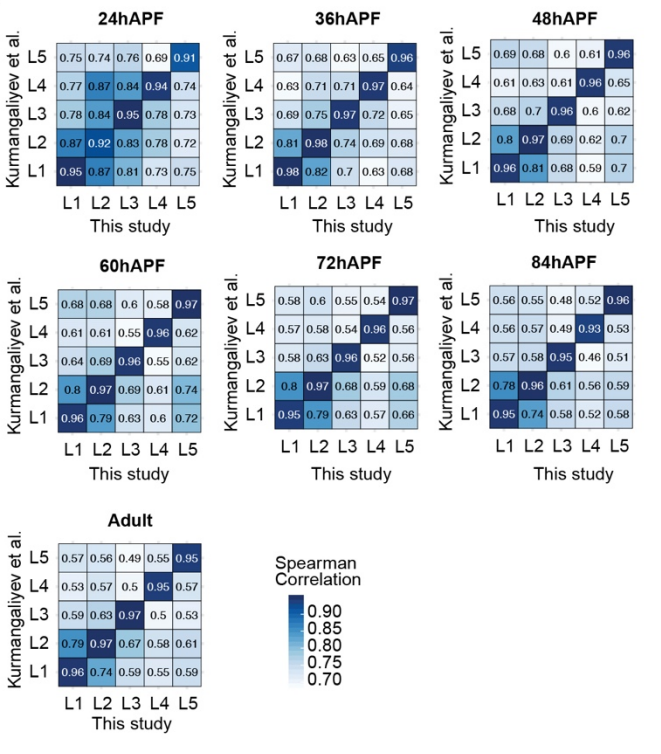

**Extended data Fig. 7. Approach for identification of EcR and Hr3 targets using scRNA-Seq.**

a, Scheme for scRNA-Seq based transcriptomic analysis of WT and mutant lamina neurons (see Kurmangaliyev et al.[12] and methods). GFP vs forward scatter 2-D plot showing criteria used to enrich for lamina neurons by FACS is shown on the right. 'Cells' highlighted in purple were excluded despite being GFP+ due to their small size. b, tSNE plots showing WT L1-L5 clusters at 24, 36, 48, 60, 72, 84 and 96 hAPF (Adult). c, Log(expression) of previously identified lamina neuron type-specific genes in L1-L5 clusters identified at each time point over development (see Tan et al.[32]). d, Comparison of lamina neuron transcriptomes generated by scRNA-Seq in this study and by scRNA-Seq in Kurmangaliyev et al. Values given are Spearman correlation values.

# Extended data Fig.8

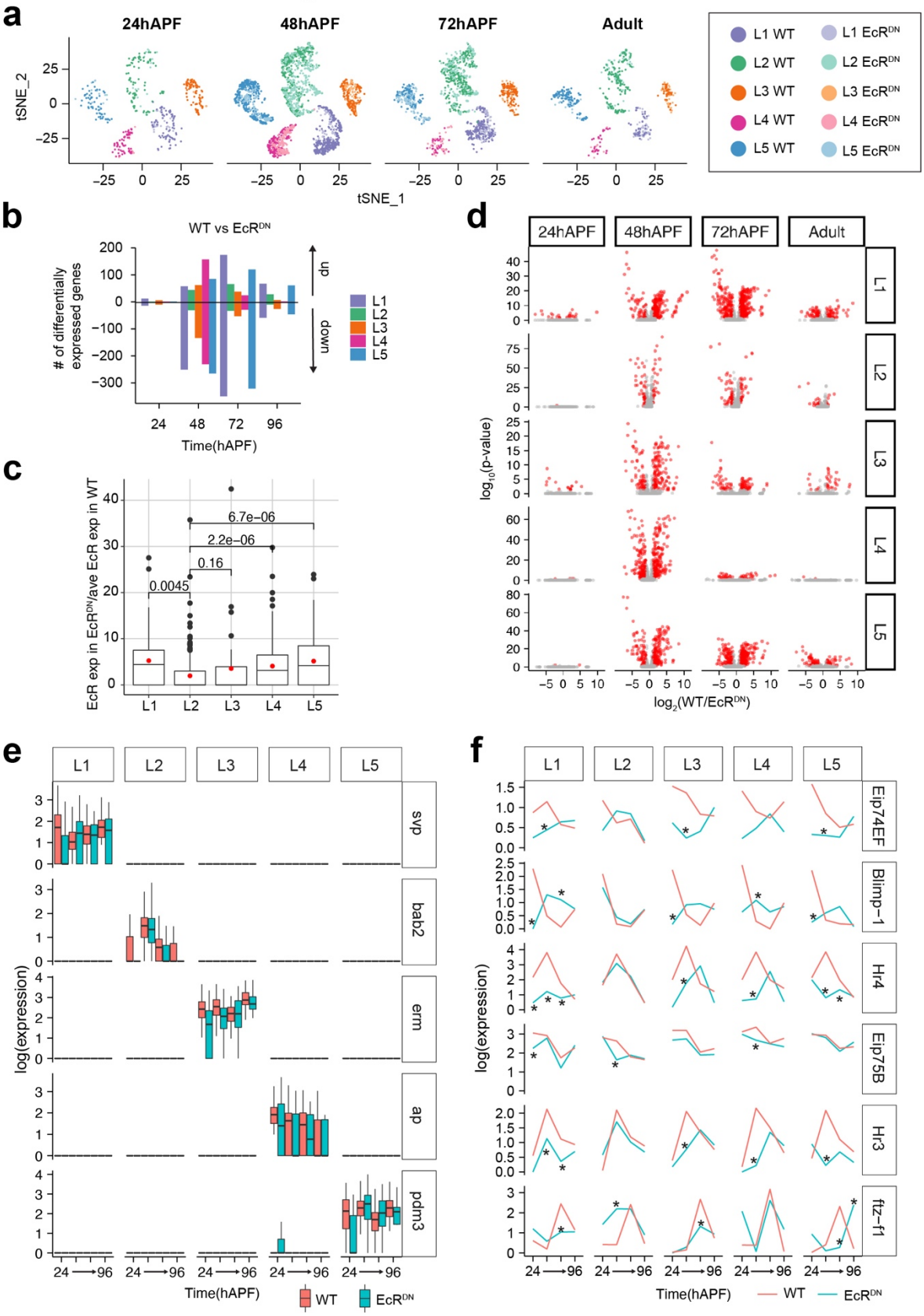

**Extended data Fig. 8. scRNA-Seq-based analysis of WT and $EcR^{DN}$ expressing lamina neurons.**

a, tSNE plots showing WT and $EcR^{DN}$-expressing L1-L5 clusters at 24, 48, 72 and 96 hAPF (Adult). b, Number of genes up or downregulated in $EcR^{DN}$ in L1-L5 neurons. c, Expression of EcR in $EcR^{DN}$-expressing lamina neurons at 48hAPF normalized to mean expression of EcR in wildtype cells at 48hAPF (done separately for each lamina neuron-type). Red dots, mean of data spread. Increase in EcR expression in $EcR^{DN}$-expressing cells over wildtype is expected to be due to the expression of the $EcR^{DN}$ transgene. Note the poor induction of $EcR^{DN}$ in L2 neurons. p-value from student's t-test are stated in the figure for comparison between L2 and other lamina neuron-types. The difference between $EcR^{DN}$ expression in L2 and L3 neurons is not significant likely due to the low cell numbers of $EcR^{DN}$-expressing L3 neurons. d, Volcano plots showing significant gene expression changes in L1-L5 neurons throughout development. Red dots: fold change > 2 and p-value < 0.05. e, Log(expression) of lamina neuron-type specific TFs with (blue) or without (red) $EcR^{DN}$. Note no change in expression of TFs ± $EcR^{DN}$. f, Log(expression) of TFs in the Ecdysone-pathway in WT (red lines) and $EcR^{DN}$-expressing (blue lines) L1-L5 neurons. *, p-value < 0.05, fold change > 2.

# Extended data Fig.9

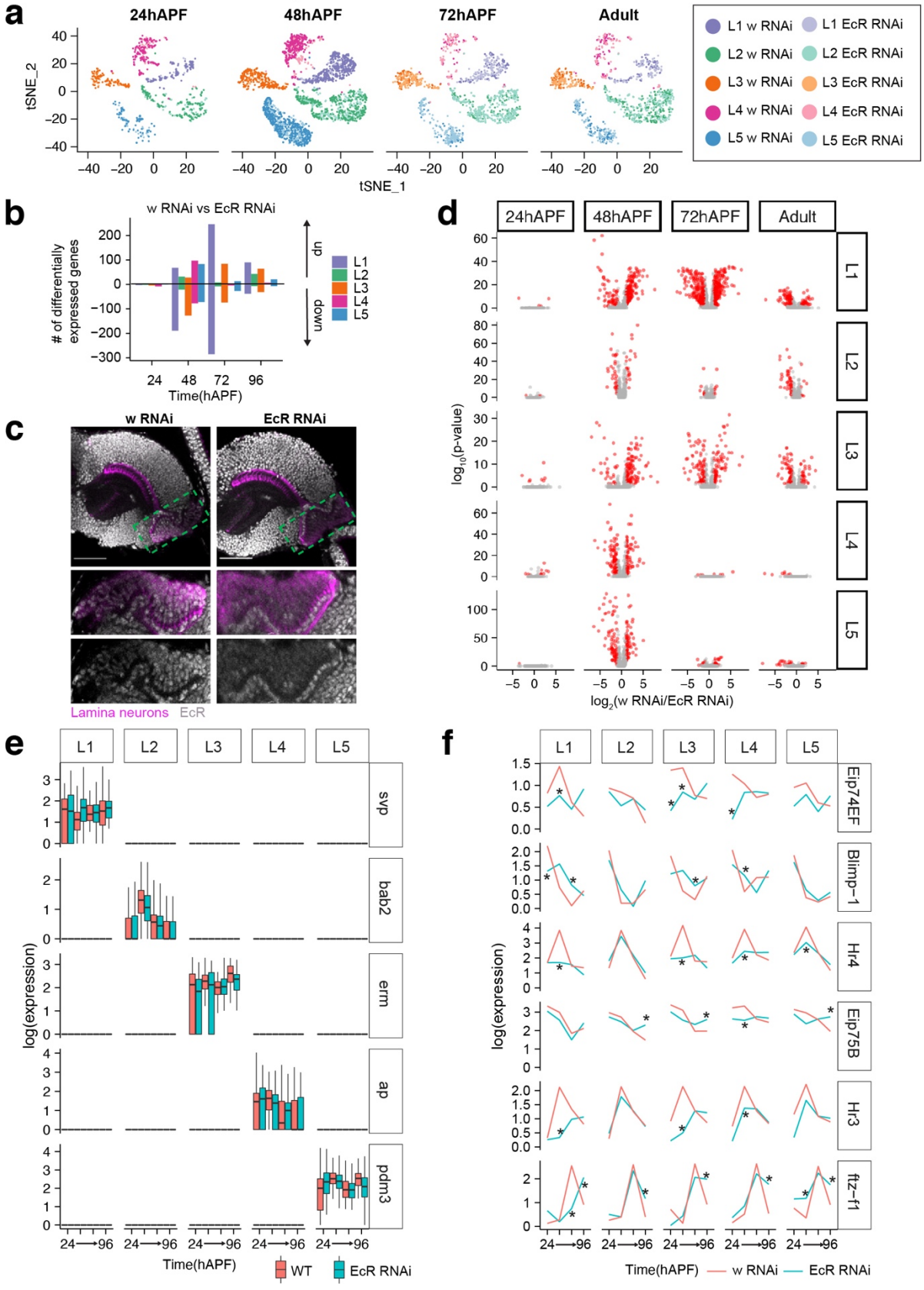

**Extended data Fig. 9. scRNA-Seq-based analysis of w RNAi and EcR RNAi expressing lamina neurons.**

a, tSNE plots showing w RNAi and EcR RNAi-expressing L1-L5 clusters at 24, 48, 72 and 96 hAPF (Adult). b, Number of genes up or downregulated in EcR RNAi in L1-L5 neurons. c, Image showing optic lobe (top) stained using an antibody targeting all EcR isoforms (grey) at 24hAPF. Box with green dotted outline marks the region containing lamina neuron cell-bodies. This region is magnified in bottom two panels. Lamina neurons are labeled in magenta. Scale bar, 50μm. d, Volcano plots showing significant gene expression changes in L1-L5 neurons throughout development. Red dots: fold change > 2 and p-value < 0.05. e, Log(expression) of lamina neuron-type specific TFs with (blue) or without (red) EcR RNAi. Note no change in expression of TFs ± EcR RNAi. f, Log(expression) of TFs in the Ecdysone-pathway in WT (red lines) and EcR RNAi-expressing (blue lines) L1-L5 neurons. *, p-value < 0.05, fold change > 2.

# Extended data Fig.10

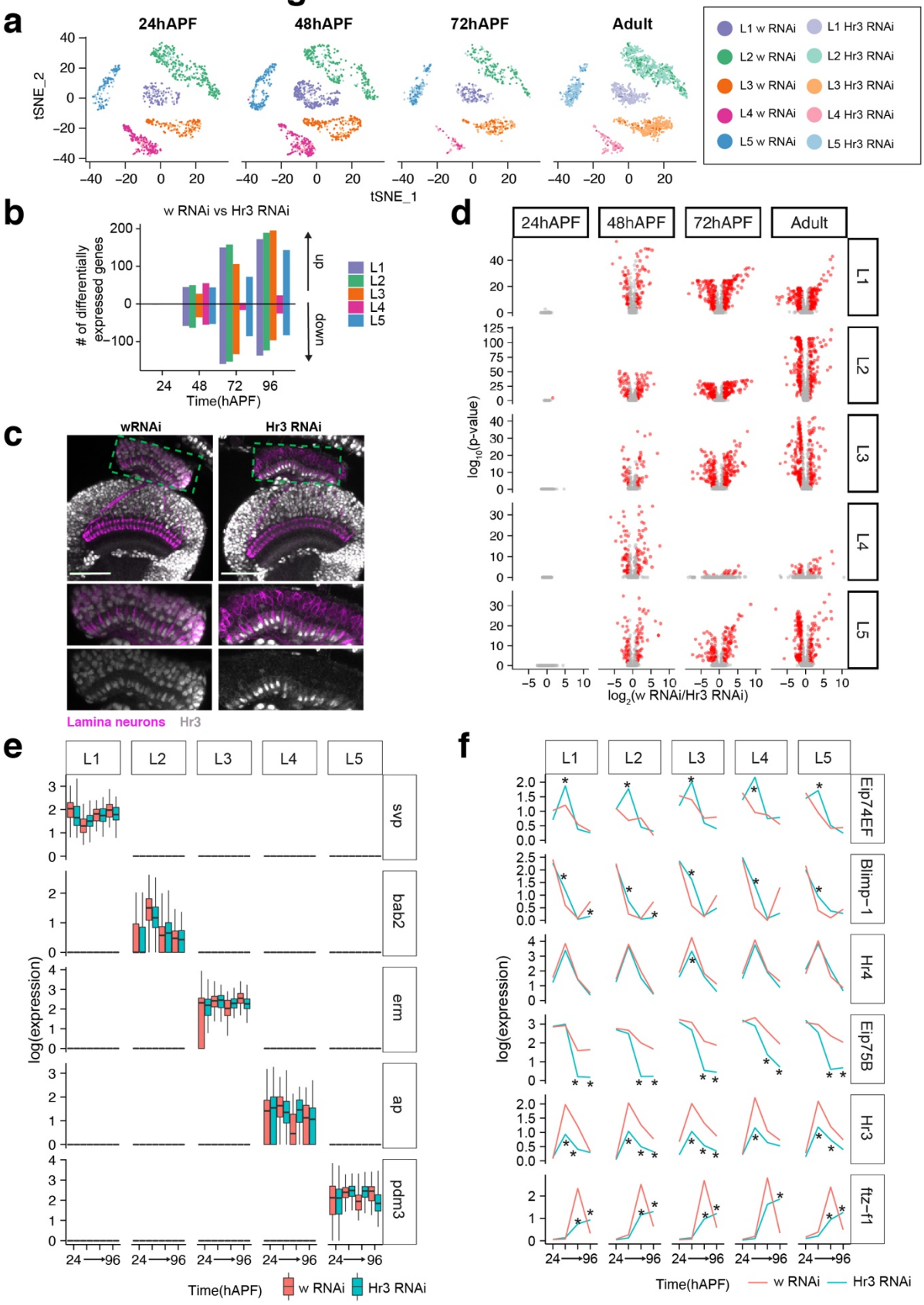

**Extended data Fig. 10. scRNA-Seq-based analysis of w RNAi and Hr3 RNAi expressing lamina neurons.**

a, tSNE plots showing w RNAi and Hr3 RNAi-expressing L1-L5 clusters at 24, 48, 72 and 96 hAPF (Adult). b, Number of genes up or downregulated in Hr3 RNAi in L1-L5 neurons. c, Image showing optic lobe (top) stained using an antibody targeting Hr3 (grey) at 24hAPF. Box with green dotted outline marks the region containing lamina neuron cell-bodies. This region is magnified in bottom two panels. Lamina neurons are labeled in magenta. Scale bar, 50μm. d, Volcano plots showing significant gene expression changes in L1-L5 neurons throughout development. Red dots: fold change > 2 and p-value < 0.05. e, Log(expression) of lamina neuron-type specific TFs with (blue) or without (red) Hr3 RNAi. Note no change in expression of TFs ± Hr3 RNAi. f, Log(expression) of TFs in the Ecdysone-pathway in WT (red lines) and Hr3 RNAi-expressing (blue lines) L1-L5 neurons. *, p-value < 0.05, fold change > 2.

# Extended data Fig.11

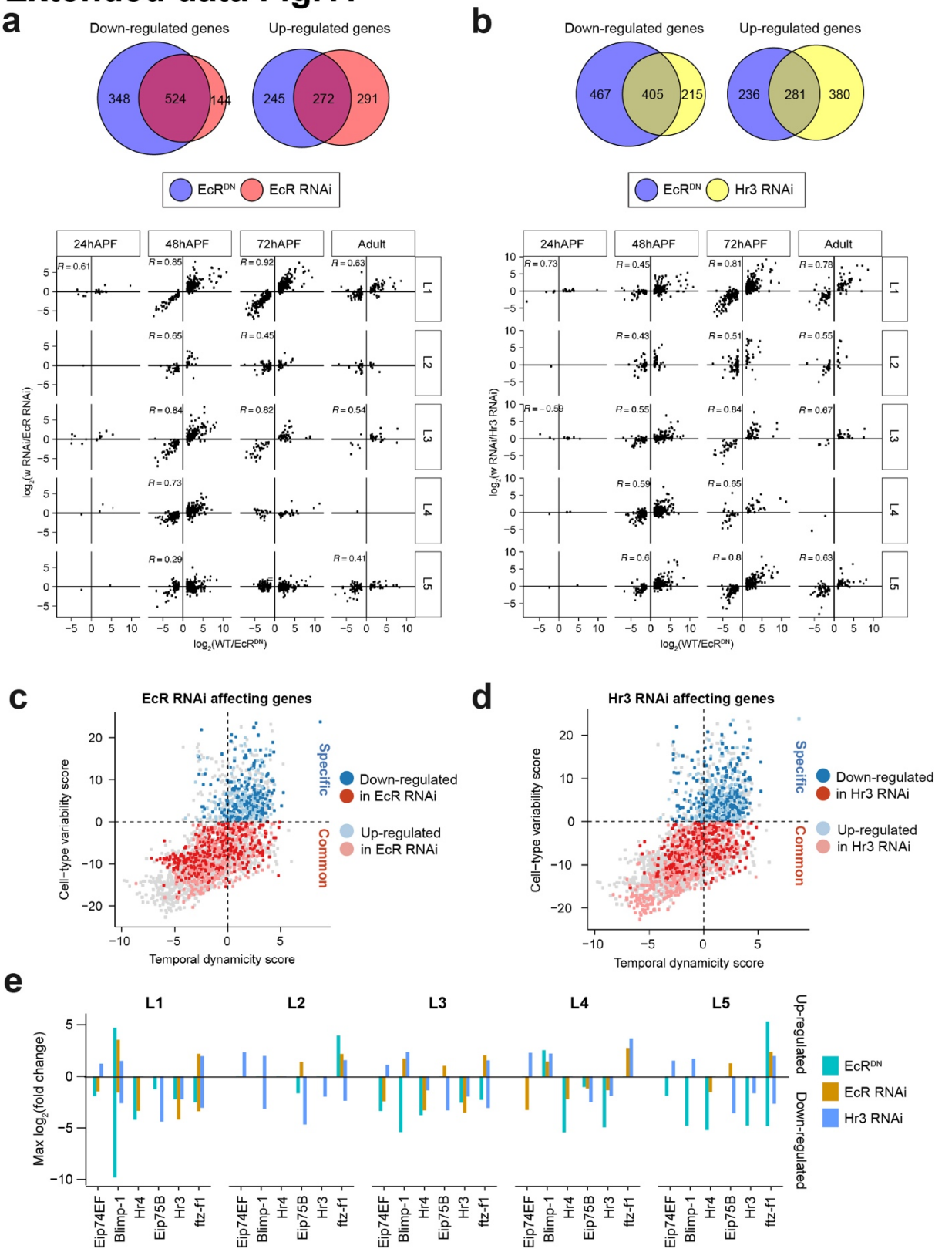

**Extended data Fig. 11. Comparison of genes affected by $EcR^{DN}$, EcR RNAi and Hr3 RNAi.**

a, Top, Venn diagram showing overlap between genes downregulated by $EcR^{DN}$ and EcR RNAi across all time points and lamina neuron-types. Below, $\log_2$(normalized expression in w RNAi/EcR RNAi) vs $\log_2$(normalized expression in WT/$EcR^{DN}$) for L1-L5 neurons throughout development. Correlation coefficient, R, is given for comparisons where $p < 0.05$. b, Top, Venn diagram showing overlap between genes downregulated by $EcR^{DN}$ and Hr3 RNAi across all time points and lamina neuron-types. Below, $\log_2$(normalized expression in w RNAi/Hr3 RNAi) vs $\log_2$(normalized expression in WT/$EcR^{DN}$) for L1-L5 neurons throughout development. Correlation coefficient, R, is given for comparisons where $p < 0.05$. c, Cell-type variability vs Temporal dynamicity plot for EcR RNAi-affected genes (fold change > 2, p-value < 0.05). Cell-type Specific (blue) and Common (red) targets are shown. Darker colors: genes reduced in EcR RNAi, lighter colors: genes increased in EcR RNAi. d, Cell-type variability vs Temporal dynamicity plot for Hr3 RNAi-affected genes (fold change > 2, p-value < 0.05). Cell-type Specific (blue) and Common (red) targets are shown. Darker colors: genes reduced in Hr3 RNAi, lighter colors: genes increased in Hr3 RNAi. e, Maximum change in expression of Ecdysone-pathway TFs in L1-L5 neurons with $EcR^{DN}$, EcR RNAi and Hr3 RNAi. Note that EcR RNAi often has weaker effect on TF expression as compared to $EcR^{DN}$.

# Extended data Fig.12

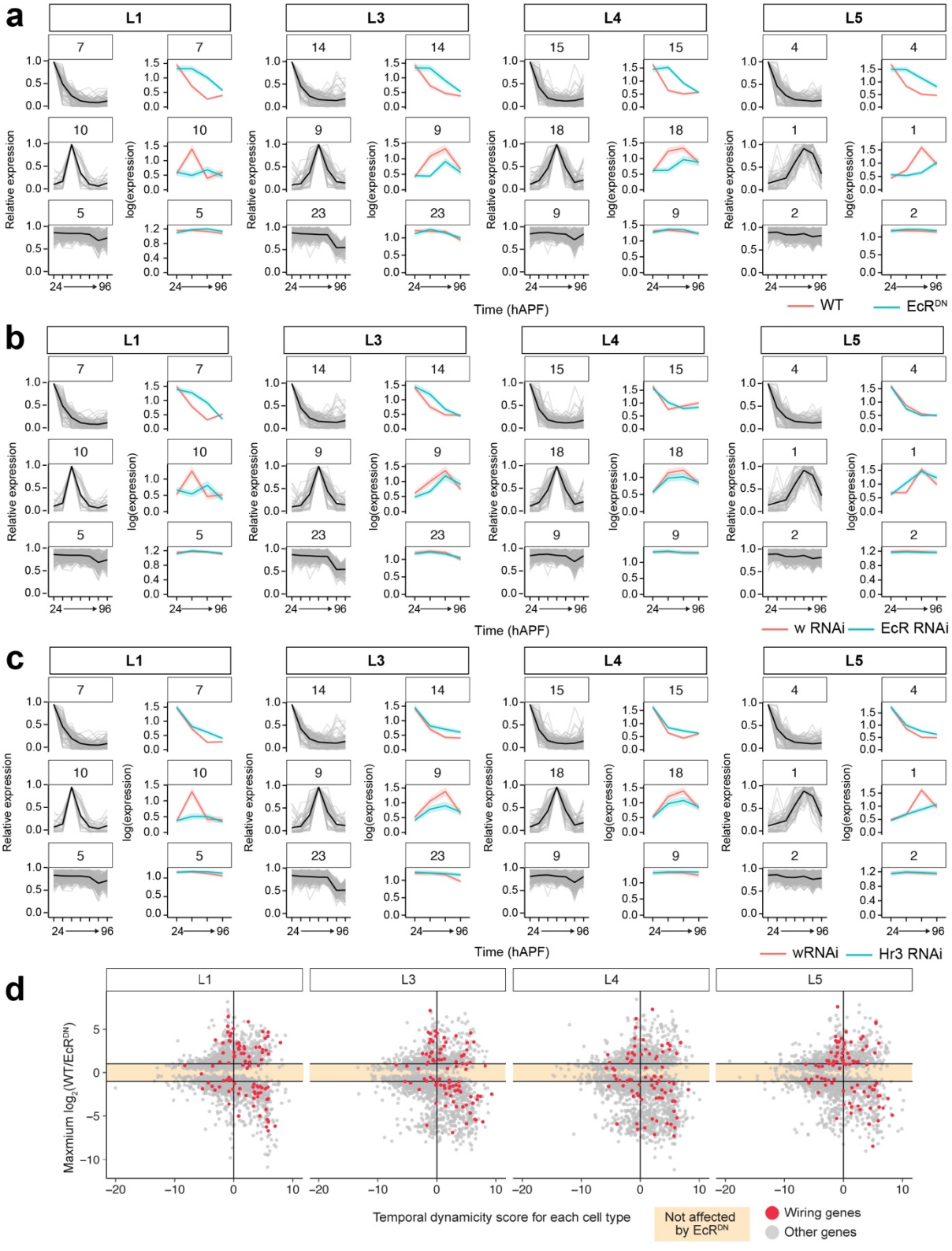

**Extended data Fig. 12. Clusters of genes most affected by $EcR^{DN}$, EcR RNAi and Hr3 RNAi.**

All genes expressed in L1-L5 neurons (done separately for each cell-type) were clustered into groups (using k-means clustering) based on their expression dynamics (see methods). Clusters that show maximum upregulation or downregulation with $EcR^{DN}$ are shown in a – c (clusters are indicated in numbers above each graph). Also shown are clusters unchanged by $EcR^{DN}$. For each panel: left, light grey lines, relative expression of all genes in the cluster; black line, mean of relative expression of all genes in the cluster. Right, red line, mean relative expression in control; blue line, mean relative expression with perturbation. Shades are SEM. d, examples of dynamic wiring genes that are not affected by $EcR^{DN}$. d, Plots showing maximum change in expression [$\log_2(WT/EcR^{DN})$] caused by $EcR^{DN}$ vs the temporal dynamicity of the gene (calculated separately for each cell-type). Shown in red are wiring genes. Colored region on the plot represents genes not affected by $EcR^{DN}$. Note many genes including wiring genes (especially in L1, L3 and L4) with high temporal dynamicity scores that are not affected by $EcR^{DN}$.

# Extended data Fig.13

**a**

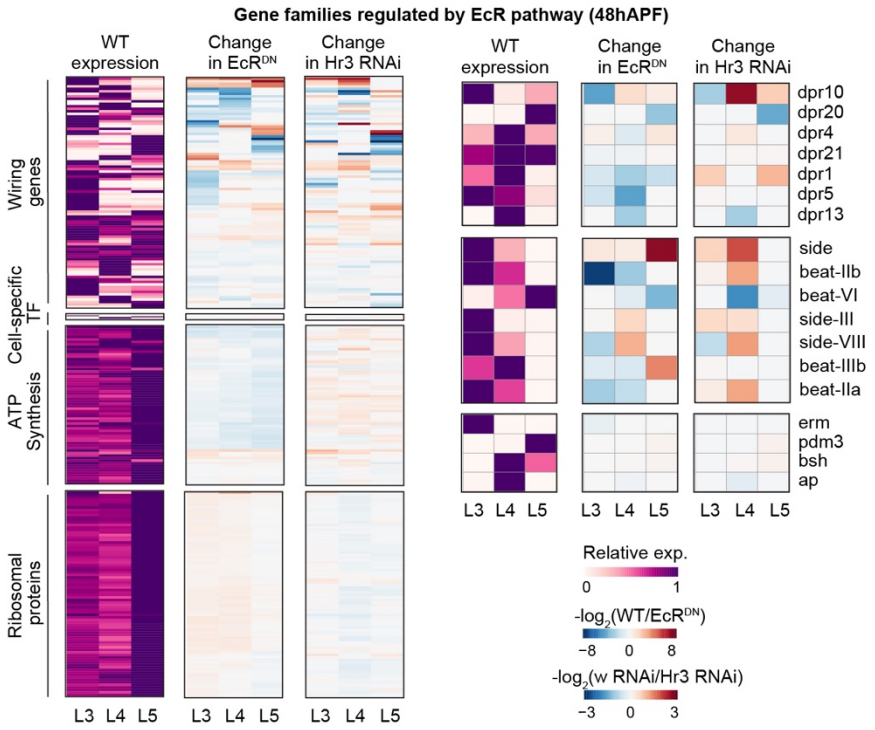


**b**

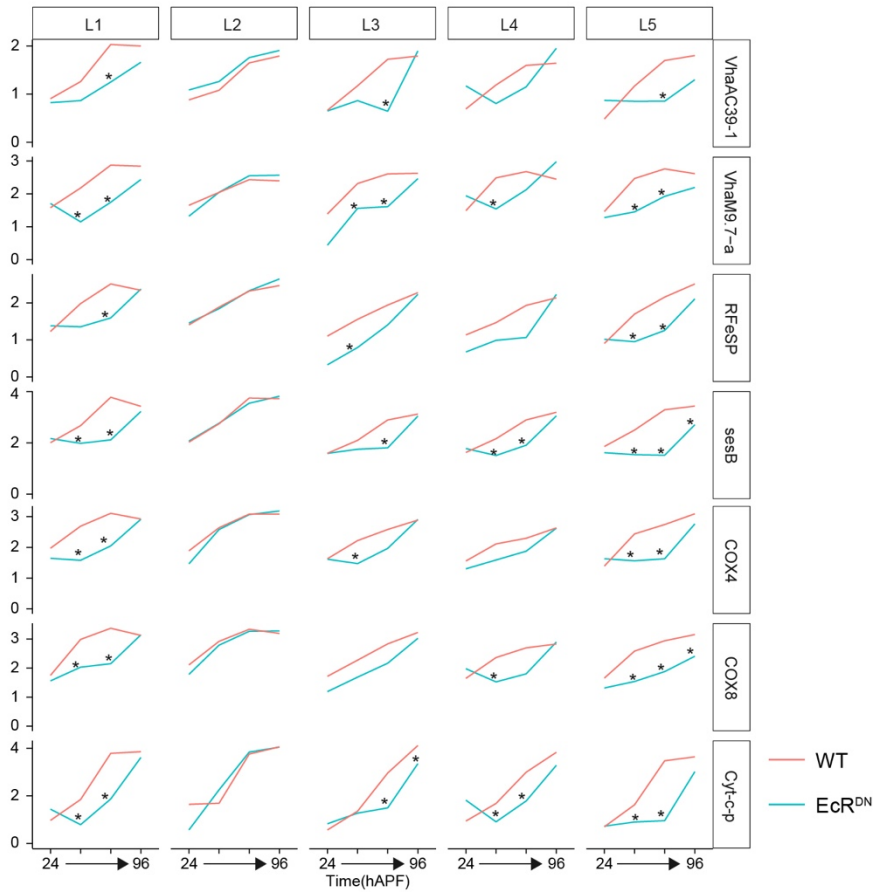

**Extended data Fig. 13. Families of genes affected by $EcR^{DN}$ and Hr3 RNAi**.

a, Relative WT expression (left), change in expression with $EcR^{DN}$ (center), and change in expression with Hr3 RNAi (right) shown as heat maps for all genes expressed in L3-L5 neurons belonging to the specified gene categories at 48hAPF (also see Extended data Fig. 13). Examples of genes belonging to the Dpr family, Side-Beat family and cell-type specific transcription factors are shown separately. b, Expression of some genes involved in ATP synthesis and vacuolar ATPase biology are shown with and without $EcR^{DN}$ in L1-L5 neurons across development. *, fold change between WT and $EcR^{DN} > 2$, p-value $< 0.05$. Note: expression in adults is not significantly affected by $EcR^{DN}$.

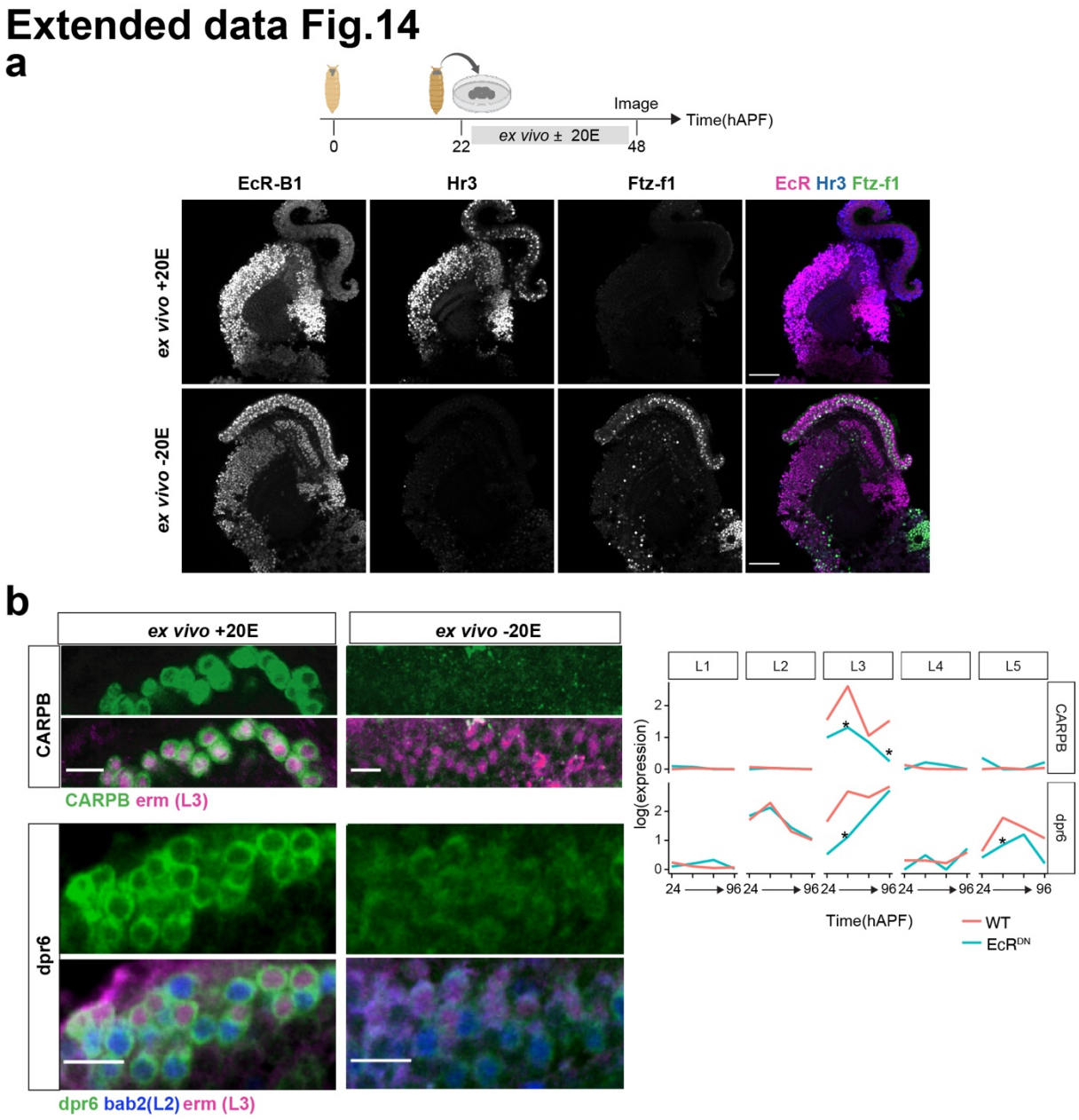


**Extended data Fig. 14. *ex vivo* culture of pupal brain with or without Ecdysone.**

a, Top, schematic of experimental setup (see methods). Briefly, brains are dissected at 22hAPF then incubated for 26h in media ± 20E (20 HydroxyEcdysone, active form of Ecdysone). Bottom, optic lobes stained for EcR-B1, Hr3 and Ftz-f1 cultured ex vivo ± 20E. Scale bar, 50 µm. b, Left, Staining for CARPB and dpr6 reporters (MiMIC lines, see methods) in lamina neuron cell-bodies

± 20E. Right, CARPB and dpr6 expression with (blue) or without (red) $EcR^{DN}$. *, fold change between WT and $EcR^{DN} > 2$, p-value < 0.05. Note: dpr6 expression is unchanged in L2 with pan-lamina expression of $EcR^{DN}$, however staining in brains cultured ex vivo without 20E in the medium shows reduced protein expression in L2 (bab2 positive cell-bodies). This is consistent with weak activity of the pan-lamina driver (9B08 Gal4) in L2 at 48hAPF leading to ineffective inhibition of the Ecdysone-pathway (see Extended data Fig. 8c).

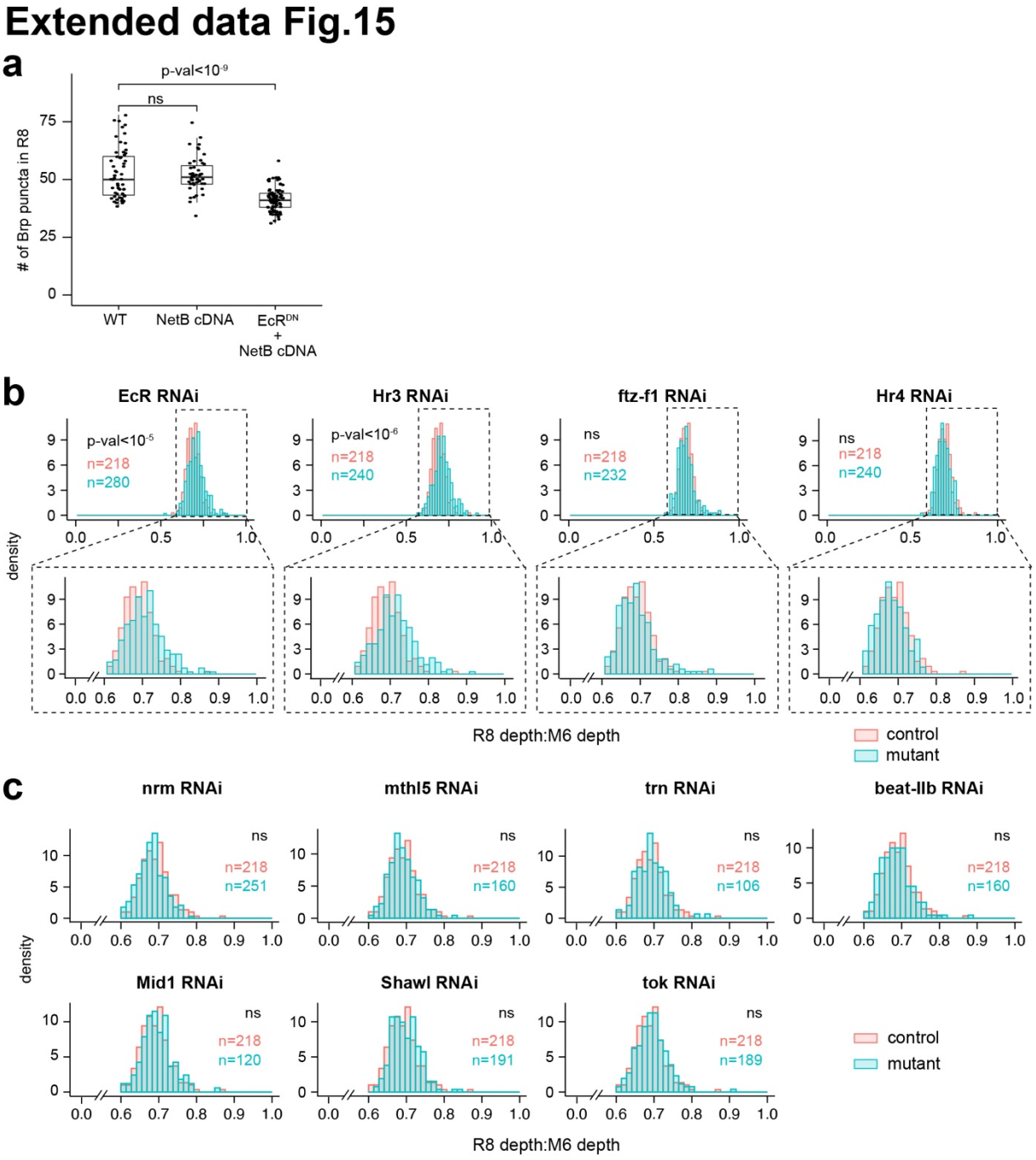


**Extended data Fig. 15. Genes expressed in L3 required for R8 wiring.**

a, Total number of presynaptic sites (Brp puncta) in R8 neurons with WT, NetB overexpressing, or $EcR^{DN}$ and NetB-expressing L3 neurons. NetB overexpression is unable to rescue the reduction in R8 presynaptic sites seen with expression of $EcR^{DN}$ in L3 neurons (see Fig. 4c). p-value

(Student's t-test) is given. b, c, Distributions of R8 axon terminal depth in w RNAi (red) or with expression of other RNAi (as shown, blue) in L3 neurons. All conditions, number of animals ≥ 3. p-values (Kolmogorov-Smirnov test) are given. ns = Not significant. b, RNAi against TFs in the Ecdysone-pathway. c, Results from RNAi screen showing genes that did not significantly affect R8 axon depth. Numbers of neurons/ condition are given.

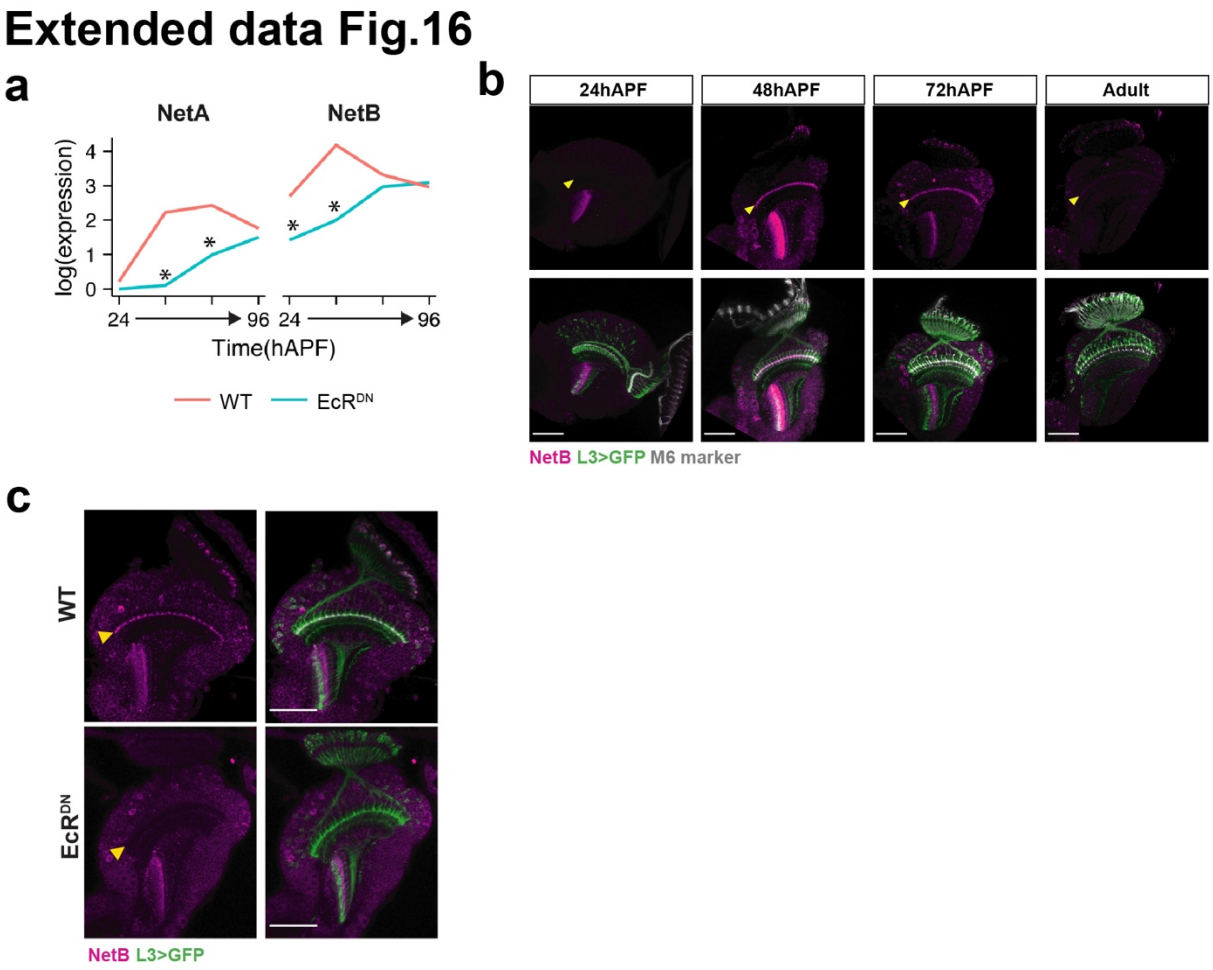


**Extended data Fig. 16. Netrin expression in L3 requires EcR activity.**

a, Expression of NetA and NetB in L3 with (blue) or without (red) $EcR^{DN}$ expression. *, fold change between WT and $EcR^{DN} > 2$, p-value $< 0.05$. b, Staining using anti-NetB antibody (magenta) at the indicated times in development. Marker for M6 medulla layer (24B10, grey) and L3 neurons labeled with GFP (green) are shown. c, Staining using anti-NetB antibody (magenta) ± $EcR^{DN}$ expression only in L3. L3 neurons labeled with GFP (green) are shown. b, c, Scale bar, 50 μm. Yellow arrowhead, M3 medulla layer.

Extended data Tables

Extended data Table 1. Fly strains used in this study

Extended data Table 2. Temporal dynamicity and cell-type variability scores

Extended data Table 3. Wiring genes

Extended data Table 4. Gene ontology and Reactome analyses

Extended data Table 5. L1 bulk ATAC-Seq

Extended data Table 6. scRNA-Seq data for wildtype Lamina neurons

Extended data Table 7. scRNA-Seq data for wildtype vs $EcR^{DN}$-expressing Lamina neurons

Extended data Table 8. scRNA-Seq data for wildtype vs EcR RNAi-expressing Lamina neurons

Extended data Table 9. scRNA-Seq data for wildtype vs Hr3 RNAi-expressing Lamina neurons

**Acknowledgements**

We thank Dr. Pecot (Harvard), Dr. Yamanaka (UC Riverside), Dr. Black (UCLA), Dr. De Robertis (UCLA), Dr. Riddiford (Univ. of Washington) and Dr. Truman (Janelia Research Campus) for helpful discussions. We thank Dr. Schuldiner (Weizmann Institute of Science) and members of the Zipursky lab for feedback on the manuscript, and Dr. Diaz de la Loza for help with figure illustrations. We would like to specifically acknowledge Juyoun Yoo's (Zipursky Lab) and Rachel Hodge's (Jones Lab, UCLA) help with ATAC-Seq library prep and immunostaining. We also thank the BSCRC Sequencing Core (UCLA) and the TCGB core (UCLA) for help with library preparation and sequencing; the BSCRC FACS core (UCLA) and the Witte lab (UCLA) for assistance with FACS purification of lamina neurons; and the IDRE Statistics Consulting (UCLA) and Dr. Balliu (UCLA) for assistance with the statistical analysis of data. Reagents provided by Dr. Akin (UCLA), Dr. Laski (UCLA), Dr. Wang (Duke-NUS), Dr. Pecot (Harvard), Dr. Thummel (Univ. of Utah) and Dr. Bashaw (Univ. of Penn.), and fly lines from the Bloomington Drosophila Stock Center were critical for this work. This work was supported by NIH T32-NS048004 Neurobehavioral Genetics Training Grant (S.J.), Helen Hay Whitney Foundation (S.J.) and Whitcome Fellowship (Y.L.). S.L.Z is an investigator of the Howard Hughes Medical Institute.

**Author contributions**

S.J., Y.L., Y.Z.K., J.V-A and S.L.Z. designed experiments. S.J., Y.L., P.M., S.A.L, J.V-A and B.P. acquired data. S.J., Y.L., J.V-A and Y.K. analyzed the data. S.J., Y.L. and S.L.Z. wrote the manuscript with input from all co-authors.

Competing interest declaration

The authors declare no competing interests.

**Additional information**

Supplementary Information is available for this paper. Correspondence and requests for materials should be addressed to: Dr. S. Lawrence Zipursky - lzipursky@mednet.ucla.edu.

**References**

1. Südhof, T. C. Towards an Understanding of Synapse Formation. Neuron 100, 276--293 (2018).

2. Zipursky, S. L. & Sanes, J. R. Chemoaffinity Revisited: Dscams, Protocadherins, and Neural Circuit Assembly. Cell 143, 343--353 (2010).

3. Hassan, B. A. & Hiesinger, P. R. Beyond Molecular Codes: Simple Rules to Wire Complex Brains. Cell 163, 285--291 (2015).

4. Yogev, S. & Shen, K. Cellular and Molecular Mechanisms of Synaptic Specificity. Annu Rev Cell Dev Bi 30, 417--437 (2014).

5. Li, H. et al. Classifying Drosophila Olfactory Projection Neuron Subtypes by Single-Cell RNA Sequencing. Cell 171, 1206--1220.e22 (2017).

6. Özel, M. N. et al. Neuronal diversity and convergence in a visual system developmental atlas. Nature 1–8 (2020) doi:10.1038/s41586-020-2879-3.

7. Hobert, O. Chapter Twenty-Five - Terminal Selectors of Neuronal Identity. in Current Topics in Developmental Biology (ed. Wassarman, P. M.) vol. 116 455--475 (Academic Press, 2016).

8. Hong, W. & Luo, L. Genetic Control of Wiring Specificity in the Fly Olfactory System. Genetics 196, 17--29 (2014).

9. Dasen, J. S. & Jessell, T. M. Chapter Six Hox Networks and the Origins of Motor Neuron Diversity. in Current Topics in Developmental Biology vol. 88 169--200 (Academic Press, 2009).

10. Larkin, A. et al. FlyBase: updates to the Drosophila melanogaster knowledge base. Nucleic Acids Res 49, D899–D907 (2020).

11. Scheffer, L. K. et al. A connectome and analysis of the adult Drosophila central brain. Elife 9, e57443 (2020).

12. Kurmangaliyev, Y. Z., Yoo, J., Valdes-Aleman, J., Sanfilippo, P. & Zipursky, S. L. Transcriptional Programs of Circuit Assembly in the Drosophila Visual System. Neuron (2020) doi:10.1016/j.neuron.2020.10.006.

13. Reilly, M. B., Cros, C., Varol, E., Yemini, E. & Hobert, O. Unique homeobox codes delineate all the neuron classes of C. elegans. Nature 584, 595–601 (2020).

14. Truman, J. W., Talbot, W. S., Fahrbach, S. E. & Hogness, D. S. Ecdysone receptor expression in the CNS correlates with stage-specific responses to ecdysteroids during Drosophila and Manduca development. Dev Camb Engl 120, 219--234 (1994).

15. Riddiford, L. M., Cherbas, P. & Truman, J. W. Ecdysone receptors and their biological actions. Vitamins Hormones 60, 1--73 (2000).

16. White, K. P., Hurban, P., Watanabe, T. & Hogness, D. S. Coordination of Drosophila metamorphosis by two ecdysone-induced nuclear receptors. Sci New York N Y 276, 114--117 (1997).

17. Agawa, Y. et al. Drosophila Blimp-1 Is a Transient Transcriptional Repressor That Controls Timing of the Ecdysone-Induced Developmental Pathway. Mol Cell Biol 27, 8739--8747 (2007).

18. Rabinovich, D., Yaniv, S. P., Alyagor, I. & Schuldiner, O. Nitric Oxide as a Switching Mechanism between Axon Degeneration and Regrowth during Developmental Remodeling. Cell 164, 170--182 (2016).

19. Pak, M. D. & Gilbert, L. I. A Developmental Analysis of Ecdysteroids During the Metamorphosis of extitDrosophila Melanogaster. J Liq Chromatogr 10, 2591--2611 (1987).

20. Buenrostro, J. D., Wu, B., Chang, H. Y. & Greenleaf, W. J. ATAC-seq: A Method for Assaying Chromatin Accessibility Genome-Wide. Curr Protoc Mol Biology Ed Frederick M Ausubel Et Al 109, 21.29.1--9 (2015).

21. Imrichová, H., Hulselmans, G., Atak, Z. K., Potier, D. & Aerts, S. i-cisTarget 2015 update: generalized cis-regulatory enrichment analysis in human, mouse and fly. Nucleic Acids Res 43, W57--W64 (2015).

22. Shlyueva, D. et al. Hormone-responsive enhancer-activity maps reveal predictive motifs, indirect repression, and targeting of closed chromatin. Mol Cell 54, 180--192 (2014).

23. Cherbas, L., Hu, X., Zhimulev, I., Belyaeva, E. & Cherbas, P. EcR isoforms in Drosophila: testing tissue-specific requirements by targeted blockade and rescue. Development 130, 271--284 (2003).

24. Xu, C. et al. Control of Synaptic Specificity by Establishing a Relative Preference for Synaptic Partners. Neuron 103, 865--877.e7 (2019).

25. Nern, A., Zhu, Y. & Zipursky, S. L. Local N-Cadherin Interactions Mediate Distinct Steps in the Targeting of Lamina Neurons. Neuron 58, 34--41 (2008).

26. Pecot, M. Y. et al. Sequential Axon-Derived Signals Couple Target Survival and Layer Specificity in the Drosophila Visual System. Neuron 82, 320--333 (2014).

27. Fisher, Y. E. et al. FlpStop, a tool for conditional gene control in Drosophila. Elife 6, (2017).

28. Yao, T.-P., Segraves, W. A., Oro, A. E., McKeown, M. & Evans, R. M. Drosophila ultraspiracle modulates ecdysone receptor function via heterodimer formation. Cell 71, 63–72 (1992).

29. Yao, T. P. et al. Functional ecdysone receptor is the product of EcR and Ultraspiracle genes. Nature 366, 476--479 (1993).

30. Schwabe, T., Borycz, J. A., Meinertzhagen, I. A. & Clandinin, T. R. Differential Adhesion Determines the Organization of Synaptic Fascicles in the Drosophila Visual System. Curr Biol 24, 1304--1313 (2014).

31. Takemura, S. et al. Synaptic circuits and their variations within different columns in the visual system of Drosophila. Proc National Acad Sci 112, 13711--13716 (2015).

32. Tan, L. et al. Ig Superfamily Ligand and Receptor Pairs Expressed in Synaptic Partners in Drosophila. Cell 163, 1756--1769 (2015).

33. Lee, C. W. & Peng, H. B. The Function of Mitochondria in Presynaptic Development at the Neuromuscular Junction. Mol Biol Cell 19, 150–158 (2008).

34. Zhou, H. & Liu, G. Regulation of density of functional presynaptic terminals by local energy supply. Mol Brain 8, 42 (2015).

35. Rangaraju, V., Lauterbach, M. & Schuman, E. M. Spatially Stable Mitochondrial Compartments Fuel Local Translation during Plasticity. Cell 176, 73--84.e15 (2019).

36. Gowrisankaran, S. & Milosevic, I. Regulation of synaptic vesicle acidification at the neuronal synapse. Iubmb Life 72, 568–576 (2020).

37. Özel, M. N., Langen, M., Hassan, B. A. & Hiesinger, P. R. Filopodial dynamics and growth cone stabilization in Drosophila visual circuit development. Elife 4, e10721 (2015).

38. Peng, J. et al. Drosophila Fezf coordinates laminar-specific connectivity through cell-intrinsic and cell-extrinsic mechanisms. Elife 7, (2018).

39. Santiago, I. J. et al. Drosophila Fezf functions as a transcriptional repressor to direct layer-specific synaptic connectivity in the fly visual system. Proc National Acad Sci 118, e2025530118 (2021).

40. Akin, O. & Zipursky, S. L. Frazzled promotes growth cone attachment at the source of a Netrin gradient in the Drosophila visual system. Elife 5, e20762 (2016).

41. Moffatt, N. S. C., Bruinsma, E., Uhl, C., Obermann, W. M. J. & Toft, D. Role of the Cochaperone Tpr2 in Hsp90 Chaperoning. Biochemistry-us 47, 8203–8213 (2008).

42. Brychzy, A. et al. Cofactor Tpr2 combines two TPR domains and a J domain to regulate the Hsp70/Hsp90 chaperone system. Embo J 22, 3613–3623 (2003).

43. Klucken, J. et al. ABCG1 (ABC8), the human homolog of the Drosophila white gene, is a regulator of macrophage cholesterol and phospholipid transport. Proc National Acad Sci 97, 817–822 (2000).

44. Suzuki, M., Suzuki, H., Sugimoto, Y. & Sugiyama, Y. ABCG2 Transports Sulfated Conjugates of Steroids and Xenobiotics*. J Biol Chem 278, 22644–22649 (2003).

45. Kurmangaliyev, Y. Z., Yoo, J., LoCascio, S. A. & Zipursky, S. L. Modular transcriptional programs separately define axon and dendrite connectivity. Elife 8, e50822 (2019).

46. Alyagor, I. et al. Combining Developmental and Perturbation-Seq Uncovers Transcriptional Modules Orchestrating Neuronal Remodeling. Dev Cell 47, 38--52.e6 (2018).

47. Uyehara, C. M. & McKay, D. J. Direct and widespread role for the nuclear receptor EcR in mediating the response to ecdysone in Drosophila. Proc National Acad Sci 116, 9893--9902 (2019).

48. Syed, M. H., Mark, B. & Doe, C. Q. Steroid hormone induction of temporal gene expression in Drosophila brain neuroblasts generates neuronal and glial diversity. Elife 6, e26287 (2017).

49. Altmann, C. R. & Brivanlou, A. H. Neural patterning in the vertebrate embryo. Int Rev Cytol 203, 447–482 (2001).

50. Briscoe, J. & Small, S. Morphogen rules: design principles of gradient-mediated embryo patterning. Development 142, 3996–4009 (2015).

51. Gaunt, S. J. Hox cluster genes and collinearities throughout the tree of animal life. Int J Dev Biol 62, 673–683 (2018).

52. Prezioso, G., Giannini, C. & Chiarelli, F. Effect of Thyroid Hormones on Neurons and Neurodevelopment. Horm Res Paediat 90, 73–81 (2018).

53. Miranda, A. & Sousa, N. Maternal hormonal milieu influence on fetal brain development. Brain Behav 8, e00920 (2018).

54. Akin, O. & Zipursky, S. L. Activity regulates brain development in the fly. Curr Opin Genet Dev 65, 8–13 (2020).

55. Ting, C.-Y. et al. Photoreceptor-Derived Activin Promotes Dendritic Termination and Restricts the Receptive Fields of First-Order Interneurons in Drosophila. Neuron 81, 830--846 (2014).

56. Mizumoto, K. & Shen, K. Two Wnts Instruct Topographic Synaptic Innervation in C. elegans. Cell Reports 5, 389–396 (2013).

57. Umemori, H., Linhoff, M. W., Ornitz, D. M. & Sanes, J. R. FGF22 and Its Close Relatives Are Presynaptic Organizing Molecules in the Mammalian Brain. Cell 118, 257–270 (2004).

58. Picelli, S. et al. Full-length RNA-seq from single cells using Smart-seq2. Nat Protoc 9, 171–181 (2014).

59. Buenrostro, J. D., Giresi, P. G., Zaba, L. C., Chang, H. Y. & Greenleaf, W. J. Transposition of native chromatin for fast and sensitive epigenomic profiling of open chromatin, DNA-binding proteins and nucleosome position. Nat Methods 10, 1213--1218 (2013).

60. Ambrosini, G., Groux, R. & Bucher, P. PWMScan: a fast tool for scanning entire genomes with a position-specific weight matrix. Bioinformatics 34, 2483–2484 (2018).

61. Xu, S. et al. Interactions between the Ig-Superfamily Proteins DIP-α and Dpr6/10 Regulate Assembly of Neural Circuits. Neuron 100, 1369--1384.e6 (2018).

# Chapter 3 Temporal specific regulation of IgSF proteins Beat-IIa/Beat-IIb

## Introduction

Developmental transcriptomic analysis revealed that gene expression is highly dynamic during neural circuit assembly in different species (Clark et al., 2019; Kurmangaliyev et al., 2020; Özel et al., 2020). Among all dynamic genes, cell recognition molecules, which play important roles in mediating specific neuronal interactions, are also expressed in a cell-type specific manner. In Chapter 2, we discussed a hormone-induced global temporal program that coordinates gene expression in different neurons and regulates specific neural connections. Previous studies in C. elegans and mouse cortex showed a strong correlation between dynamic expression of recognition molecules and specific synaptic connections (Favuzzi et al., 2019; Sengupta et al., 2020). However, little evidence directly proves that the temporal specificity of recognition molecules is important for building functional neural networks. The precise temporal control would explain how so many synapses ($\sim 10^7$) can be specified by a limited set of cell recognition molecules ($\sim 10^3$) (Scheffer et al., 2020).

From the developmental transcriptome of Drosophila visual system, we found that IgSF proteins Beat-IIa and Beat-IIb are used at different times by neurons in the same region. Lamina neuron L1-L5 terminate and arborize in specific layers of the outer medulla and have distinct connectivity and function (Figure 3-1a) (Nern et al., 2008; Rivera-Alba et al., 2011; Takemura et al., 2015; Tuthill et al., 2013). Among all five lamina neurons, Beat-IIa/Beat-IIb is only expressed in L3-L5, and interestingly, they are expressed in a sequential way during circuits assembly (Figure 3-1b). The dynamic expression of Beat-IIa/Beat-IIb is regulated by the global temporal program induced by steroid hormone ecdysone (Figure 3-1c) (Jain et al., 2021). However, it is unclear whether the specific timing control of Beat-IIa/Beat-IIb in L3-L5 plays a role their circuit assembly.

The re-use of Beat-IIa /Beat-IIb in lamina neurons provides a good system to study the function of temporal specificity of cell recognition molecules.

Beat-IIa and Beat-IIb belong to Beat subfamily of Immunoglobulin super family (IgSF) and it contains 14 paralogs (Figure 3-1d) (Pipes et al., 2001). Biochemistry assays showed that different Beat proteins bind specifically to members of another IgSF subfamily, Side, which contains 8 paralogs (Figure 3-1e) (Li et al., 2017). Among these paralogs in the Beat and Side subfamily, Beat-Ia and Side protein have been shown to regulate motor neuron axon guidance and target recognition (Siebert et al., 2009). The expression of Side protein, which shows highly dynamic pattern during embryogenesis, strongly correlates with the position of motor neuron growth cones, which express Beat-Ia protein (Figure 3-1f). It is unclear whether Beat-IIa/Beat-IIb regulates axon guidance in the visual system, and more importantly, whether the timing of their expression can coordinate axon guidance in different neurons. We hypothesize that the global temporal program, combined with other co-factors, turns on the expression of Beat-IIa/Beat-IIb at different time in L3-L5, and the temporal specific regulation of Beat-IIa/Beat-IIb coordinates axon/dendrite growth. The choreographed axon/dendrite growth restricts neuronal interaction in certain time and space, so less recognition molecules are needed to distinguish among neurons and form specific neural networks.

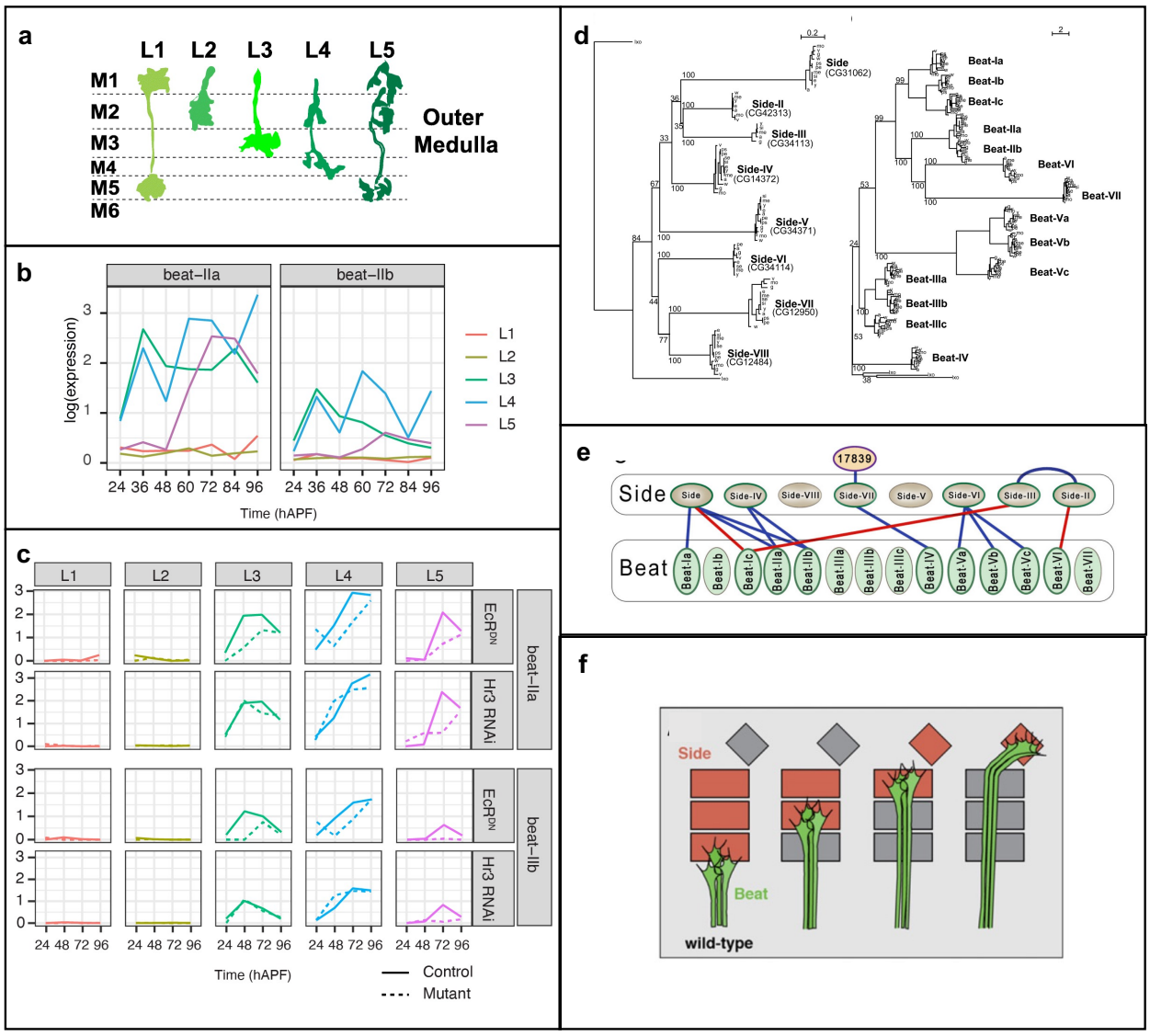


**Figure 3-1 Temporal specific expression of Beat-IIa/Beat-IIb in different lamina neurons.**

(a) Morphology of lamina neuron L1-L5 in medulla. (Millard and Pecot, 2018) (b) Beat-IIa and Beat-IIb are dynamically expressed in L3-L5. Data is from Kurmangaliev et al. 2020. (c) Beat-IIa/Beat-IIb expression is controlled by EcR but not Hr3 in L3 and controlled by both in L5. Data is from Jain et al., 2020 (d) Phylogeny of Beat family proteins and Side family proteins. (Li et al., 2017)(e) Beat and Side family proteins have specific heterophilic binding pattern.(Li et al., 2017)

(f) Beat-Ia and dynamic Side expression is important for motor neuron axon guidance (Siebert et al., 2009).

**Genetic analysis of Beat-IIa/Beat-IIb and Side in L3 and L5 neurons**

L3 neurons provide important signals for proper targeting of photoreceptor R8. In the middle of pupal stage, R8 neurons project their axons to medulla layer M3 (~ 48 hours after pupa formation (hAPF) (Akin and Zipursky, 2016). In this process, Netrin expression in L3 is required to interact with Frazzled protein expressed in the surface R8 and stabilize R8 axons at M3. Without Netrin-Frazzled interaction, R8 retracts to the top of medulla. In our studies discussed in Chapter 2, we showed that disrupting the global temporal program induced by ecdysone not only leads to R8 retraction but also causes R8 to target to deeper layers (M4-M5). The deeper targeting R8 phenotype type can be also found when knocking down Beat-IIa, which is a downstream gene of the ecdysone pathway, with RNAi in L3. This demonstrated that Beat-IIa expression in L3 is important for R8 targeting to the proper layer.

To test whether the interactions between Beat-IIa/Beat-IIb and Side protein are important for R8 proper targeting, we need to perform genetic analysis on Side, which is expressed in R8 neurons. In our preliminary data, whole animal Side mutant generated from Side[C137]/Side-deficiency showed significant R8 mistargeting phenotype. To confirm this result, we are generating another Side null allele using CRIPSR/Cas9. After that, we will perform mosaic analysis on R8 neurons to test if this is from cell-autonomous effects. In addition, since Beat-IIa/Beat-IIb might work redundantly, we are using RNAi to knock down both Beat-IIa and Beat-IIb in L3 and test if R8 neurons show a more severe mistargeting phenotype.

L5 neurons also express Beat-IIa/Beat-IIb but at a late time point (72hAPF), and the timing of their expression coincidence with the extension of L5 branches into the M2 layer (Nern et al.,

2008). Homophilic interactions of N-Cadherin in L5 and L2 are involved in this process, but the expression of N-cadherin does not appear to be tightly linked to L5 branching (Nern et al., 2008). To ask whether Beat-IIa/Beat-IIb expression is required in L5 branching, we will knock down Beat-IIa or Beat-IIb or both in L5 using RNAi and assess L5 morphology. Our preliminary data shows that Beat-IIa RNAi disrupts normal L5 arbors in M2. It is still unclear what neurons provide the Side or Side-IV protein that interact with the Beat-IIa/Beat-IIb in L5. We set a Side/Side-IV RNAi screen with different cell-type specific Gal4 drivers to test which neighboring neurons provide the signal to direct L5 branches into M2.

The genetic analysis of Beat-IIa/Beat-IIb and Side in L3 and L5 will show whether molecular interactions between Beat and Side at different times are important for coordinating axon/dendrite growth of different neurons. Interestingly, in both L3 and L5 neurons, Beat-IIa/Beat-IIb is highly dynamic but Side is expressed in a relatively constant way. This suggests that controlling the timing of one of the binding proteins might be sufficient to generate dynamic interaction.

**Alter the timing of Beat-IIa/Beat-IIb expression in L3 and L5 neurons**

Although the expression of Beat-IIa/Beat-IIb in L3-L5 are temporally correlated with different neural developmental processes, it is unclear whether the temporal control of Beat-IIa/Beat-IIb helps to generate wiring specificity. To study the role of the temporal specificity of gene expression, we can change the timing of Beat-IIa//Beat-IIb expression in L3 and L5. We are generating cDNA lines to express Beat-IIa/Beat-IIb early in L5 or extend their expression in L3. Combining cell-type specific Gal4 and temperature sensitive Gal80, we can precisely control when and where Beat-IIa/Beat-IIb are expressed. The temporal alteration can be also achieved by Cas9 based transcriptional activation (CRISPRa) (Jia et al., 2018). We hypothesize that changing the

timing of Beat-IIa/Beat-IIb will disrupt the order of R8 and L5 innervating their designated regions and affect their specific synaptic connections.

Loss of function analysis only show whether Beat-IIa/Beat-IIb is required in specific neural development, but it does not explain why the same molecules are used in different time windows. Precise control of when and where Beat-IIa/Beat-IIb are expressed is technically challenging, but it will provide direct evidence to support if temporal specificity can increase molecular diversity in developing neurons.

**Mechanisms of differential temporal control of Beat-IIa/Beat-IIb expression**

In L3-L5, Beat-IIa/Beat-IIb expression is controlled by different temporal transcription factors (TFs) in the ecdysone pathway, although these TFs are expressed globally. In different tissues or cell types, Ecdysone receptor, EcR, binds to distinct sets of target genes over development, and combinations of cis-regulatory motif can also specify their target genes (Shlyueva et al., 2014; Uyehara and McKay, 2019). This suggests that cell-type specific TFs might set distinct chromatin landscape in different cell types so that globally expressed temporally TFs preferentially bind to certain sites and regulate their target genes. To understand how Beat-IIa/Beat-IIb are differentially controlled in lamina neurons, we need to examine their chromatin landscape.

Janssens et al. recently published a single cell Assay for Transposase-Accessible Chromatin using sequencing (ATAC-seq) dataset that contains cells in the entire Drosophila brain, including the visual system, at multiple developmental stages (Janssens et al., 2021). This dataset would provide great information to reveal how Beat-IIa/Beat-IIb is expressed at different times in L3-L5. However, only L2/3 neurons are currently annotated in their dataset. We can re-analyze their single cell ATAC-seq data and improve the bioinformatic analysis of unsupervised clustering

and cluster annotation. After extracting data of different lamina neurons, we will identify differential chromatin open regions near Beat-IIa/Beat-IIb. Since Beat-IIa and Beat-IIb are close related genes generated from recent gene duplication event and they have very similar expression pattern, they might share the same enhancer region, or the enhancer region is also duplicated. It is still possible that the enhancer regions of Beat-IIa/Beat-IIb are distant from the gene body and it will be challenging to identify. After identifying the enhancer regions for Beat-IIa/Beat-IIb, we can clone those enhancers to Gal4 drivers and see if it reflects the expression patterns. TF motif analysis in different enhancer regions will be performed to understand the molecular mechanisms of differential temporal control.

In addition to Beat-IIa and Beat-IIb these two examples that have differential temporal regulations, more recognition molecules like these are re-used over development. There are about a thousand genes encoded for cell surface molecules, but only a fraction of them are expressed in developing brains and can act as recognition molecules. To build a complex brain containing billions of synapses, having precise temporal control of gene expression can generate more combination of molecular codes over time to specify synaptic connections. When neuronal interactions are restricted to certain times and places, fewer recognition molecules are needed to establish specific connections.

**References**

Akin, O., and Zipursky, S.L. (2016). Frazzled promotes growth cone attachment at the source of a Netrin gradient in the Drosophila visual system. ELife Sciences 5, e20762.

Clark, B.S., Stein-O'Brien, G.L., Shiau, F., Cannon, G.H., Davis-Marcisak, E., Sherman, T., Santiago, C.P., Hoang, T.V., Rajaii, F., James-Esposito, R.E., et al. (2019). Single-Cell RNA-Seq Analysis of Retinal Development Identifies NFI Factors as Regulating Mitotic Exit and Late-Born Cell Specification. Neuron 102, 1111-1126.e5.

Favuzzi, E., Deogracias, R., Marques-Smith, A., Maeso, P., Jezequel, J., Exposito-Alonso, D., Balia, M., Kroon, T., Hinojosa, A.J., Maraver, E.F., et al. (2019). Distinct molecular programs regulate synapse specificity in cortical inhibitory circuits. Science 363, 413–417.

Jain, S., Lin, Y., Kurmangaliyev, Y.Z., Valdes-Aleman, J., LoCascio, S.A., Mirshahidi, P., Parrington, B., and Zipursky, S.L. (2021). A global timing mechanism regulates cell-type specific wiring programs. Biorxiv 2020.09.18.304410.

Janssens, J., Aibar, S., Taskiran, I.I., Ismail, J.N., Spanier, K.I., Gonzalez-Blas, C.B., Quan, X.J., Papasokrati, D., Hulselmans, G., Makhzami, S., et al. (2021). Decoding gene regulation in the fly brain. BioRxiv.

Jia, Y., Xu, R.-G., Ren, X., Ewen-Campen, B., Rajakumar, R., Zirin, J., Yang-Zhou, D., Zhu, R., Wang, F., Mao, D., et al. (2018). Next-generation CRISPR/Cas9 transcriptional activation in Drosophila using flySAM. Proc National Acad Sci 115, 201800677.

Kurmangaliyev, Y.Z., Yoo, J., Valdes-Aleman, J., Sanfilippo, P., and Zipursky, S.L. (2020). Transcriptional Programs of Circuit Assembly in the Drosophila Visual System. Neuron 108, 1045-1057.e6.

Li, H., Watson, A., Olechwier, A., Anaya, M., Sorooshyari, S.K., Harnett, D.P., Lee, H.-K. (Peter), Vielmetter, J., Fares, M.A., Garcia, K.C., et al. (2017). Deconstruction of the beaten Path-Sidestep interaction network provides insights into neuromuscular system development. Elife 6, e28111.

Millard, S.S., and Pecot, M.Y. (2018). Strategies for assembling columns and layers in the Drosophila visual system. Neural Development 13, 11.

Nern, Zhu, Aljoscha;, Zipursky, Yan;, and Lawrence, S. (2008). Local N-Cadherin Interactions Mediate Distinct Steps in the Targeting of Lamina Neurons. Neuron 58, 34–41.

Özel, M.N., Simon, F., Jafari, S., Holguera, I., Chen, Y.-C., Benhra, N., El-Danaf, R.N., Kapuralin, K., Malin, J.A., Konstantinides, N., et al. (2020). Neuronal diversity and convergence in a visual system developmental atlas. Nature 589, 1–8.

Pipes, G.C., Lin, Q., Riley, S.E., and Goodman, C.S. (2001). The Beat generation: a multigene family encoding IgSF proteins related to the Beat axon guidance molecule in Drosophila. Dev Camb Engl 128, 4545–4552.

Rivera-Alba, M., Vitaladevuni, S.N., Mishchenko, Y., Lu, Z., Takemura, S., Scheffer, L., Meinertzhagen, I.A., Chklovskii, D.B., and Polavieja, G.G. de (2011). Wiring Economy and Volume Exclusion Determine Neuronal Placement in the Drosophila Brain. Current Biology 21, 2000–2005.

Scheffer, L.K., Xu, C.S., Januszewski, M., Lu, Z., Takemura, S., Hayworth, K.J., Huang, G.B., Shinomiya, K., Maitlin-Shepard, J., Berg, S., et al. (2020). A connectome and analysis of the adult Drosophila central brain. Elife 9, e57443.

Sengupta, T., Koonce, N.L., Moyle, M.W., Duncan, L.H., Vázquez-Martínez, N., Han, X., Shao, L., Wu, Y., Santella, A., Fan, L., et al. (2020). A neurite-zippering mechanism, mediated by layer-specific expression of IgCAMs, regulates synaptic laminar specificity in the C. elegans nerve ring neuropil. Biorxiv 2020.08.28.271437.

Shlyueva, D., Stelzer, C., Gerlach, D., ˜ez-Cuna, J.O.Y. ´n, Rath, M., Bory, qukasz M., Arnold, C.D., and Stark, A. (2014). Hormone-Responsive Enhancer-Activity Maps Reveal Predictive Motifs, Indirect Repression, and Targeting of Closed Chromatin. Molecular Cell 54, 180–192.

Siebert, M., Banovic, D., Goellner, B., and Aberle, H. (2009). Drosophila motor axons recognize and follow a Sidestep-labeled substrate pathway to reach their target fields. Gene Dev 23, 1052–1062.

Takemura, S., Xu, C.S., Lu, Z., Rivlin, P.K., Parag, T., Olbris, D.J., Plaza, S., Zhao, T., Katz, W.T., Umayam, L., et al. (2015). Synaptic circuits and their variations within different columns in the visual system of Drosophila. PNAS 112, 13711–13716.

Tuthill, J.C., Nern, A., Holtz, S.L., Rubin, G.M., and Reiser, M.B. (2013). Contributions of the 12 Neuron Classes in the Fly Lamina to Motion Vision. Neuron 79, 128–140.

Uyehara, C.M., and McKay, D.J. (2019). Direct and widespread role for the nuclear receptor EcR in mediating the response to ecdysone in Drosophila. PNAS 116, 9893–9902.

## Chapter 4 Discussion

### Dynamic gene expression in post-mitotic neurons during neural circuit assembly

High-throughput transcriptomic analysis allows us to profile gene expression at multiple stages in developing neurons. Before single cell RNA-seq, it is hard to imagine profiling so many types of neurons at different time points. Now we have a near-complete cell atlas for the Drosophila brain, including the visual and the olfactory systems (Kurmangaliyev et al., 2020; Li et al., 2017; McLaughlin et al., 2021; Özel et al., 2020; Simon and Konstantinides, 2021). Additionally, a substantial effort has been put into understanding the gene expression trajectory of mammalian neurons (Cheng et al., 2021; Franjic et al., 2021; Yao et al., 2021). We will soon have the complete cell atlas containing the transcriptomes of all cell types in developing brains in many different species. By analyzing their gene expression patterns, we will significantly improve our knowledge of the mechanisms of brain assembly during development.

From the single cell transcriptomic data in Drosophila visual system, we found that gene expression levels change dramatically over time in post-mitotic neurons (see Chapter 2). During neurogenesis, sequential expression of temporal transcription factors (TFs) was observed in neural stem cells and the timing of their expression determine their cell fate (Erclik et al., 2017; Syed et al., 2017). After neurons become fully matured, their expression levels only change mildly while aging (Davie et al., 2018). It is interesting that in between the neural stem cell stage and fully matured neuron stage, post-mitotic neurons present highly dynamic expression patterns, suggesting their critical roles in neural circuit assembly.

Cell recognition molecules are not only expressed dynamically during development, but also expressed in a cell-type specific fashion. In the past several decades, many recognition molecules were found to be important for specific neural connections, while it is still a small set

of molecules compared to the large number of synapses (Sanes and Zipursky, 2020). The combination of spatial and temporal controls of recognition molecules allows neurons to generate diverse molecular codes for wiring from a relatively small number of genes. More examples like Beat-IIa and Beat-IIb (see Chapter 3) are expressed at different time in neurons arborizing in the same region. Therefore, the precise temporal regulation of gene expression, especially recognition molecules, in post-mitotic neurons would be critical for establishing specific connections. However, the mechanisms controlling when genes are expressed during neural circuit formation are unclear. Our studies showed that a global temporal program induced by a steroid hormone ecdysone can control when many genes are expressed (See Chapter 2). The expression of other genes is not controlled by ecdysone signaling, so it suggests that there are other mechanisms controlling the timing of gene expression during circuit assembly.

**Global temporal mechanism coordinates neural development**

To study the temporal control of gene expression during neural circuit formation, we focused on dynamically expressed TFs in the Drosophila visual system. As shown in Chapter 2, dynamic TFs are enriched for nuclear hormone receptors and interestingly they form a TF cascade initiated by a steroid hormone, ecdysone. Ecdysone is produced in prothoracic gland and circulated through hemolymph to be delivered to different tissue (Ou et al., 2016). The growth of different parts of the body can be coordinated by ecdysone signaling and insulin-like peptide Dilp8 (Vallejo et al., 2015). In addition to the global circulation of ecdysone, its receptor EcR is also expressed in all neurons in the brain (see Chapter 2). All neurons switch from one EcR isoform (EcR-B1) to another (EcR-A) during metamorphosis, although the function of this isoform switch remains unclear. Other downstream TFs in the cascade are also expressed and changed in a highly

synchronized fashion during neural development. This suggests that the ecdysone signaling is used globally during neural circuit formation.

To test the role of ecdysone signaling in different types of neurons, we used Gal4-UAS system to drive the expression of dominant negative EcR, which cannot bind to ecdysone and disrupts normal EcR function. From the data in Chapter2, we showed that the ecdysone signaling is required for many different types of neurons to develop their proper axon, dendrite, synapse, and connectivity. This is consistent with our hypothesis that the ecdysone signaling induces a global temporal program that regulates neuronal development.

The global temporal program works with cell-type specific TFs to generate distinct outputs. In Chapter 2, we showed that many dynamic genes in lamina neuron L3 are co-regulated by the global ecdysone signaling and the cell-type specific TF erm. In Chapter 3, we showed that Beat-IIa/Beat-IIb are expressed in different temporal domains in lamina neurons. Although the TFs in the temporal program are expressed in all neurons, their target genes can be differentially regulated in distinct cellular contexts. Similar with Hox genes, which are used as a common module for A/P patterning in different developmental contexts, the EcR pathway may work as a common timing module in combination with distinct cell-type specific factors to control when and where genes are expressed in developing neurons. This global temporal program provides an elegant mechanism that coordinates steps of neuronal differentiation in different neurons.

Ecdysone signaling is highly conserved across different insects but is not used in mammalian systems. Steroid hormones in mammals such as glucocorticoid and estrogen have been shown to have significant impact on neuronal circuits and animal behavior (Clemens et al., 2019; Garabedian et al., 2017). Thyroid hormones are also important for brain development. They can control the time window of neurogenesis, differentiation, and synapse formation (Bernal, 2005).

These suggest that mammalian hormones might induce a common temporal program similar to the TF cascade induced by ecdysone in Drosophila to coordinate gene expression changes during brain development.

**Choreographed gene expression coordinates brain wiring**

As discussed in Chapter 1, a century ago, John Langley and Roger W. Sperry proposed that the molecular differences between neurons are keys to generate wiring specificity (Yogev and Shen, 2014). In this model, neurons express different cell recognition molecules that selectively interact with their receptors on the other neurons, and the specific molecular interactions help them to choose synaptic partners. Both biochemical and genetic analysis are consistent with this model (Honig and Shapiro, 2020; Sanes and Zipursky, 2020). When removing some recognition molecules or disrupting their binding affinities, neurons are re-wired to a different layer or column that might lead to malfunction of neural circuits. However, there are only a small number of recognition molecules compared to the large number of synapses. Additionally, gene redundancy further reduces the number of unique combinations.

Matching cell recognition molecules are important for synaptic specificity, but additional mechanisms are also required to increase the molecular diversity and ensure the precision of synaptic connections. The global temporal program we discovered helps to improve our understanding of brain wiring logic in three aspects. First, the dynamic expression of recognition molecules increases the diversity of matching codes over time. Recognition molecules can be matched at a certain time or throughout the entire circuit assembly to select for proper partners. Second, gene expression can be coordinated in different neurons so that both spatial and temporal cues are integrated for the expression of recognition molecules. Third, the timing of recognition molecule expression could direct stepwise neuronal growth. Within a given temporal and spatial

domain, fewer recognition molecules are required to select proper partners since a neuron only has a small pool of candidates to choose from. This idea fits with the stepwise layer formation in Drosophila medulla or mouse retina where neurons target to broad domains first and then refine their structures in specific layers (Matsuoka et al., 2011; Millard and Pecot, 2018). At different stages of circuit assembly, the corresponding recognition molecules are expressed to guide or sculpt certain wiring features.

**Future directions**

In Chapter 2, we showed ecdysone signaling regulated genes in lamina neurons using single cell RNA-seq (scRNA-seq), but how it controls gene expression in other cell types remains unclear. Ideally, we would perform scRNA-seq analysis on EcR dominant negative or EcR RNAi expressing neurons for each cell type. However, proper Gal4 lines that are expressed at the right time in targeting cells are hard to find. Alternatively, we could culture brains *ex vivo* with/without ecdysone in the media. After *ex vivo* culture, we can dissociate brain tissue and perform scRNA-seq as described in Kurmangaliyev et al (Kurmangaliyev et al., 2020). All cell types can be mapped according to the cell atlas dataset and analyze differentially expressed genes in each cell type. There are still two major limitations of this method. First, we need to improve our *ex vivo* system to culture brains for longer period so that we can sample late time points (the current method can only grow brains up to 48 hours). Second, we cannot distinguish between cell autonomous and non-cell autonomous effect since the entire brain lacks ecdysone signaling. Therefore, we need to develop better assays to analyze ecdysone signaling in targeting genes in the entire brain.

In addition to loss of function analysis, we can also utilize the recently published single cell ATAC-seq (scATAC-seq) dataset to understand the gene regulatory network during neural circuit formation. The scATAC-seq data set contains neurons from the entire brain at multiple

developmental stages (Janssens et al., 2021). From bioinformatic analysis of the whole optic lobe scATAC-seq and scRNA-seq, we will map the TFs in different neurons that act as cell-type specific input to work with the common temporal program. We can also identify enhancers that are important for specific regulation of cell recognition molecules (i.e., Beat-IIa and Beat-IIb are expressed at different times in lamina neurons). Knowing how the spatial and the temporal inputs are integrated might help us to further improve our understanding of the logic underlying brain wiring.

**References**

Bernal, J. (2005). Thyroid Hormones and Brain Development. Vitamins Hormones 71, 95–122.

Cheng, S., Butrus, S., Xu, V., Sagireddy, S., Tan, L., Shekhar, K., and Zipursky, S.L. (2021). Vision is Required for Cell Type Specification in the Visual Cortex. Biorxiv 2021.08.10.455824.

Clemens, A.M., Lenschow, C., Beed, P., Li, L., Sammons, R., Naumann, R.K., Wang, H., Schmitz, D., and Brecht, M. (2019). Estrus-Cycle Regulation of Cortical Inhibition. Curr Biol 29, 605-615.e6.

Davie, K., Janssens, J., Koldere, D., Waegeneer, M.D., Pech, U., Kreft, qukasz, Aibar, S., Makhzami, S., Christiaens, V., González-Blas, C.B., et al. (2018). A Single-Cell Transcriptome Atlas of the Aging Drosophila Brain. Cell 174, 982-998.e20.

Erclik, T., Li, X., Courgeon, M., Bertet, C., Chen, Z., Baumert, R., Ng, J., Koo, C., Arain, U., Behnia, R., et al. (2017). Integration of temporal and spatial patterning generates neural diversity. Nature 541, 365.

Franjic, D., Skarica, M., Ma, S., Arellano, J.I., Tebbenkamp, A.T.N., Choi, J., Xu, C., Li, Q., Morozov, Y.M., Andrijevic, D., et al. (2021). Transcriptomic taxonomy and neurogenic trajectories of adult human, macaque, and pig hippocampal and entorhinal cells. Neuron.

Garabedian, M.J., Harris, C.A., and Jeanneteau, F. (2017). Glucocorticoid receptor action in metabolic and neuronal function. F1000research 6, 1208.

Honig, B., and Shapiro, L. (2020). Adhesion Protein Structure, Molecular Affinities, and Principles of Cell-Cell Recognition. Cell 181, 520–535.

Janssens, J., Aibar, S., Taskiran, I.I., Ismail, J.N., Spanier, K.I., Gonzalez-Blas, C.B., Quan, X.J., Papasokrati, D., Hulselmans, G., Makhzami, S., et al. (2021). Decoding gene regulation in the fly brain. BioRxiv.

Kurmangaliyev, Y.Z., Yoo, J., Valdes-Aleman, J., Sanfilippo, P., and Zipursky, S.L. (2020). Transcriptional Programs of Circuit Assembly in the Drosophila Visual System. Neuron 108, 1045-1057.e6.

Li, H., Horns, F., Wu, B., Xie, Q., Li, J., Li, T., Luginbuhl, D.J., Quake, S.R., and Luo, L. (2017). Classifying Drosophila Olfactory Projection Neuron Subtypes by Single-Cell RNA Sequencing. Cell 171, 1206-1220.e22.

Matsuoka, R.L., Nguyen-Ba-Charvet, K.T., Parray, A., Badea, T.C., Chédotal, A., and Kolodkin, A.L. (2011). Transmembrane semaphorin signaling controls laminar stratification in the mammalian retina. Nature 470, 259–263.

McLaughlin, C.N., Brbić, M., Xie, Q., Li, T., Horns, F., Kolluru, S.S., Kebschull, J.M., Vacek, D., Xie, A., Li, J., et al. (2021). Single-cell transcriptomes of developing and adult olfactory receptor neurons in Drosophila. Elife 10, e63856.

Millard, S.S., and Pecot, M.Y. (2018). Strategies for assembling columns and layers in the Drosophila visual system. Neural Development 13, 11.

Ou, Q., Zeng, J., Yamanaka, N., Brakken-Thal, C., O'Connor, M.B., and King-Jones, K. (2016). The Insect Prothoracic Gland as a Model for Steroid Hormone Biosynthesis and Regulation. Cell Reports 16, 247–262.

Özel, M.N., Simon, F., Jafari, S., Holguera, I., Chen, Y.-C., Benhra, N., El-Danaf, R.N., Kapuralin, K., Malin, J.A., Konstantinides, N., et al. (2020). Neuronal diversity and convergence in a visual system developmental atlas. Nature 589, 1–8.

Sanes, J.R., and Zipursky, S.L. (2020). Synaptic Specificity, Recognition Molecules, and Assembly of Neural Circuits. Cell 181, 536–556.

Simon, F., and Konstantinides, N. (2021). Single-cell transcriptomics in the Drosophila visual system: Advances and perspectives on cell identity regulation, connectivity, and neuronal diversity evolution. Developmental Biology 479, 107–122.

Syed, M.H., Mark, B., and Doe, C. (2017). Steroid hormone induction of temporal gene expression in Drosophila brain neuroblasts generates neuronal and glial diversity. Elife 6, e26287.

Vallejo, D.M., Juarez-Carreño, S., Bolivar, J., Morante, J., and Dominguez, M. (2015). A brain circuit that synchronizes growth and maturation revealed through Dilp8 binding to Lgr3. Science 350, aac6767.

Yao, Z., Velthoven, C.T.J. van, Nguyen, T.N., Goldy, J., Sedeno-Cortes, A.E., Baftizadeh, F., Bertagnolli, D., Casper, T., Chiang, M., Crichton, K., et al. (2021). A taxonomy of transcriptomic cell types across the isocortex and hippocampal formation. Cell 184, 3222-3241.e26.

Yogev, S., and Shen, K. (2014). Cellular and Molecular Mechanisms of Synaptic Specificity. Annu Rev Cell Dev Bi 30, 417–437.